THE UNIVERSITY OF MANITOBA

TURBULENCE STRUCTURE IN A CONICAL DIFFUSER

by

RUDOLF HENRY HUMMEL

A THESIS

SUBMITTED TO THE FACULTY OF GRADUATE STUDIES
IN PARTIAL FULFILMENT OF THE REQUIREMENTS FOR THE
DEGREE OF DOCTOR OF PHILOSOPHY

DEPARTMENT OF MECHANICAL ENGINEERING

WINNIPEG, MANITOBA
FEBRUARY, 1978

TURBULENCE STRUCTURE
IN A CONICAL DIFFUSER

BY

RUDOLF HENRY HUMMEL

A dissertation submitted to the Faculty of Graduate Studies of the University of Manitoba in partial fulfillment of the requirements of the degree of

DOCTOR OF PHILOSOPHY

© 1978

Permission has been granted to the LIBRARY OF THE UNIVERSITY OF MANITOBA to lend or sell copies of this dissertation, to the NATIONAL LIBRARY OF CANADA to microfilm this dissertation and to lend or sell copies of the film, and UNIVERSITY MICROFILMS to publish an abstract of this dissertation.

The author reserves other publication rights, and neither the dissertation nor extensive extracts from it may be printed or otherwise reproduced without the author's written permission.

THE UNIVERSITY OF MANITOBA LIBRARIES

ABSTRACT

Using hot-wire anemometry experiments were conducted to investigate the turbulence structure in a conical diffuser with fully developed pipe flow at entry. Total divergence angle and area ratio were 8° and 4:1 respectively. For most experiments a pipe Reynolds number of 137,000 was used.

Presented for several axial locations are probability densities of U, profiles of; $\bar{U}$, u', moments of u up to the fourth-order, $\overline{uv}$, and the four truncated components of $\overline{uv}$. Also given, for a profile located 30 cm upstream of the diffuser exit plane for measurements of u spectra, dissipation, length scales, longitudinal vorticity, structure functions, as well as several fine-structure parameters which include the skewness, flatness factor, and intermittency factor of $\partial u/\partial t$.

For the core region the results show a structure similar to that of fully developed pipe flow, but gradually being replaced in the down stream direction by a more energetic structure expanding toward the centre line. At approximately the entry radius throughout, the turbulence structure exhibits characteristics, in several ways similar to those of a boundary layer in the vicinity of $y^+ = 15$. Near the wall the fine structure is very intermittent, and

tends to coincide with fluid having an axial velocity above the local mean. Except possibly near the wall, the structure functions demonstrate the existence of an inertial subrange for a separation range of about one decade.

ACKNOWLEDGEMENTS

The author would like to thank Dr. R.S. Azad who initiated the project and guided its progress throughout. The many hours of stimulating conversation with fellow students, Paul Okwuobi, Jim Reichert and Subash Arora were most helpful. Special thanks are due to my wife, Betty for her endless patience and continuing encouragement.

During the first three years of the work the author held a Post Industrial Experience Research (PIER) Fellowship in Engineering from the National Research Council of Canada. The financial assistance thus provided is gratefully acknowledged.

TABLE OF CONTENTS

LIST OF FIGURES

LIST OF TABLES

NOMENCLATURE

A	characteristic of large scale motion
A_1, A_2, τ_1, τ_2	parameters of envelope autocorrelation or spectrum
D_{LL}, D_{LLL}, D_{LLLL}	longitudinal structure functions
D_{NN}, D_{NNNN}	transverse structure functions
$E_1(k_1)$	one-dimensional energy spectrum
f	frequency
$F_{\Delta x}$	flatness factor of Δ_{xr}
$F_{\Delta y}$	flatness factor of Δ_{yr}
f_k	Kolmogoroff frequency
f_h	cut-off frequency of high-pass filter
f_e	cut-off frequency of low-pass filter
f_m	filter centre frequency $(f_e f_h)^{0.5}$
$f_{\varepsilon\varepsilon}(f)$	spectrum of $(\partial u/\partial t)^2$
$f_{\varepsilon\varepsilon}(k_1)$	wave-number spectrum of $(\partial u/\partial x)^2$
$I(t)$	two-state intermittency signal
k_1	longitudinal wave-number
L_f	transverse integral length scale
r	separation distance
R	radial distance, measured from centre line
R_{REF}	radius of diffuser at entry
Re	Reynolds number (based on centre line velocity and diameter at entry)

R_λ	turbulence Reynolds number
Station number	axial position in cms from diffuser exit, measured on centre line
S	skewness
$\bar{U}$	mean velocity in longitudinal direction
u'	rms velocity in longitudinal direction
U	instantaneous longitudinal velocity $(\bar{U} + u)$
$\overline{uv}$	correlation factor of u and v
$u_+v_+, u_+v_-, u_-v_+, u_-v_-$	truncated uv correlation factors
u^*	friction velocity
v'	rms velocity in transverse direction
v_k	Kolmogoroff velocity scale
x	longitudinal direction
y	transverse or radial direction
y^+	non-dimensional distance from the wall $(y_1 u^*/\nu)$
y_1	distance from wall
z	peripheral or lateral direction
Δ_{xr}	$u(x + r) - u(x)$
Δ_{yr}	$u(y + r) - u(y)$
Δ_f	filter bandwidth $(f_h - f_e)$
γ	intermittency factor
$\bar{\varepsilon}$	mean viscous dissipation
u	fluctuating velocity in longitudinal direction
v	fluctuating velocity in transverse direction
uv_c	any one of the truncated uv correlation factors

η	Kolmogoroff length scale
λ	Taylor microscale
μ	universal constant
ν	kinematic viscosity
ξ	fluctuating component of longitudinal vorticity
ξ'	rms value of ξ
τ_k	Kolmogoroff time scale

ABBREVIATIONS

PDF	probability density function
DIVM	digital integrating voltmeter
$\overline{\quad}$	overbar, denotes time average
db	decibels
rms	root mean square
kHz	kilohertz

1.0 INTRODUCTION

A conical diffuser is a fluid mechanical element often used in turbomachinery as a pressure recovery device. The diffuser flow is a developing axisymmetric (in the mean) flow with an adverse pressure gradient. Information on flows with adverse pressure gradient is generally meager and this work attempts to increase the knowledge of such flows.

For the present work an 8° included angle conical diffuser, with an area ratio of 4 to 1, and fully developed pipe flow at the inlet was utilized. Sovran and Klomp (1967) have shown that such a diffuser possesses optimum pressure recovery characteristics.

The most detailed work presently available on such a diffuser is given by Okwuobi and Azad (1973). They have reported data concerning mean velocities, turbulence intensities, the Reynolds stress tensor and a turbulent kinetic energy budget. They have postulated the existence of a "wall turbulent layer" extending from the wall to the point of maximum u'. In this region $\overline{u^2}$ was found to increase linearly with distance from the wall. A detailed literature survey of diffuser research up to that time was also given. Azad and Hummel (1971) have shown that for the same region (which they call the wall intermittent region) the fine

structure is very intermittent. The intermittency factor of $\frac{\partial^2 u}{\partial y \partial t}$ was found to approach zero close to the wall.

1.1 Turbulence Structure

The meaning of the word "structure" when used in the context of turbulent flow has been discussed by Morrison (1969). The following paragraphs are a review of that discussion and are included here in the interest of completeness.

When used in the context of turbulent flow the word structure has many connotations. Generally, it is used to refer to those characteristics which describe order in a flow situation which is not well ordered. It seeks to display the repetitive or predictable aspects of a flow situation which at first glance is apparently random.

Structure is commonly used to refer to order at many levels; to order of gross overall characteristics of the flow; to order in the distribution of the time averaged fluctuating variables as well as to order in distinguishable discrete phenomena. So called isotropic turbulence is completely devoid of structure because the velocity field is completely random in space and time*. Other flows, such as the vortex streets in the wake of a cylinder have a well defined structure because the velocity field is

* Corrsin suggests that "isotropic turbulence is well structured and its structure has been studied both theoretically and experimentally from 1935 up to today".

largely deterministic. In between these extremes lies a broad class of flows which are partially random and partially ordered. Diffuser flows belong to this class.

Flow variables can be measured or assessed by two methods; flow visualization and the use of transducers. Flow visualization uses a tracer such as smoke, dye or hydrogen bubbles to follow the flow. This provides a dynamic three-dimensional view of the flow field over a large volume simultaneously. The technique is most useful where the flow field is highly ordered such as near the wall in a boundary layer. While intuitively very appealing, the major disadvantages of the technique are that the results are very qualitative; the true statistical properties are often difficult and tedious to obtain.

More quantitative information on flow structure can be obtained with transducers such as hot-wires. While such transducers can measure the instantaneous velocity at a relatively small number of fixed points in space very accurately, it is often difficult to infer much about the turbulence structure without the results of flow visualization studies to serve as a guide.

Historically, turbulence research can be divided into an early era (up to 1955), and a modern era (from 1955) to the present. Measurements in the early period consisted

largely of,

a) The spacial distribution of averaged quantities such as mean velocity, and turbulence intensities. These have been used to separate flows into distinct regions in which different flow structures probably exist.

b) Turbulent energy and momentum balances.

c) Space-time correlations.

d) Spectra measurements.

While all of the above have been useful in providing some information concerning turbulence structures, the basic fact remains that they are all the result of long time averages which has a strong tendency to obscure the physics of the flow* More recently, (since 1955) modern flow visualization and conditional sampling techniques have intensified interest in shear flows, especially those with zero pressure gradient. In an attempt to quantify the qualitative picture provided by the visualization studies many investigators have proposed additional experiments expanding upon the conditional sampling techniques as well as other innovative methods for processing the hot wire signals.

* Corrsin points out that long time averages can be justified mathematically and physically.

1.2 Objectives

Diffuser research is an ongoing project at The University of Manitoba. The present work is essentially a continuation of the work of Okwuobi and Azad (1973). The same diffuser geometry and inlet flow conditions were used. Okwuobi and Azad restricted their experiments to the measurement of more "conventional" quantities such as mean velocities, turbulence intensities, etc. By using more advanced techniques the present work seeks to obtain more information not only on turbulence structure in a diffuser, but also on "laboratory" or "wind tunnel" turbulence in general.

The objectives of the work reported in this thesis may be characterized as follows:

a) A more advanced experimental investigation of diffuser flow with emphasis on the developing nature of the flow and its relationship to other wall-bounded flows.

b) Evidence for the existence of an inertial subrange in laboratory turbulence by measuring structure functions in a diffuser.

c) The development of a scheme to study the structure of bursts near a wall.

d) Advanced instrumentation development for modern turbulence research.

In the following section these objectives are discussed in greater detail.

1.2.1 The Developing Nature of Diffuser Flow - Its Relationship to Other Wall-Bounded Flows

The flow in a conical diffuser is a developing axisymmetric flow with adverse pressure gradient. Near the inlet it maintains many properties of the entering flow which, in this case, is fully developed pipe flow. Proceeding down stream the radial position of maximum shear stress and energy production move further away from the wall, remaining nearly at constant (inlet pipe) radius throughout. Thus proceeding down stream the maximum shear stress layer starts to attain some of the properties of a free shear layer since the maximum shear now takes place relatiyely far from a solid boundary. Further down stream the flow will separate from the wall if the diffuser is sufficiently long and with sufficiently large opening angle. An important objective of the present work was to investigate the developing nature of diffuser flow and to watch for any flow characteristics which may suggest that separation is imminent.

Consistent with boundary layer theory recent findings of the bursting pehnomena also divides the boundary layer into two zones, the inner zone ($y^+ < 40$) and the outer zone ($y^+ > 40$). Most of the turbulence production takes place in the inner zone; its innermost layer is the viscous sublayer. A more detailed discussion of this topic is given in Chapter 2. Following the work of Okwuobi and Azad (1973) and Azad and Hummel (1971), it was conjectured that perhaps the region in the diffuser between the maximum shear stress layer and the wall was in many ways similar to the inner region of a boundary layer. Boundary layer flows with near zero pressure gradients have been thoroughly investigated with the aid of flow visualization. This has lead to new experiments designed to corroborate and quantify the results of these visual observations. In the absence of a viable flow visualization experiment in the diffuser, an important objective was to repeat some of these experiments in diffuser flow and compare the results with those of boundary layer flows, already well documented in the literature.

1.2.2 On the Existence of an Inertial Subrange

For turbulent flows with sufficiently high Reynolds number, Kolmogoroff's (1941) origin theories predict power

law relationships for structure functions in the inertial subrange. Van Atta and Chen (1970) have verified the theory by measuring structure functions in the atmospheric boundary layer where the Reynolds number is very large. A major objective of the present work was to determine if the theories have any validity in laboratory flows where the Reynolds number is much smaller. In this case, the diffuser served as a convenient flow regime for an experimental examination of these theories.

1.2.3 Experiments Using an Envelope Detector

Following the discovery of the bursting phenomenon in a boundary layer by flow visualization techniques, several experiments have attempted to measure the mean time between bursts and related quantities by using hot wire anemometry. To date no consistent method has been given. A major objective of the present work was to study this important phenomenon by examining the properties of the envelope of narrow-band filtered signals. The results of this investigation are given in Chapter 7.

1.2.4 Instrumentation Development

The modern era of experimental turbulence research

depends largely on the development of new electronic devices and circuits. Because of their specialized nature and limited use, these circuits have not been commercially available. Accordingly, a major aim of the present work was to construct a number of these specialized circuits and to test them in diffuser flow.

2.0 THEORETICAL CONSIDERATIONS

As mentioned in the previous chapter, turbulence is neither a completely random, nor well ordered phenomenon; it therefore has structure, the subject of many theoretical and experimental investigations. Up to the present time there are no viable theories which completely describe real turbulent flows. A number of concepts, helpful in understanding the basic turbulence mechanisms, have however been developed. Of these, some of the more important will be discussed in the present chapter.

In 1941, Kolmogoroff postulated the important concept of local isotropic turbulence. The reasoning was that at sufficiently high Reynolds number, turbulence is generated at large scales which cascade to small scales with a small-scale structure independent of the large-scale structure.

A second important concept (often referred to as Kolmogoroff's modified theory) recognizes that the fine-scale (or dissipation) structure cannot be truly independent of the large-scale structure, and does in fact become spacially localized.

A third important development (due largely to modern flow visualization) has demonstrated that for shear flows

near a wall the large scale motion becomes more highly organized. Furthermore, the fine scale structure is more related to the large scale structure which thus becomes even more spacially localized.

2.1 Local Isotropic Turbulence

Monin and Yaglom (1975) have recently reviewed the postulates of Kolmogoroff (1941), and much of what follows is an abridgement of their work.

Kolmogoroff postulated that the largest disturbances in a developed flow have a length scale λ_1 which is of the same order as L_1 the length scale of the flow as a whole. These large fluctuations have amplitudes which are of the same order of magnitude as the change in the mean flow velocity over distance L_1. They draw their energy directly from the mean motion which affects all of their characteristics; i.e., the fluctuations are inhomogeneous and anisotropic almost to the extent that the mean-velocity field is inhomogeneous and anisotropic.

For an eddy of size λ_1 with velocity u_1, the time of emergence is $\lambda_1/u_1 = t_1$. Its energy is u_1^2. Therefore the energy converted per unit time is $u_1^2/t_1 = u_1^2 u_1/\lambda_1 = u_1^3/\lambda_1$. The dissipation equals ν x (velocity gradient)^2 $(= \nu\, u_1^2/\lambda_1^2)$. For an emerging eddy not to decline, it

is necessary that production be much larger than dissipation; i.e.,

$$\frac{u_1^3}{\lambda_1} >> \nu \frac{u_1^2}{\lambda_1^2} ,$$

or $$\frac{u_1 \lambda_1}{\nu} \equiv Re_1 >> 1 .$$

The Reynolds number Re_1 characterizes the large eddies and is usually several times smaller than the Reynolds number, UL_1/ν of the whole flow. Since it is still large these eddies are unstable, breaking down into eddies with length scale λ_2 and velocity scale u_2, characterized by Reynolds number Re_2 which is smaller than Re_1, but nevertheless still large. These eddies in turn break down into eddies with Reynolds number Re_3 and so on. This process terminates when length and velocity scales λ_n and u_n are reached such that,

$$Re_n = \frac{\lambda_n u_n}{\nu} = 1 .$$

These small eddies are hydrodynamically stable because viscosity has now become important. Their energy is

converted directly into heat in overcoming the frictional forces.

For eddies with high Reynolds number the effect of viscosity is unimportant and very little direct energy dissipation takes place. Since developed turbulence is accompanied by dissipation of kinetic energy, it can only be maintained by a continuous supply of energy from some external source. When a disturbance of length scale λ_n decays to length scale λ_{n+1}, the new disturbance has components not only along the direction of the original motion but also in all other directions. This is caused by the pressure fluctuations. Thus the directional effect of the mean motion is lost in the small eddies, which will tend to be statistically isotropic. Turbulence with this property is said to exhibit "local isotropy".

2.1.1 Kolmogoroff's Original (1941) Theories

If L is a typical length scale of the energy-containing eddies, then a necessary condition for the existence of local isotropy is that there exist disturbances with wavenumber k, much greater than 1/L. Kolmogoroff's (1941) first hypothesis states that for $k >> 1/L$, the turbulence is specified statistically by a single flow parameter (the

dissipation rate $\bar{\varepsilon}$) and a single fluid parameter (the kinematic viscosity ν). From these can be formed, using dimensional analysis the Kolmogoroff velocity, length and time scales given by,

$$v_k = (\nu\bar{\varepsilon})^{1/4} ,$$

$$\eta = (\nu^3/\bar{\varepsilon})^{1/4} ,$$

$$\tau_k = (\nu/\bar{\varepsilon})^{1/2} .$$

This wavenumber region is referred to as the quasi-equilibrium range. Kolmogoroff (1941) further postulated, as a second hypothesis that if there exists a range of disturbances with wavenumber k such that

$$\eta << 1/k << L ,$$

then for these disturbances the predominant activity is the inertial transfer of energy with little energy production or dissipation. Therefore the statistical properties should not depend on ν and therefore only on $\bar{\varepsilon}$. This subrange of the quasi-equilibrium range is called the inertial subrange.

2.1.2 Structure Functions

To test the validity of the hypothesis of Kolmogoroff

it is useful to introduce the concepts (as Kolmogoroff did) of structure functions of various order. These are essentially mean-values of various powers of velocity differences measured at two points in space separated by a distance r. The power defines the order of the structure function.

From the theories of isotropic (and locally isotropic) turbulence it follows that only two types, longitudinal and transverse structure functions, need be considered. These are $\overline{[u_L(x) - u_L(x + r)]^n}$, the nth order longitudinal structure function and $\overline{[u_N(x) - u_N(x + r)]^n}$, the nth order transverse structure function. u_N and u_L are velocity components perpendicular and parallel, to r respectively

Kolmogoroff reasoned that in the inertial subrange ($\eta << r << L$) the structure function can depend only on the separation r and $\bar{\varepsilon}$. Thus by dimensional reasoning

$$\overline{[u(x) - u(x + r)]^n} = C_n (\bar{\varepsilon} r)^{n/3},$$

where C_n is a constant.

Thus the relevent structure functions up to the fourth order become,

$$D_{LL}(r) = C_1 (\bar{\varepsilon} r)^{2/3}$$
$$D_{NN}(r) = C_2 (\bar{\varepsilon} r)^{2/3}$$
$$D_{LLL}(r) = C_3 \bar{\varepsilon} r$$
$$D_{NNNN}(r) = C_4 (\bar{\varepsilon} r)^{4/3}$$
$$D_{LLLL}(r) = C_5 (\bar{\varepsilon} r)^{4/3}$$

where C_1, C_2, C_3, C_4 and C_5 are constants .

The previous results on the statistical properties of locally isotropic turbulence were obtained strictly by dimensional reasoning and did not require the use of any fluid dynamic equations such as the Navier-Stokes equations. However, it does not follow that the dynamic equations are useless for studying local structure as they can be used to extend the predictions based on dimensionality. A useful equation is due to Kolmogoroff (1941) and named after him. This equation, which can be derived from the Navier-Stokes equations with the Karman-Howarth equation as an intermediate step, is

$$D_{LLL}(r) - 6\nu \frac{d}{dr} D_{LL}(r) = -\frac{4}{5} \bar{\varepsilon} r .$$

It relates the second and third order longitudinal structure functions, and is valid only in the quasi-equilibrium range. In the inertial subrange where viscosity is unimportant, the second term on the left-hand side can be neglected. Thus

$$D_{LLL}(r) = -0.8\,\bar{\varepsilon}\,r \quad , \quad \eta \lesssim r \lesssim L \quad ,$$

which gives a specific form for the third-order longitudinal structure function.

2.1.3 The One-Dimensional Energy Spectrum

The one dimensional energy spectrum $E_1(k_1)$ is defined such that

$$\int_0^\infty E_1(k_1)dk_1 = u'^2.$$

Thus dimensionally,

$$[E_1(k_1)] = \left[\frac{u'^2}{k_1}\right] \quad .$$

In the inertial subrange according to Kolmogoroff (1941), E(k) can depend only on k and $\bar{\varepsilon}$ from which it follows by dimensional reasoning and mathematical manipulation that,

$$E_1(k_1) = C_1\,\bar{\varepsilon}^{2/3}\,k_1^{-5/3}, \quad \eta \lesssim \frac{1}{k_1} \lesssim L$$

where C_1 is a constant

This is the important 'five-thirds law' often used to test for the existence of an inertial subrange.

2.1.4 Skewness of the Longitudinal Structure Function

According to Kolmogoroff (1941) this skewness, S $(= D_{LLL}(r)/D_{LL}(r)^{2/3})$, should depend only on $\bar{\varepsilon}$ and r in the inertial subrange. Since it is impossible to construct a non-dimensional group from the two quantities that make up the skewness, it is concluded that,

$$S = \text{constant}, \qquad \eta << r << L$$

This result provides a further test for the existence and extent of the inertial subrange.

2.2 Kolmogoroff's Modified Theory

Immediately, following the formulation of Kolmogoroff's (1941) original theories a critical remark was made by Landau concerning the effect of fluctuations in the energy dissipation rate on the small scale properties of turbulence. The original theories assumed that the energy transfer $\bar{\varepsilon}$, to small scale disturbances was the same throughout and the statistical properties of the small scale structure depended only on $\bar{\varepsilon}$. In fact, however, the statistical characteristics of the instantaneous dissipation,

$$\varepsilon = .5\ \nu \sum_{i,j} \left(\frac{\partial u_i}{\partial x_j} + \frac{\partial u_j}{\partial x_i}\right)^2 \qquad 2.1$$

may depend on properties of the large scale motion. Thus it is expected that the dispersion of the dissipation will depend on a large scale property, Reynolds number. Accordingly, Kolmogoroff (1962) modified his original theories as outlined in the following discussion.

Let ε_r be the rate of dissipation of turbulent energy averaged over a fixed volume of linear dimension r. With large Reynolds number and $r << L$ where L is a large eddy length scale, Kolmogoroff postulated that ε_r has a log-arithmically normal distribution with dispersion,

$$\sigma = A + \mu \ln \left(\frac{L}{r}\right) , \qquad 2.2$$

where - A is a characteristic of the large scale motion,

- μ is a universal constant.

Gurvich and Yaglom (1967) provided a model which attempts to explain the log-normal hypothesis described above. By using a form of cascade process and the central-limit theorem, they concluded that any positive fine structure quantity has a log-normal distribution.

The log-normal hypothesis has a number of important consequences, some of which are discussed in the following sections.

2.2.1 The Spectrum of $(\partial u/\partial t)^2$

15 ν $(\partial u/\partial x)^2$ is often used as an estimate for dissipation. This result is obtained from equation 2.1, and the assumption of local isotropy (Tennekes and Lumley, 1972). With $f_{\varepsilon\varepsilon}(k_1)$ the wavenumber spectrum of $(\partial u/\partial x)^2$, Novikov (1965) was able to show that under the original assumptions of Kolmogoroff (1941), this spectrum should have been constant, i.e., the spectrum of white noise. Experiments for example by Pond and Steward (1965) indicate the spectrum to be more of the form,

$$f_{\varepsilon\varepsilon}(k_1) \approx k_1^{-0.6}$$

in the inertial subrange. Gurvich and Yaglom (1967) have shown from theoretical considerations that

$$f_{\varepsilon\varepsilon}(k_1) \approx k_1^{\mu-1}$$

in the inertial subrange; μ is the universal constant in equation 2.2. By using Taylor's hypothesis this equation can be written

$$f_{\varepsilon\varepsilon}(f) \approx f^{\mu-1},$$

where f is frequency and $f_{\varepsilon\varepsilon}(f)$ is the frequency spectrum of $(\partial u/\partial t)^2$. This spectrum is readily measured and the result can be used to estimate μ.

2.2.2 The Relationship of $\partial u/\partial x$ to R_λ

According to the modified theory the statistical properties of the dissipation field ε, depend on the large scale motion, namely the Reynolds number Re_L (= UL/ν) which is proportional to R_λ^2 (Tennekes and Lumley 1972). A useful expression relating the non-dimensional moments of $\partial u/\partial x$ to R_λ is given by (Monin and Yaglom 1975).

$$\frac{\overline{\left(\frac{\partial u}{\partial x}\right)^n}}{\overline{\left(\frac{\partial u}{\partial x}\right)^2}^{n/2}} = R_\lambda^{3\mu n(n-2)/16}$$

where n is a positive integer.
For $n = 4$, it states that the flatness factor of $\partial u/\partial x$ equals $R_\lambda^{(3/2)\mu}$.

2.2.3 Spacial Localization of Fine Structure

An important consequence of the modified theory is that the fine structure tends to be spacially localized. Thus fine structure (or high frequency) signals derived from hot wires fixed in space will be very intermittent.

A large number of experiments have been performed to show the highly non-gaussian nature of the small scale

turbulence component. An often-used test is to measure the flatness factor (FF) of the time derivative $\frac{\partial^n u}{\partial t^n}$ (where n is usually 1 or 2) and observe how the FF differs from 3, the gaussian value. This difference is known as the excess. Batchelor and Townsend (1949) found the FF's of $\frac{\partial^n u_1}{\partial t^n}$ measured in grid generated turbulence to increase with n, indicating increased deviation from normality with increased wavenumber.

To explain the intermittent nature of the fine structure, a number of models have been proposed. Of particular interest is a model proposed by Corrsin (1962) and later modified by Tennekes (1968). By assuming the dissipation to be concentrated in vortex tubes, Tennekes predicted skewness and flatness factor values for velocity derivatives along with their Reynolds number dependence. Kuo and Corrsin (1971) measured flatness factors of narrow-band filtered signals and found them to increase sharply in the dissipation region. This increased flatness factor is often used as an indicator of increased spacial localization. They also found,

a) that the FF of $\partial u/\partial x$ (a fine scale quantity) increased with turbulence Reynolds number, R_λ.

b) fine structure quantities (such as $\partial u/\partial x$) have an approximate log-normal distribution in limited agreement with Kolmogoroff's (1962) hypothesis.

2.3 Coherent Structures in Wall Bounded Shear Flows

The study of wall bounded shear flows, or boundary layer flows has been given new impetus in the last two decades by the use of flow visualization techniques. A major conclusion of these studies is that turbulent motion near a solid boundary is not completely random, but proceeds in a semi-organized and partially predictable manner; hence the name, coherent structures.

In analyzing boundary-layer flows, it is often convenient to partition the regions near the wall into layers. The extent of each layer is usually indicated in terms of the non-dimensional viscous length y^+ $(= \frac{yu^*}{\mu})$ where y is the distance from the wall.

The inner layer $(0 < y^+ < 40)$ consists of the viscous sublayer $(0 < y^+ < 5)$ and the buffer layer $(5 < y^+ < 40)$. The outer layer $(y^+ > 40)$ consists of the log layer followed by the wake region which is furthest from the wall. For a pipe flow, the outer region is also referred to as the core region.

The viscous sublayer is dominated by its proximity to the wall which guarantees zero mean velocity at the wall (no slip condition). Shear stresses in this region are predominantly viscous, the Reynolds stresses being very small.

The mean velocity profile is linear with distance from the wall.

The inner part of the outer layer, starting from a y^+ value of 40 up to the law of the wake is often referred to as the log layer because its mean velocity profile is logarithmic. In this layer the effect of the wall is not dominant and most of the shear stress is due to Reynolds stress, which is essentially constant across the layer. Hence, the names constant shear layer, and inertial sublayer are also used when discussing this region. Between the viscous sublayer and the log layer is a region which characterizes a transition from viscous shear stress to inertial shear stress, appropriately called the buffer layer.

The wake region, which actually consists of the largest part of the boundary layer does not exist in fully developed pipe flows or diffuser flow as considered in the present work. Therefore it will not be considered further.

Detailed flow visualization studies in boundary layers have been conducted by essentially two different experimental groups, the Stanford group led by Kline, and the Ohio-Göttingen groups led by Brodkey. The essential results of the Stanford group have been summarized by

Kim et al (1971). Near the wall in the viscous sublayer, they observed low speed streaks consisting of alternating regions of high and low (axial) momentum fluid which were very much elongated in their streamwise extent* The low speed streaks were seen to slowly lift away from the wall, begin a growing oscillation (often accompanied by a streamwise vortex motion) and finally to break up into more chaotic motion. This whole cycle they termed bursting and they concluded that essentially all of the turbulence production occurs during the burst cycle.

A somewhat different sequence of events is described by Nychas et. al. (1973) in a paper summarizing the results of Brodkey and his co-workers. According to them, the main sequence of events began with a local deceleration of the flow over a relatively large extent near the wall. From further upstream a large scale fluid mass with higher velocity began to accelerate the decelerated fluid. Between the accelerated and decelerated fluid were regions of intense local shear. Immediately after the acceleration began, there occurred an ejection of fluid from the decelerated region outward from the wall, followed finally by the higher speed fluid sweeping the field of the low speed fluid. Transverse vortices appeared as the result of a Helmholz-type of instability at the interface between

* Sublayer streakiness was originally observed by Hama whose observations were reported by Corrsin in Proc. First U.S. Naval Hydrodynamics Sympos., 1957.

the high speed and low speed fluid.

There is general agreement among the two experimental groups that the different observations are due to the different visualization techniques used, and do not indicate different physical phenomena. Be that as it may, the visual observations have spawned many new hot-wire experiments, some of which have been repeated in the present work in the hope of a better understanding of the structure of turbulence in a diffuser.

3.0 FLOW FACILITY, PROCEDURE, AND SPECIALIZED INSTRUMENTATION

3.1 Flow Specification - Wind Tunnel, Diffuser and Traversing Mechanism

The low speed open circuit wind tunnel, diffuser and traversing mechanism have been described by Azad and Hummel (1971) and Okwuobi and Azad (1973). Seventy-eight diameters of straight pipe separated the contraction cone from the inlet of the diffuser which was machined from cast aluminum. Reichert and Azad (1976) have shown that the pipe flow is fully developed upstream from the diffuser inlet, but is somewhat modified at the diffuser inlet due to the diffuser itself. Figure 3.1 shows the diffuser geometry. Station numbers, identifying position in the x direction correspond to the x position measured (in cm) from the diffuser outlet. Position in the radial (transverse, or y) direction is specified by the non-dimensional length R/R_{REF} where R is the position, measured from the centre line and R_{REF}, is the radius of the pipe (5.08 cm). The probes were mounted on a tube entering the diffuser from the down stream end. This could be rotated on its axis, slid in and out (in the x direction) and positioned in the y direction with a micrometer graduated in 0.001 inches. The overall mechanical structure of the traversing mechanism (Figure 3.2) was sufficiently robust to minimize probe

vibration without unduly blocking the flow. The Reynolds number of the flow was varied by changing the fan speed and observing the pressure across the contraction cone which was calibrated in terms of velocity at the diffuser inlet. Okwuobi and Azad (1973), by using forward and reverse-facing pitot tubes, have also shown that the flow in the diffuser does not separate.

3.2 Hot Wires, Anemometers, and Linearizers

Standard DISA hot-wire equipment included two constant-temperature anemometers 55M01, two 55D10 linearizers, two 55D35 RMS voltmeters and a 55D31 digital voltmeter. To measure the transverse structure functions, 6 different hot wire assemblies (custom made by DISA) were used, each consisting of two independent hot wires with its own anemometer and linearizer. Wire separations (in the transverse direction) were 1, 2, 4, 6, 8 and 10 mm. The platinum-plated tungsten wires were 5 microns in diameter with an effective length of 0.8 mm. An overheat ratio of 0.8 was used. Measurements involving only one hot wire were taken with one of the two wires of the 10 mm probe. The X-probe was a DISA type 55A38. Linearization was done with the probes on the center line at station 75 where the actual velocity was known from a pitot tube calibration.

The four-wire probe for measuring the streamwise component of vorticity was custom made by DISA and is similar to one described by Kistler (1952). Mechanical and calibration details are given in Appendix A.

3.3 Measurement of Mean Quantities

Accurate averages of quantities fluctuating in time are difficult to obtain when these averages are small (possibly only a few millivolts) but the fluctuations are intermittent and very large (up to $\pm$ 10 volts). Time averaging by conventional analogue methods thus becomes long, tedious and often inaccurate. In an attempt to overcome this problem, a true digital integrating voltmeter (DIVM) was constructed. It consisted of a voltage controlled oscillator with oscillation frequency proportional to the input voltage. Thus counting these oscillations over a preset time interval in effect integrates the input voltage, and the total count serves as a minimum variance unbiased estimator for the time average; i.e., for the given preset time no other averaging technique can give a "better" average.

3.4 Probability Distribution and Density Measurement

Figure 3.3 shows a block diagram of a circuit designed to plot both ordinary and conditional probability distributions and densities with an xy plotter. When used in the probability density mode, the window width was 4% and no attempt was made to correct the results for the small error incurred by these finite window widths. For a proper probability density function, (PDF) the area must equal unity. A numerical technique for normalizing the PDF's is given in Appendix B.

3.5 Skewness and Flatness Factor Measurement

The skewness S, and the flatness factor FF, of a random variable $e(t)$, with probability density $P(e)$, are defined by,

$$S = \overline{e^3}/(\overline{e^2})^{3/2}$$

$$FF = \overline{e^4}/(\overline{e^2})^2$$

where t indicates time and the overbar indicates time average.

Figure 3.4 is a block diagram of the circuit used. The multiplier was specially selected from a group of six as follows. A 1 kHz sine wave was filtered by a low pass four-pole Butterworth filter set to 950 Hz. This removed

any harmonics from the sine wave making it essentially pure; i.e., with zero skewness or very nearly so. Using this as the signal e (with a peak-to-peak value of 20 volts) the multiplier with the smallest $\overline{e^3}/100$ value was selected. The fourth power was obtained from the second using four thermocouples, a technique suggested by Kuo and Corrsin (1971). The four thermocouples have their inputs connected in parallel and their outputs in series (to give a larger output voltage). This technique helps neutralize the different characteristics of the individual thermocouples. Because the output of a thermocouple is very small, a chopper stabilized amplifier was used. These have very small input offset voltages and temperature drift.

The flatness factor circuit was tested by using a chopped gaussian white-noise signal with variable but known duty cycle, γ. For such a signal γ x flatness factor = 3. The measured results fit this theoretical relationship well for flatness factor values up to about 70 as shown in Figure 3.5. For all measurements the amplitude of the input signal e was adjusted so that the largest excursions of e just reached the saturation level ($\pm$ 10 volts) as observed on an oscilloscope. Simultaneous measurement of $\overline{e^4}/1000$ (or $\overline{e^3}/100$) with the DIVM, and the normalizing quantity $\overline{e^2}/10$ with a DISA 55D31 voltmeter,

(on 100 second-time constant) give more consistent results than separate time-sequential measurements with the DIVM. This technique was therefore universally adopted.

Following Kuo and Corrsin (1971), the FF of the narrow-band filtered signals were tested for variation with band-width. It was verified that minimum bandwidth $\Delta f/f_m$ on the Kron-Hite (KH) Model 3700 filters gave near maximum FF. $(\Delta f/f_m)_{min}$ was measured to be 0.43, where $\Delta f = f_h - f_e$; $f_m = (f_h\ f_e)^{1/2}$; and f_h and f_e are the upper and lower 3 db points of the bandpass filters respectively.

3.6 Spectra Measurement

All spectra were measured with the Kron-Hite Model 3700 filters on the smallest bandwidth, $(\Delta f/f_m = 0.43)$. Nearly identical results were obtained when measuring the same spectrum with both a KH 3700 filter and an HP 3590A spectrum analyzer with a bandwidth of 10 Hz. From these measurements it was concluded that the relatively large bandwidth of the KH 3700 filter did little to adversely distort the shape of the spectrum.

3.7 Truncated uv Correlation Measurement

Figure 3.6 shows a block diagram of the circuit used.

The two truncating circuits are identical to those described by Wallace et al (1972). The non-truncated uy correlation was found to equal the algebraic sum of the truncated components within 5%.

3.8 An Envelope Detector Circuit

A circuit was designed to generate the envelope of a narrow-band filtered signal (which generally has the appearance of a slowly varying amplitude-modulated sine wave).

For the present purposes the envelope was defined as that signal whose instantaneous value equals the absolute value of the most recent peak of the input signal. A typical pulse sequence and block diagram for the envelope detector are given in Figure 3.7. Each time the absolute value of the input reaches a maximum, a sampling gate pulse is generated which samples the input. This sample value is then held until the next maximum and so on. The output of the hold-circuit thus forms the required envelope.

3.9 Intermittency Measurement

A circuit was constructed to measure the intermittency of the time derivative of a signal, and also the intermittency of the envelope of a signal. Figure 3.8 shows a

block diagram of the experimental set-up. The intermittency circuit proper (similar to that described by Kuo and Corrsin, 1971) consisted of two level detectors separated by a low pass filter. The two levels and the low pass filter were adjusted by comparing the ON-OFF output signal I(t), with the input to the first level detector on a dual-beam storage oscilloscope. The intermittency factor γ, was then readily measured using the digital integrating voltmeter.

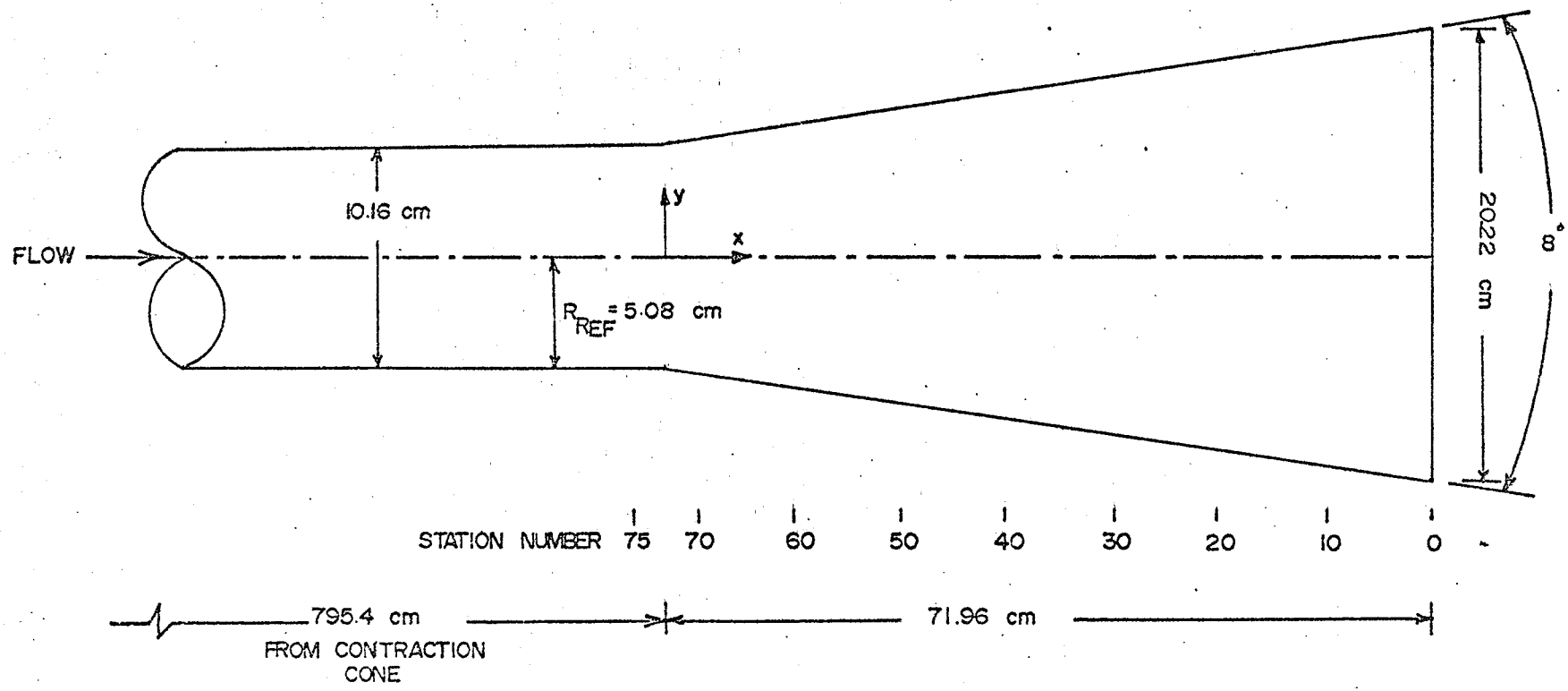

Figure 3.1 Diffuser Geometry

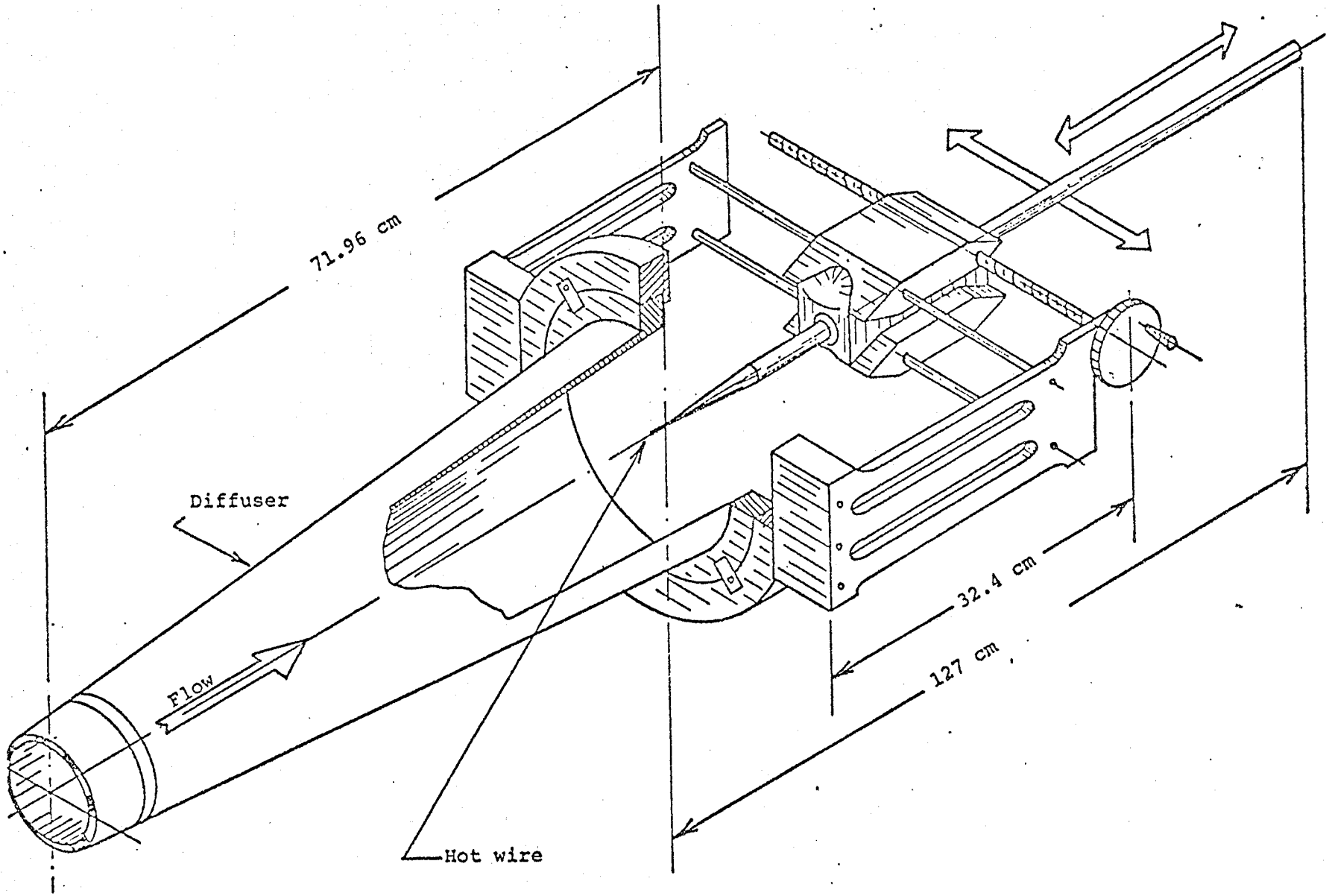

Figure 3.2 Diffuser Traversing Mechanism

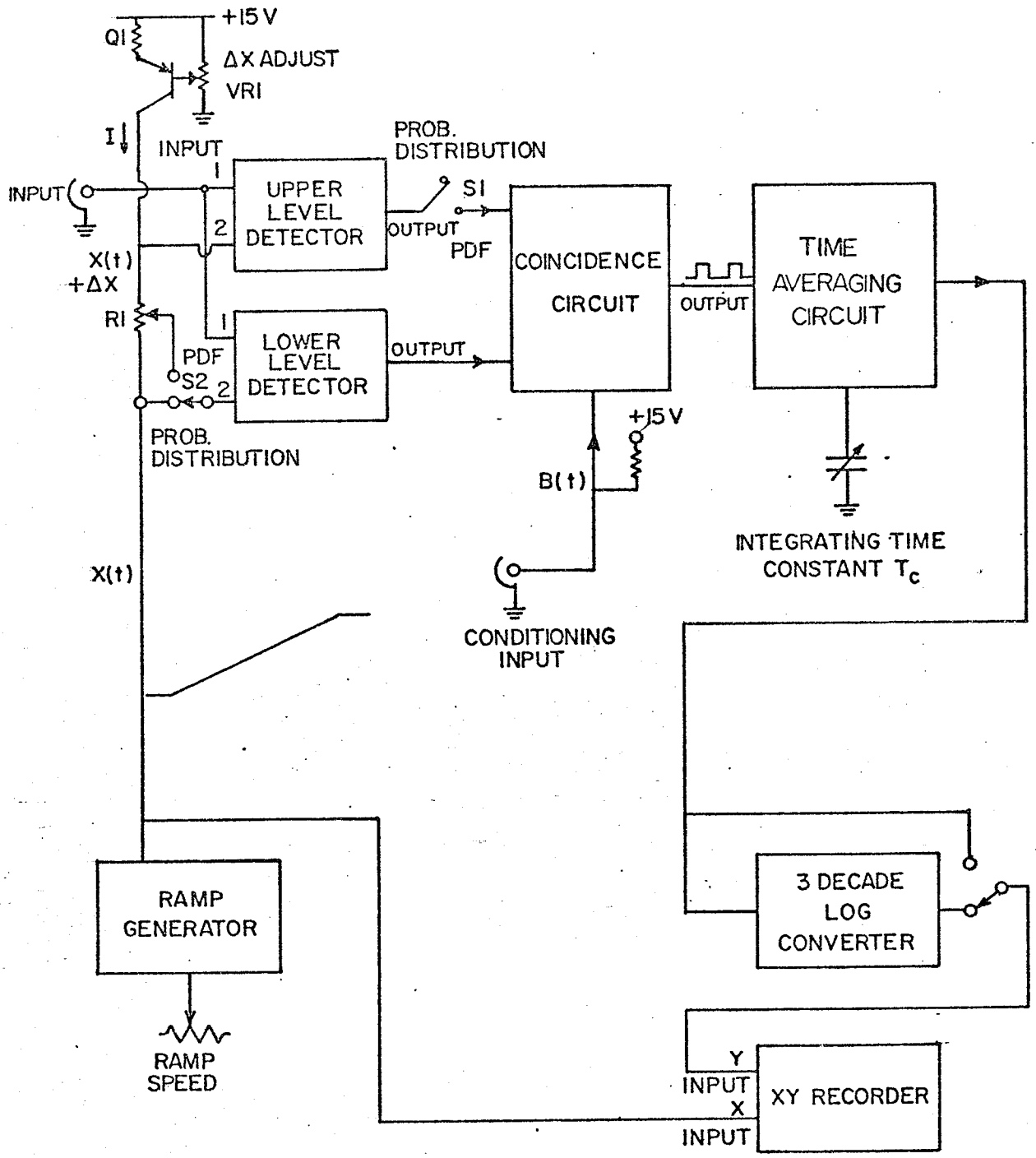

Figure 3.3 Block Diagram - Probability Density Analyzer

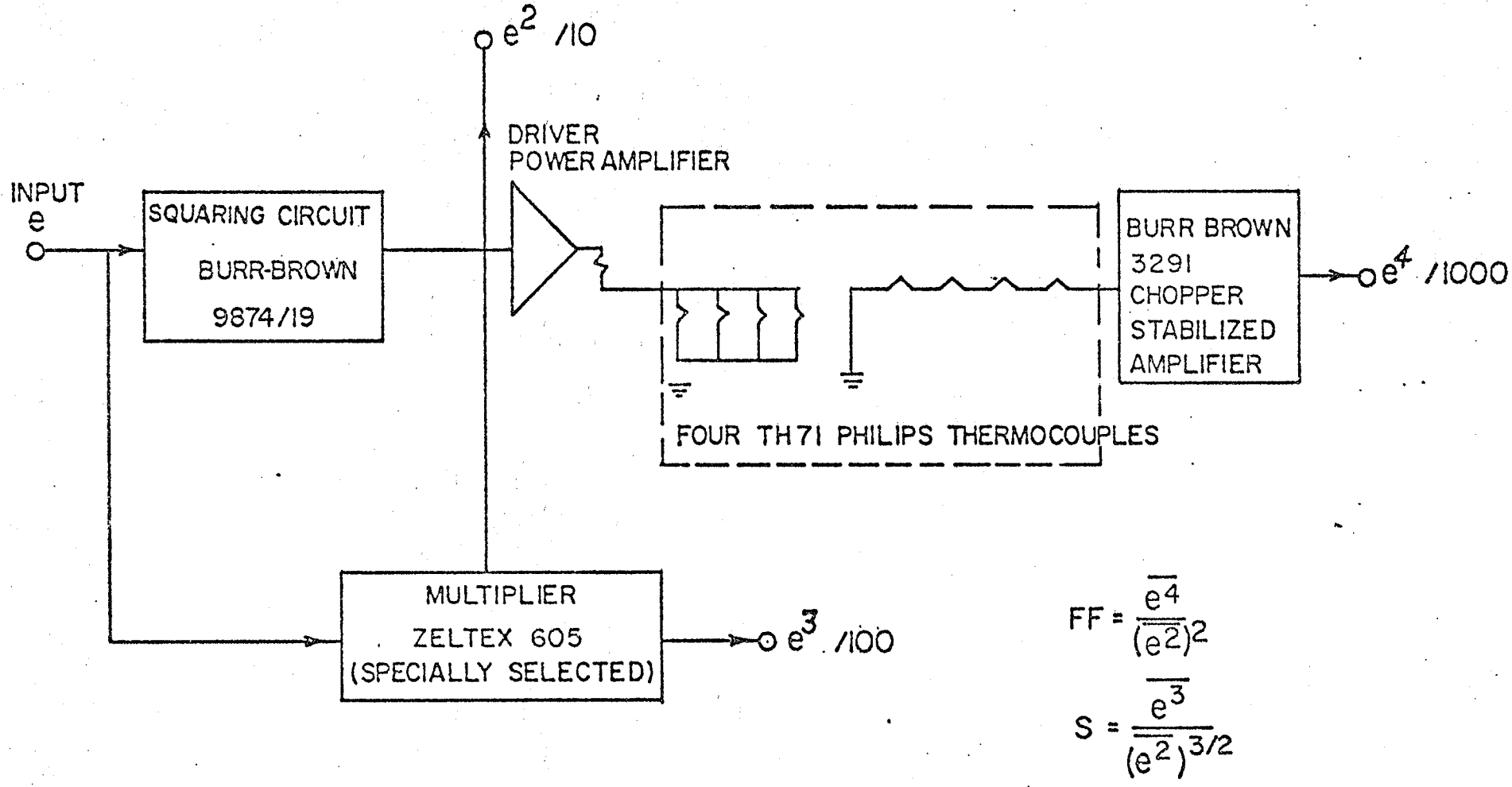

Figure 3.4 Circuit for Measuring Skewness and Flatness Factor

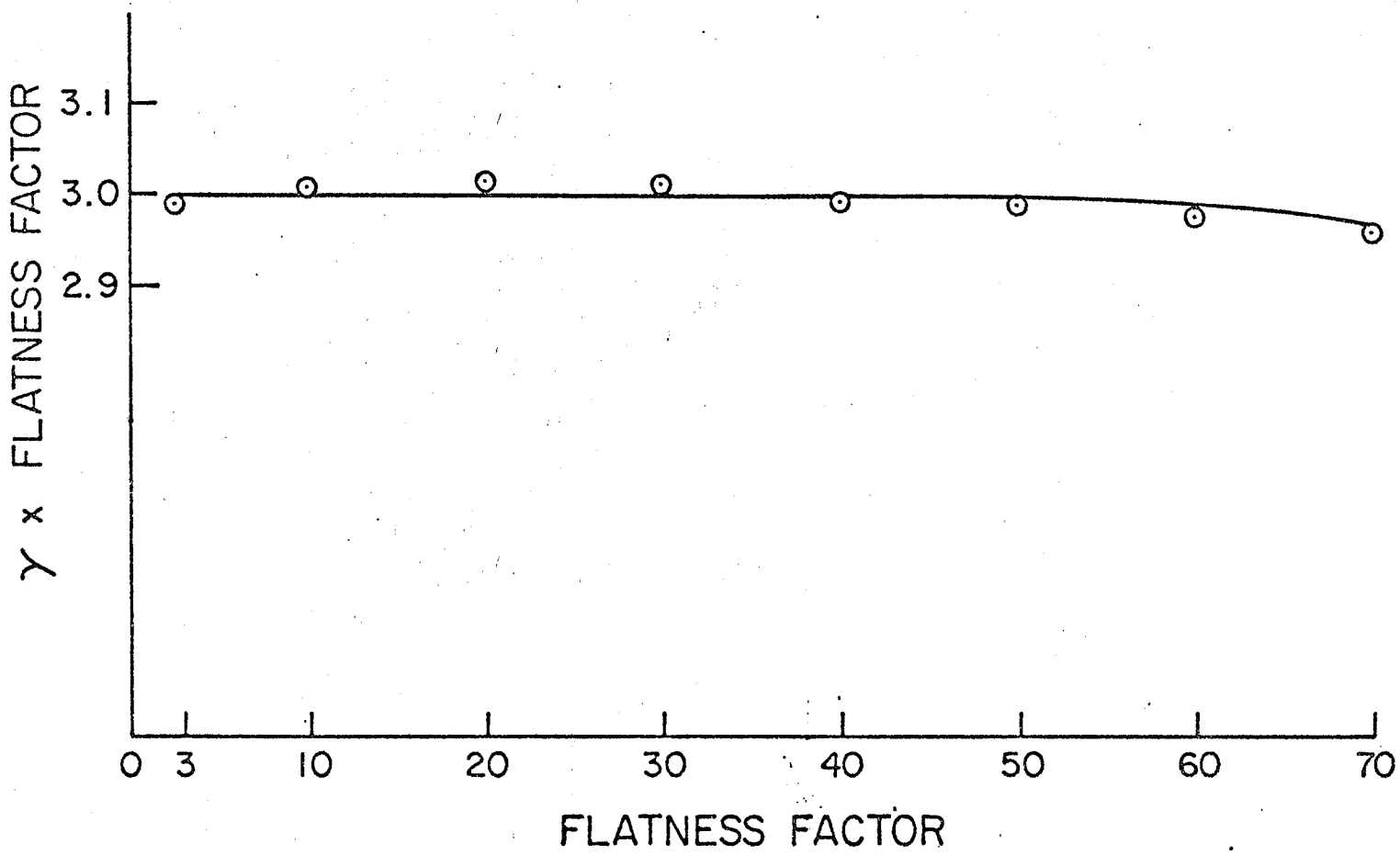

Figure 3.5 γ. Flatness Factor VS. Flatness Factor for Chopped Gaussian Signal.

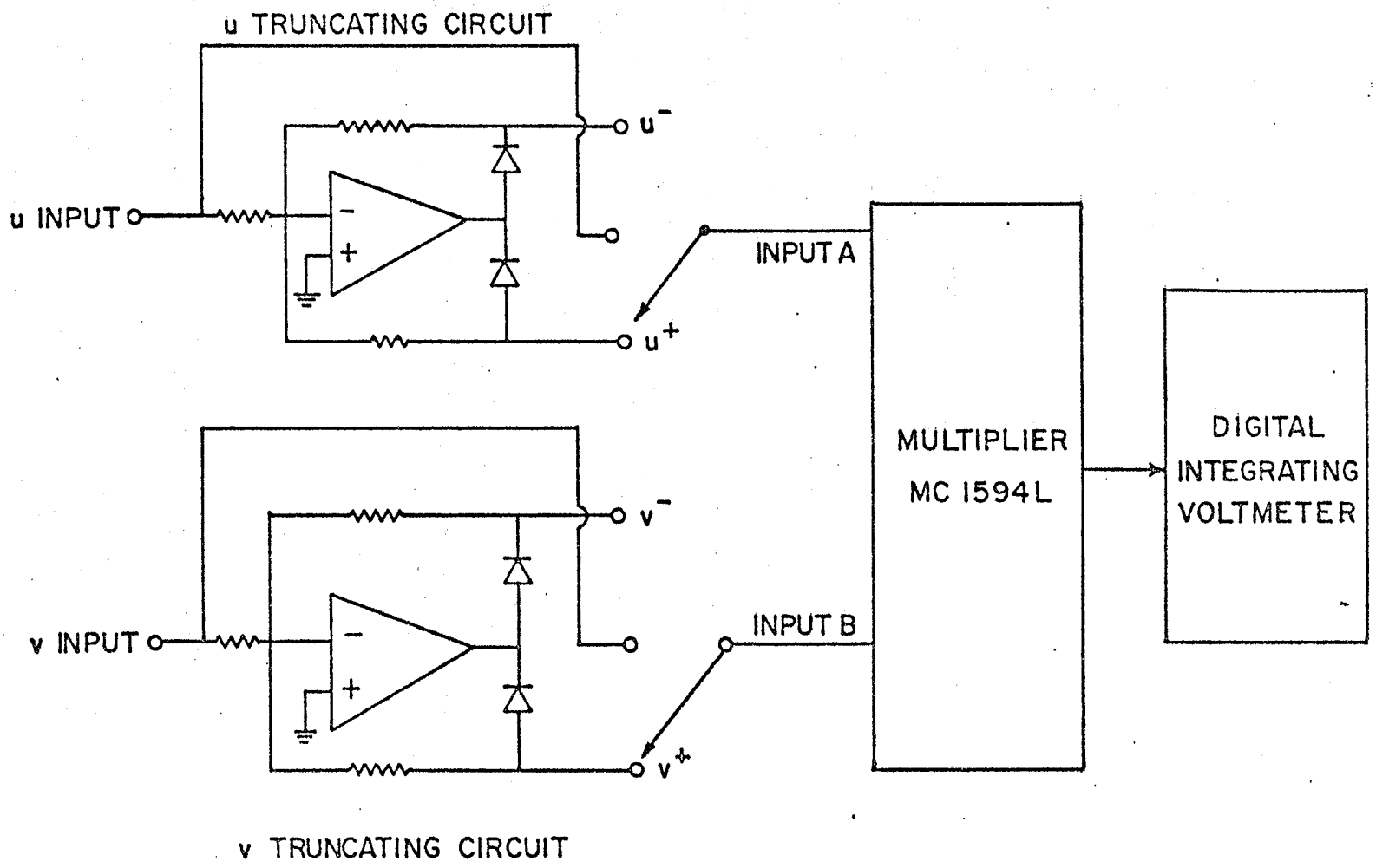

Figure 3.6 Circuit for Measuring Truncated uv Correlations

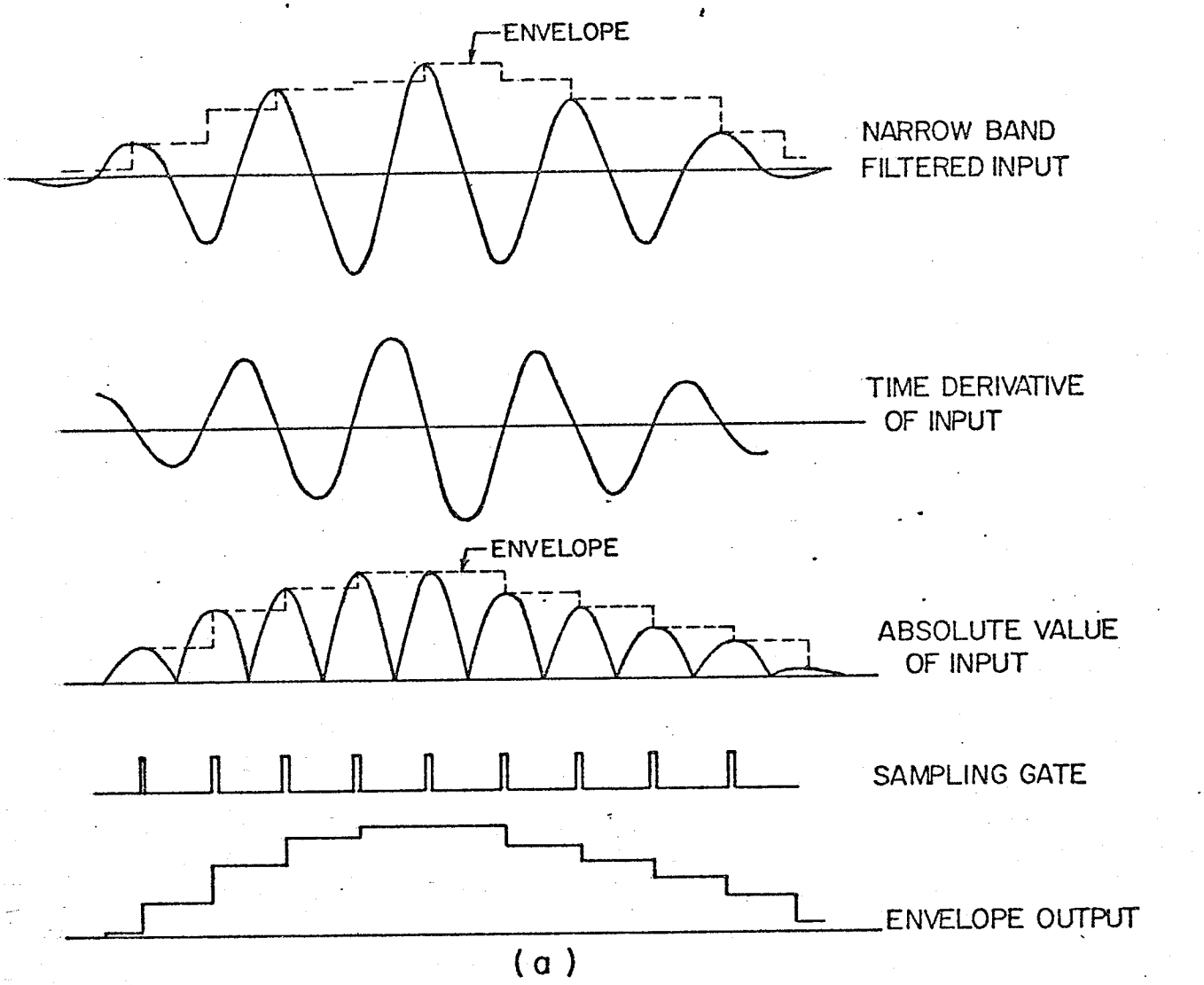

Figure 3.7 Envelope Detector (a) Wave Shapes
(b) Block Diagram

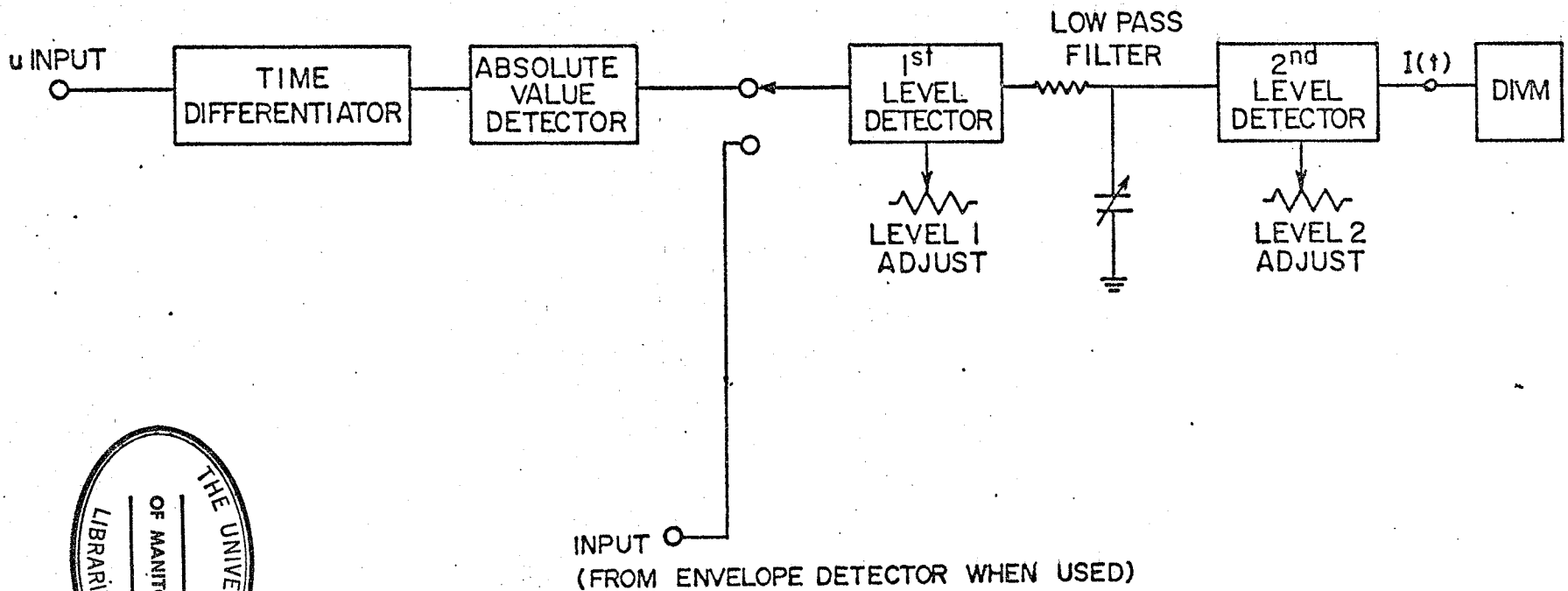

THE UNIVERSITY OF MANITOBA LIBRARIES

Figure 3.8 Block Diagram of Intermittency Detector

4.0 PRELIMINARY EXPERIMENTS

Since a rather large number of experiments were planned it was decided at the outset to perform most of these at a single axial position which should be representative of diffuser flow*. To find the desired axial position and to obtain more information on the developing nature of the flow, some statistical properties of U were measured at several stations. These results are given in the present chapter with the more extensive measurements at a single station given in subsequent chapters.

4.1 Probability Density Measurements

Using the circuit of Figure 3.3, probability densities (PDF's) of U were measured at various stations for Re = 137,000 (based on the centre line velocity at station 75 and a pipe diameter of 10.16 cm). These were "faired", normalized, (as discussed in Appendix B) and

*It has been recognized that the flow is developing in the downstream direction and no single axial position is truly representative of "developing" diffuser flow.

replotted by computer. A general feature of all the results, shown in Figures 4.1 to 4.7 is that the PDF's are negatively skewed toward the centre line and positively skewed toward the wall. At stations 75, 65 and 55 no measurements were taken sufficiently close to the wall to show positive skewness.

Figure 4.5 shows the results at station 30, considered for the moment as a typical station. The negative skewness of the PDF's toward the centre line is attributed to the intermittent ejection of low momentum fluid away from the wall region. Moving away from the centre line at R/R_{REF} = 1.03 the distribution becomes symmetric;* i.e., the skewness is zero but the turbulence intensity is very large with the flatness factor less than 3. This point corresponds approximately to the point of maximum shear stress in Okwuobi and Azad (1973). It is also the farthest point from the wall where the velocity, U, is sometimes zero. Moving closer to the wall the skewness becomes positive with an increase in flatness factor. While undoubtedly some of the positive skewness is due to the intermittent flow of high momentum fluid toward the wall, a substantial part may also be due to the action of the hot wire itself which is insensitive to flow direction for flow components

* By interpolation of the results in Fig. 4.5.

normal to the wire. Thus wallward, from $R/R_{REF} = 1.03$ the flow is occasionally flowing upstream since one must suppose the flow to be sometimes negative if it is sometimes zero. This was verified at the wall by gluing very fine threads there and observing that they "sometimes" pointed in the upstream direction. This effect became more pronounced closer to the diffuser exit.

4.2 Skewness and Flatness Factor Measurements

While these quantities could be obtained from the PDF's discussed in the previous section, they were measured directly using the circuit in Figure 3.4. To show Reynolds number similarity, measurements were made for both Re = 137,000 and 340,000. Detailed results for the higher Reynolds number are shown for various stations in Figures 4.8 to 4.11.

Figure 4.10 shows the results for both Reynolds numbers at station 30. Here the flatness factor shows negligible Reynolds number dependence; the skewness values are however, slightly lower at the higher Reynolds number. The results thus confirm, that for large values of Reynolds number as used here, the actual value of the Reynolds number plays only a secondary role in determining

the overall turbulence structure; i.e., the flow displays Reynolds number similarity.

Figures 4.13a,b show contours of iso-skewness and flatness factor respectively throughout the diffuser. At the inlet (fully developed pipe flow) the skewness is negative, (except possibly very close to the wall where no measurements were taken) and decreases gradually in magnitude toward the wall (Figure 4.8). The most negative value is at ($R/R_{REF} \approx 0.2$) where it remains in the down stream direction to about station 45. Proceeding down stream from station 45 this ridge of maximum negative skewness first moves slightly away from the centre line which it subsequently approaches and touches at station 5. Below station 5 the ridge again diverges from the centre line. In the region down stream from station 35 the ridge is more prominent and is coincident with a ridge of maximum flatness factor (Figure 4.13b). The words "maximum" and "minimum" as used in this discussion refer to a given axial position.

Throughout the entire length of the diffuser there is also a contour of zero skewness accompanied by a valley of minimum flatness factor at approximately the pipe radius. The minimum flatness factor values are slightly less than 3, the gaussian value. Starting from the inlet they

bulge out slightly towards the wall near station 30 and then return toward the centre line in the exit region.

On the centre line, as shown in Figure 4.12 the skewness and flatness factor remain essentially constant, except near the diffuser exit where there is a sudden increase in skewness (magnitude) and flatness factor. Because of this rather dramatic change in structure near the diffuser exit, station 30 (further upstream) was selected for the detailed experiments described in the following chapters. This station is also sufficiently far down stream from entry for the flow to be representative of developing diffuser flow*. To insure that no signals contained high frequency components in excess of 20 kHz, the upper frequency limit for the KH 3700 filters, all further measurements were restricted to the lower Reynolds number, Re = 137,000.

4.3 Mean Velocity and Turbulence Intensity Measurements

$\bar{U}$ and u' were measured at seven stations with

*See footnote at beginning of chapter

Re = 137,000. Figure 4.14 shows iso-contours of $\bar{U}$ and u'. $\bar{U}$ decreases montonically from the diffuser inlet to the outlet and also from the centre line toward the wall. For purposes of analyzing u', the diffuser is divided into three regions.

a) For $(R/R_{REF} < 0.8)$, u' increases monotonically in the down stream and wallward directions.

b) At $(R/R_{REF} \approx 1)$, u' increases in the down stream direction up to about station 28 and then decreases again toward the outlet.

c) Wallward from $(R/R_{REF} \approx 1)$, u' decreases.

It is important to notice that in the wall region all measurements are subject to errors because of the very large turbulence intensities. Figure 4.15 shows turbulence intensities near the wall at station 30 of up to 57%. As mentioned previously, the basic problem is that hot wires are not direction sensitive for flow components normal to the wire. Thus the PDF's taken near the wall are probably folded back on themselves because hot-wires always indicate positive U values even when they are in fact negative. Thus in the wall region it may be expected that $\bar{U}$ is estimated high and

u' is estimated low. The mean velocity profiles (Figure 4.16) exhibit points of inflexion which are especially noticeable for stations near the diffuser outlet. It is suggested that these points of inflexion are at least partially caused by the over-estimated $\bar{U}$ values near the wall.

If the mean velocity near the wall does indeed become negative then the flow is said to separate. Considering the velocity profile at station 0 and the errors discussed above, it would appear that the flow there is just on the verge of separation and would in fact do so if the opening angle were slightly increased.

4.4 Error Considerations

As discussed in the previous section, the results near the wall are subject to large errors because of the high turbulence intensity. Under these circumstances any attempt to correct even a most fundamental quantity such as the mean velocity is very difficult. Thus, for the present work, generally involving more complex quantities, assessment of error is practically impossible and not attempted.

Possibly more important than absolute accuracy is

the trend accuracy. It is the trends which allow identification of the different regions with different flow structure - a most important aspect of the present work. Also many of the results in the present work are non-dimensionalized (e.g., skewness and flatness factor) in which case the errors may tend to cancel. A more detailed discussion of errors in hot-wire anemometry is given by Trupp (1973).

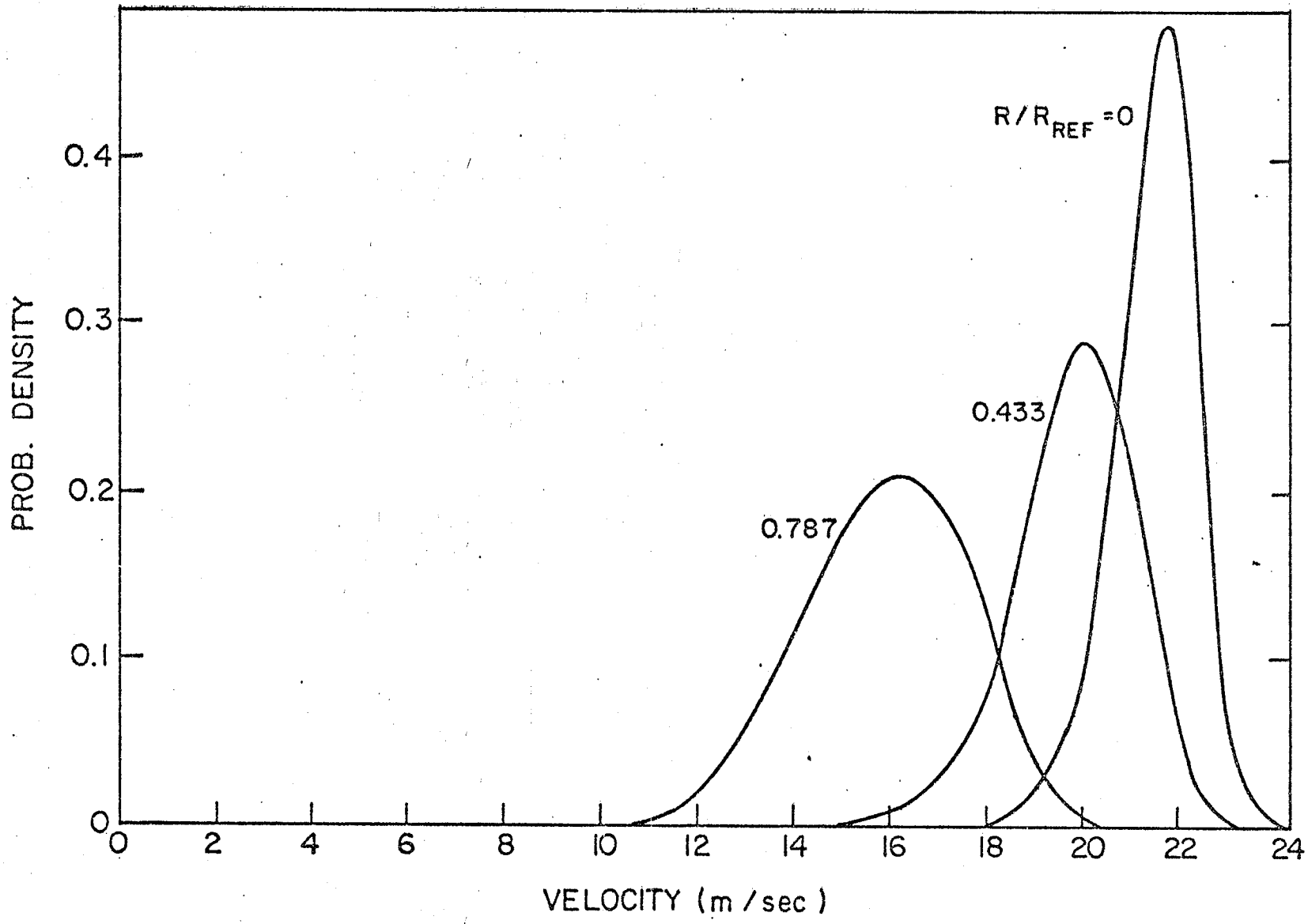

Figure 4.1 Probability Density of U at Station 75. Re = 137,000

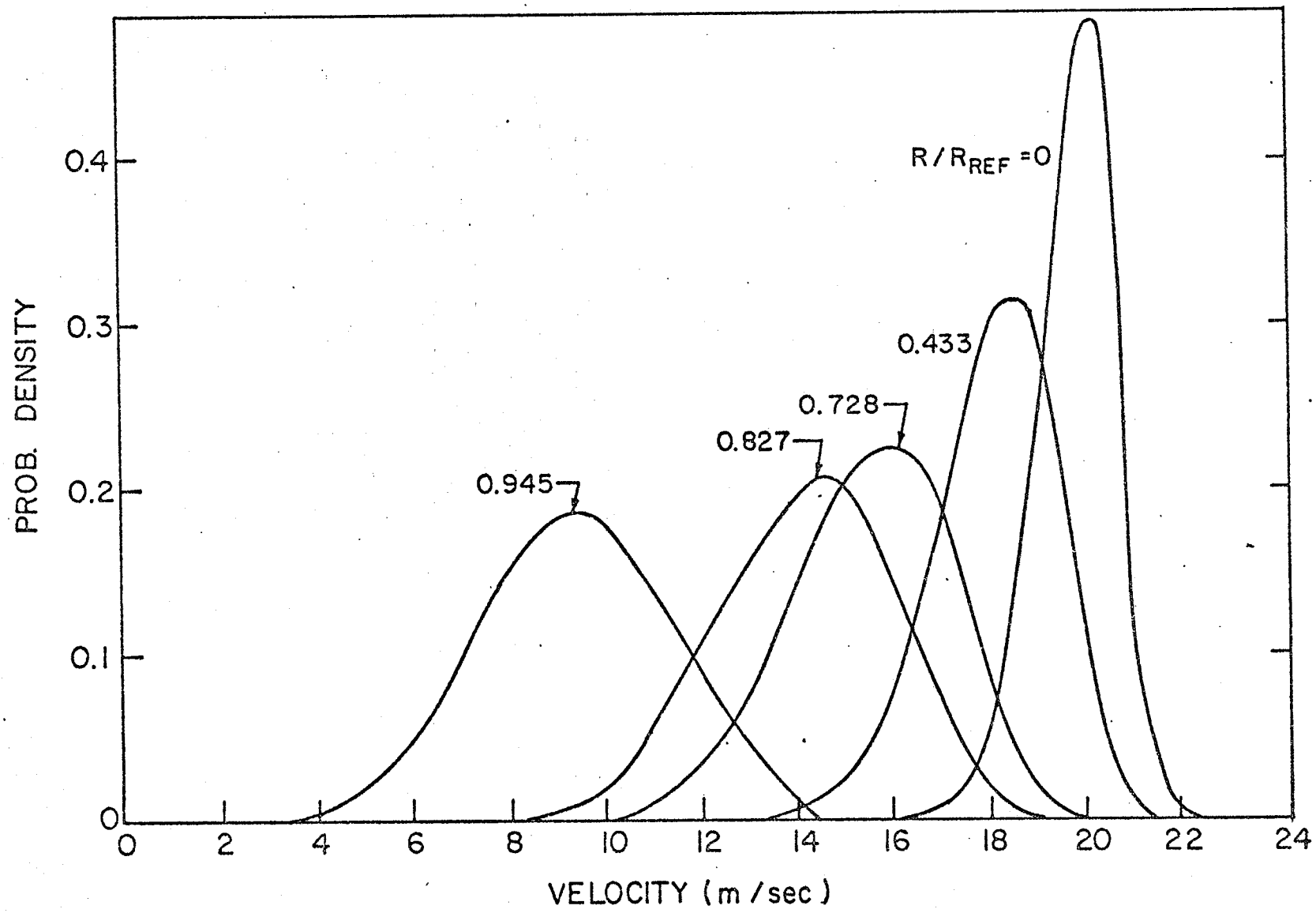

Figure 4.2 Probability Density of U at Station 65. Re = 137,000

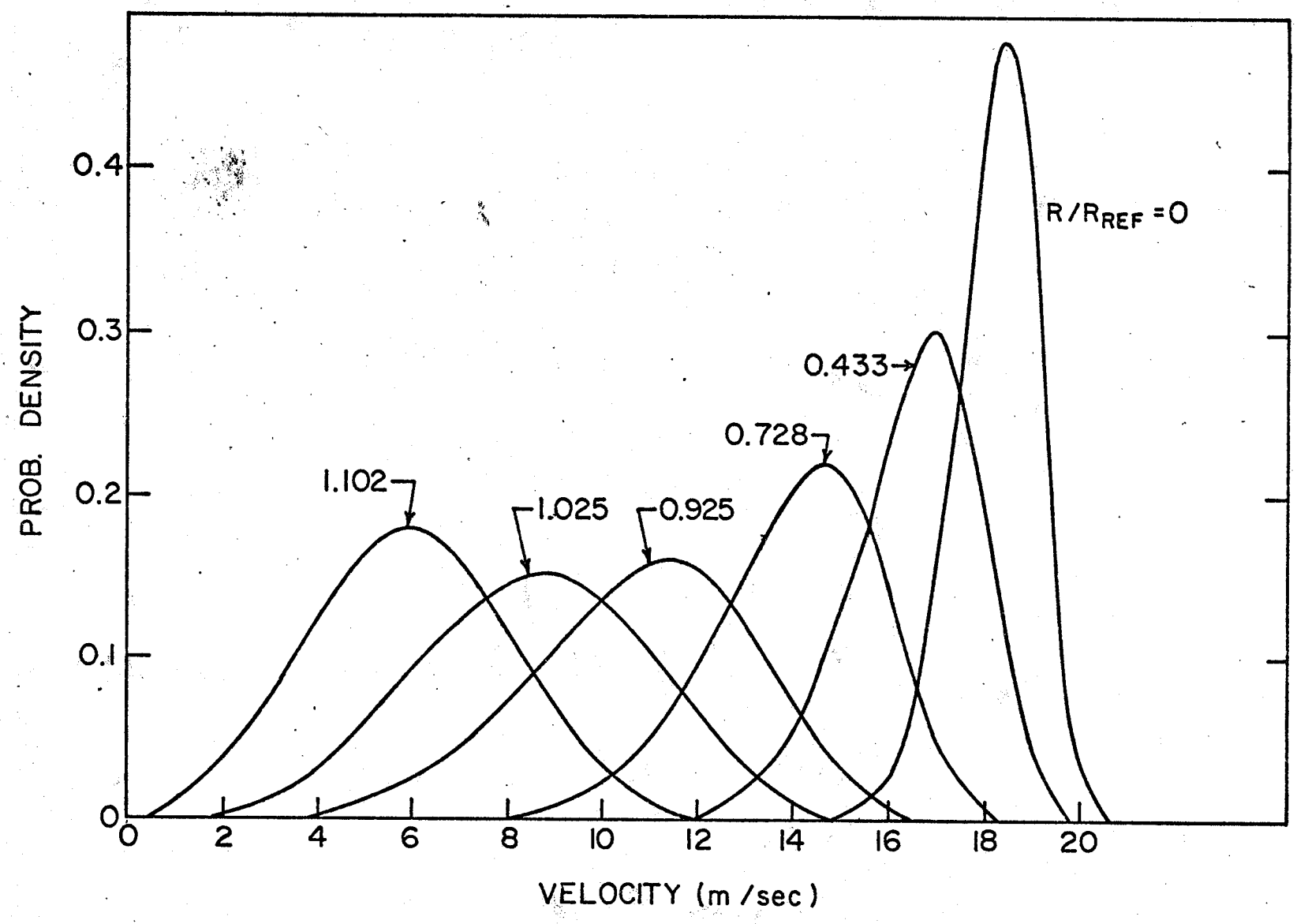

Figure 4.3 Probability Density of U at Station 55. Re = 137,000

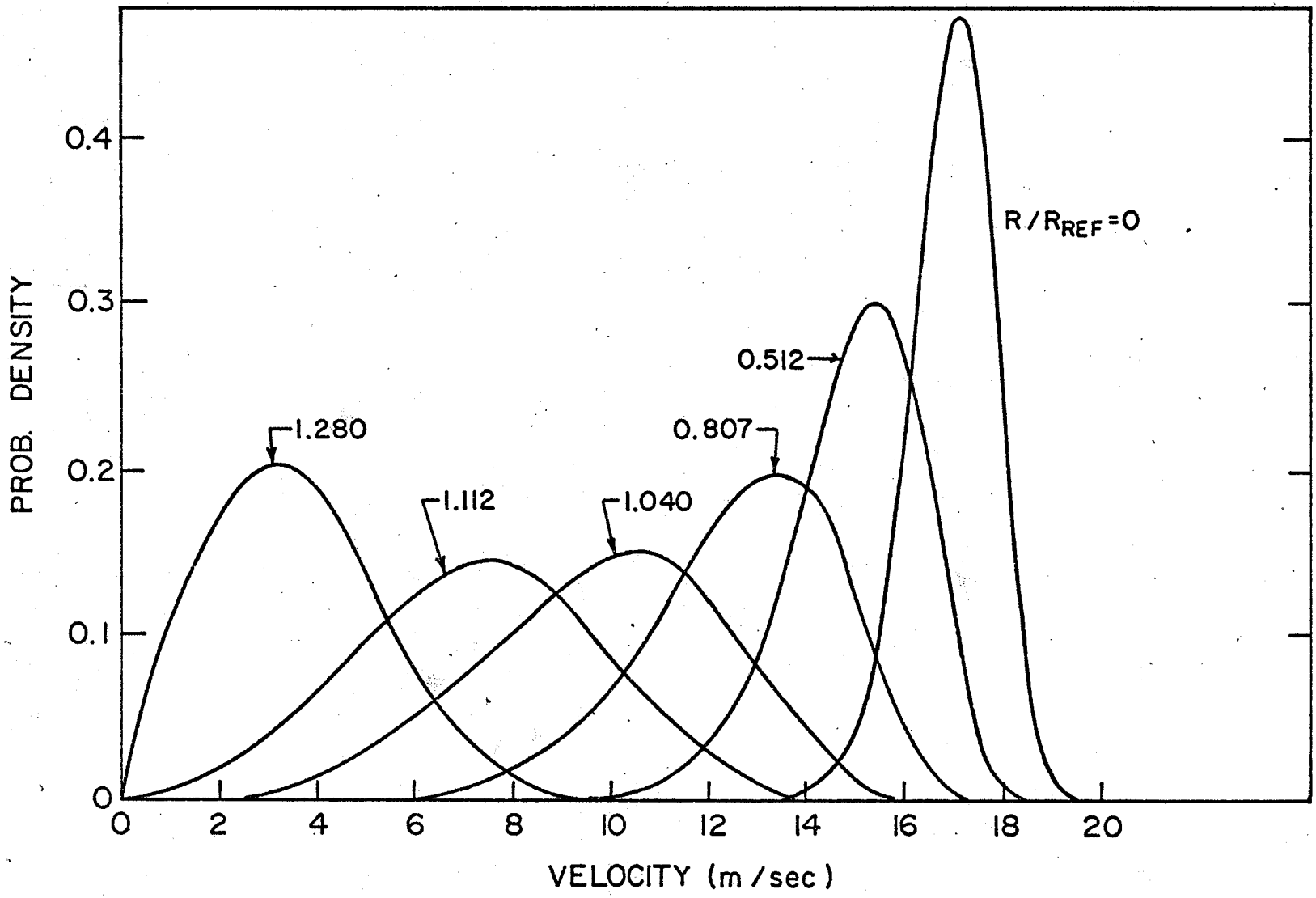

Figure 4.4 Probability Density of U at Station 45. Re = 137,000

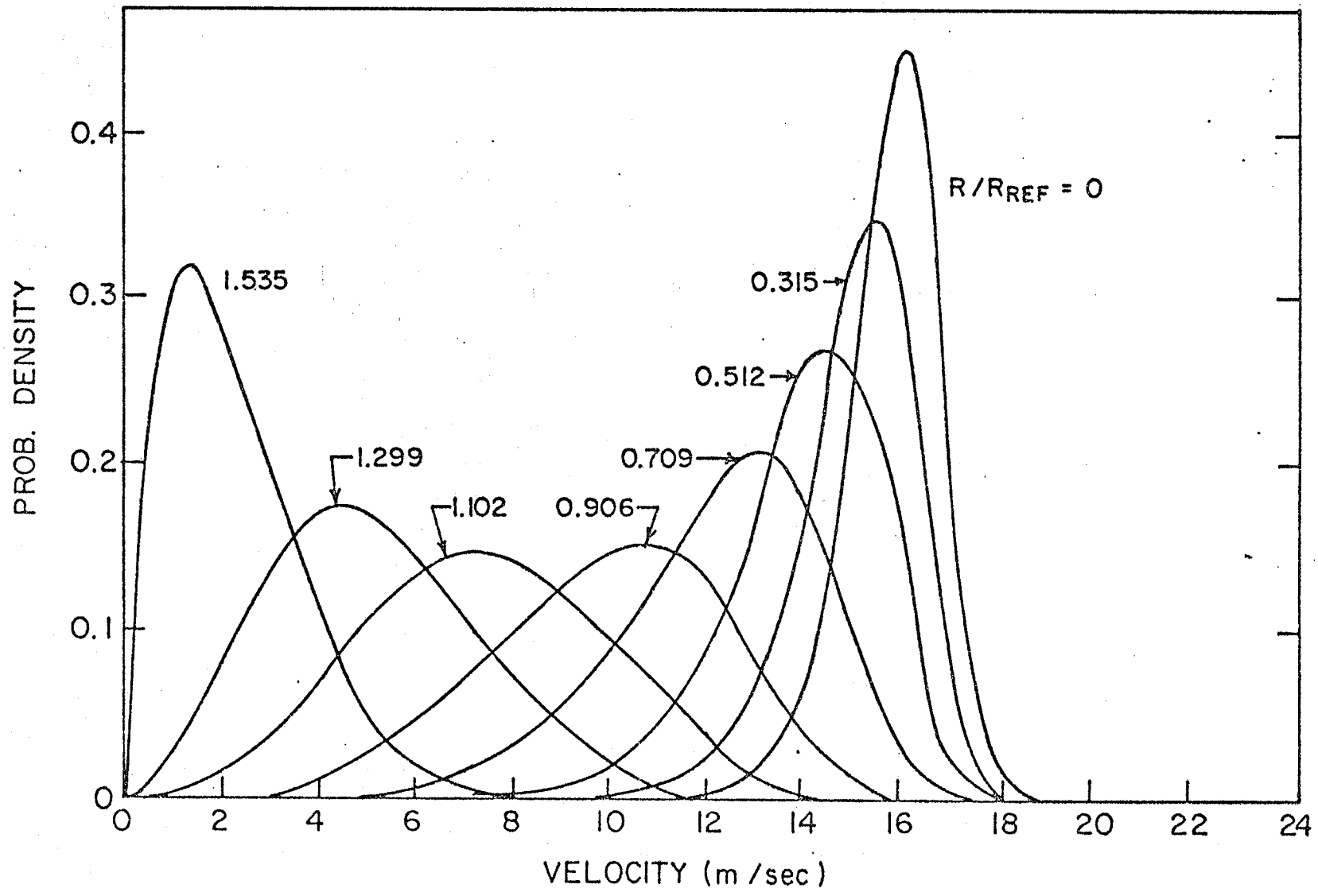

Figure 4.5 Probability Density of U at Station 30. Re = 137,000

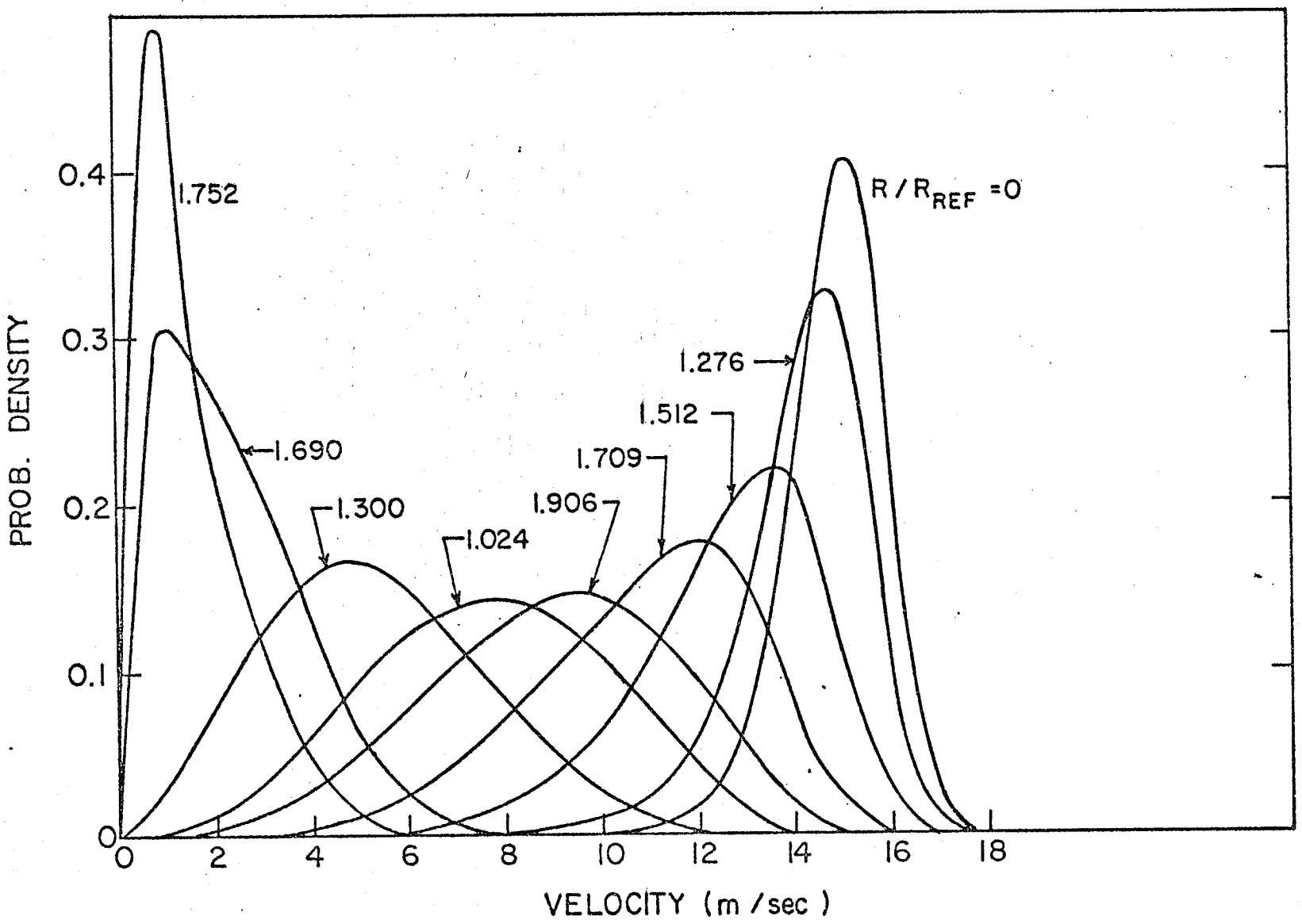

Figure 4.6 Probability Density of U at Station 15. Re = 137,000

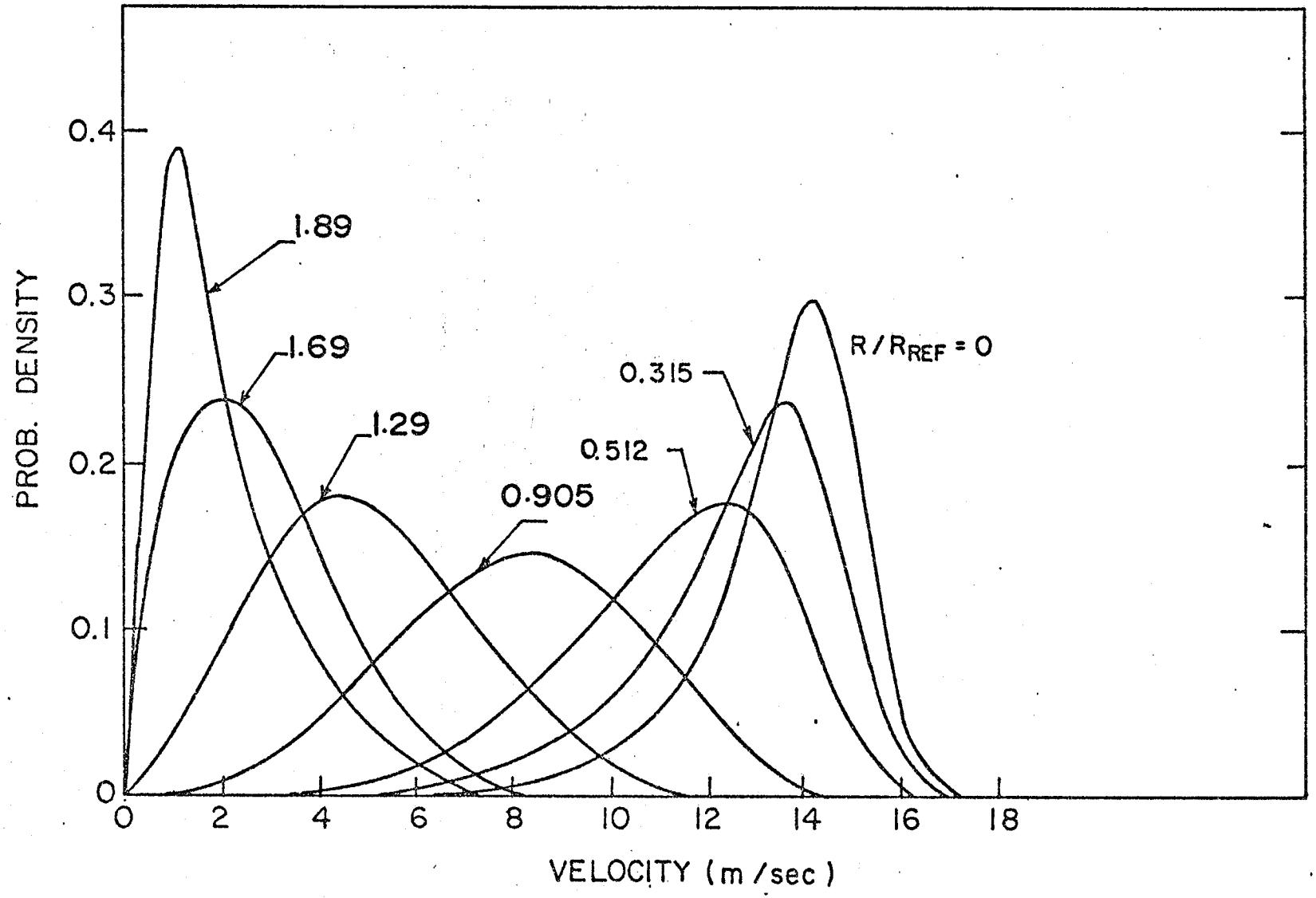

Figure 4.7 Probability Density of U at Station 0. Re = 137,000

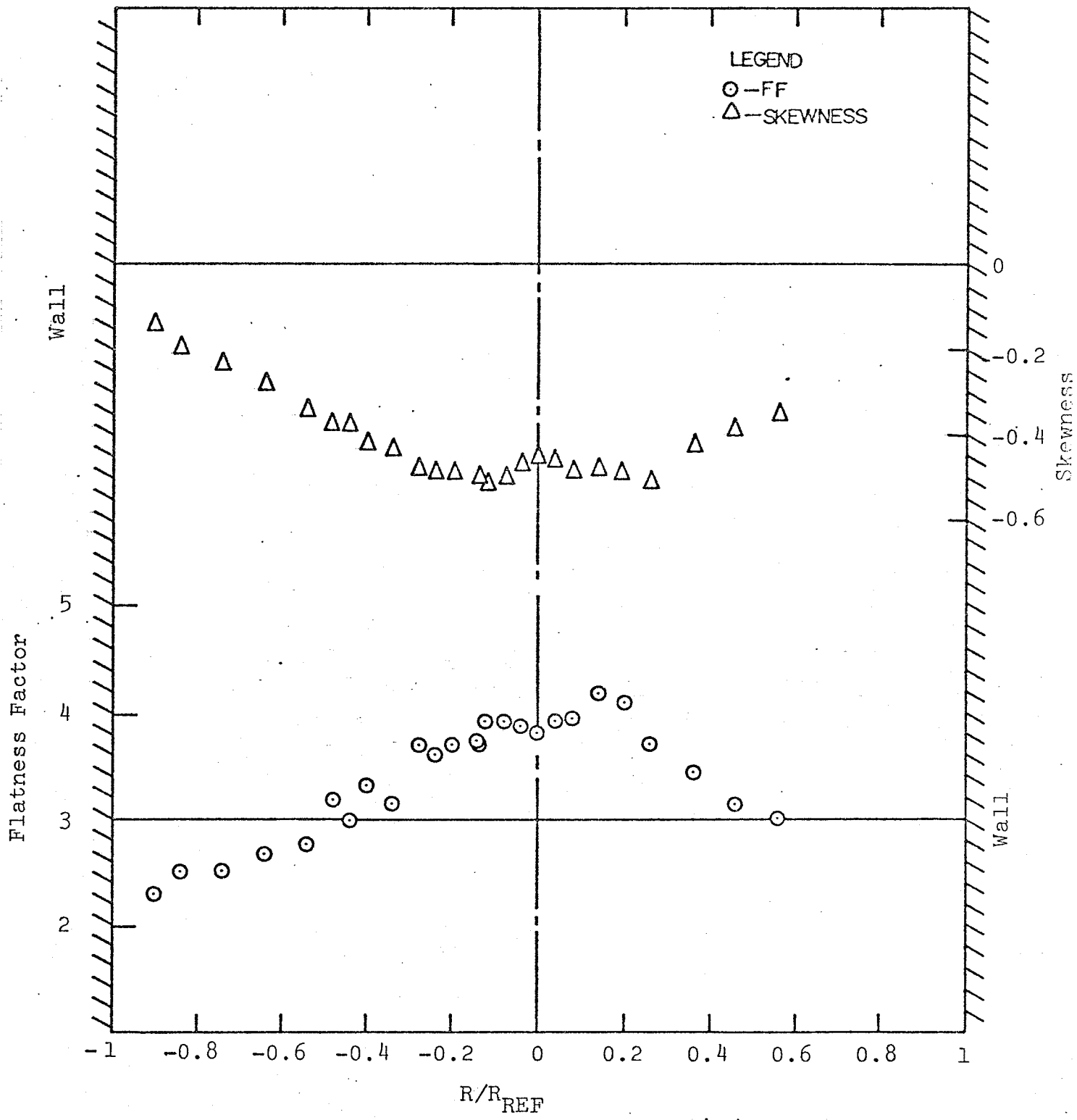

Figure 4.8 Skewness and Flatness Factor of u at Station 75.
Re = 340,000

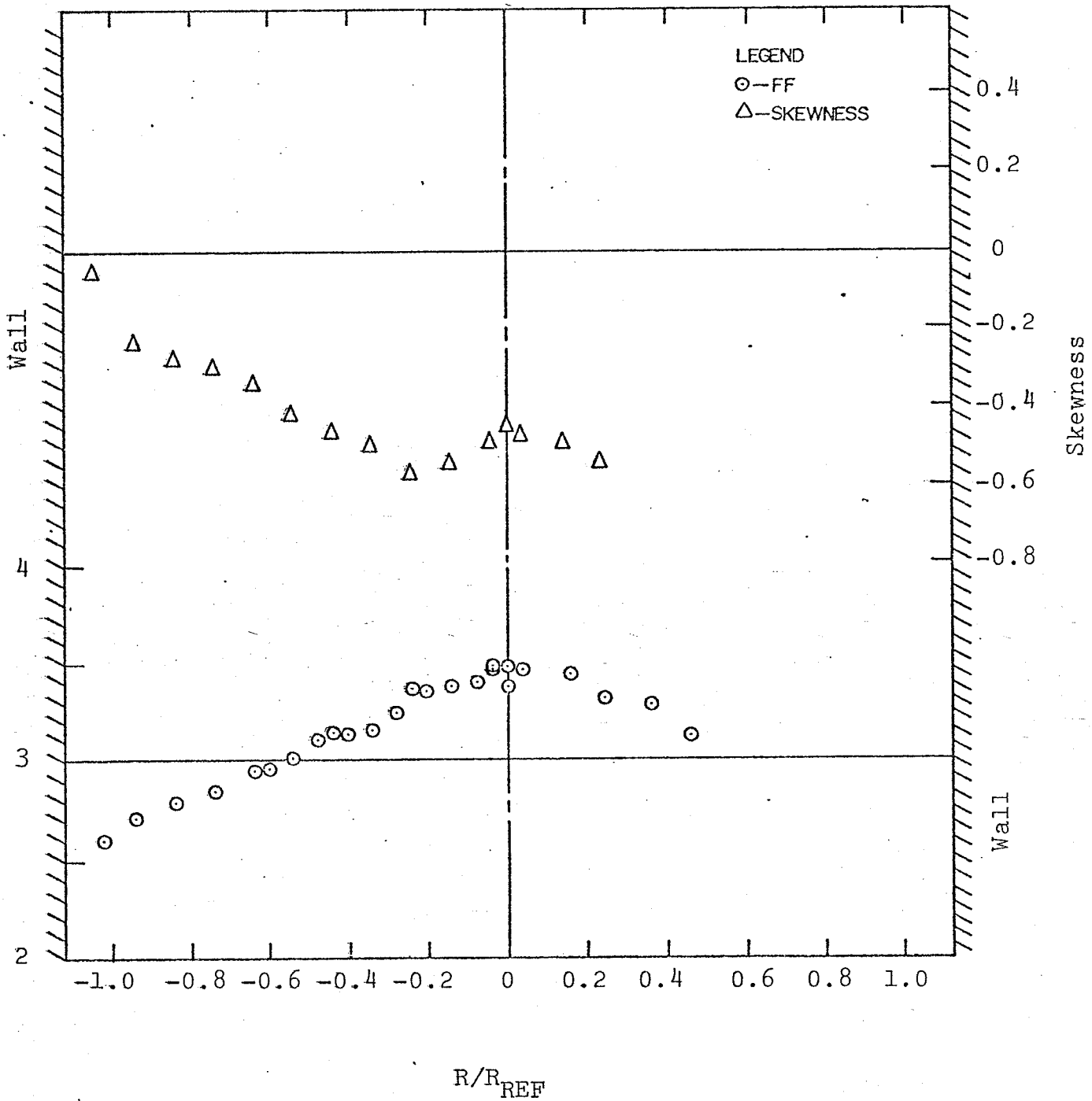

Figure 4.9 Skewness and Flatness Factor of u at Station 65.
Re = 340,000

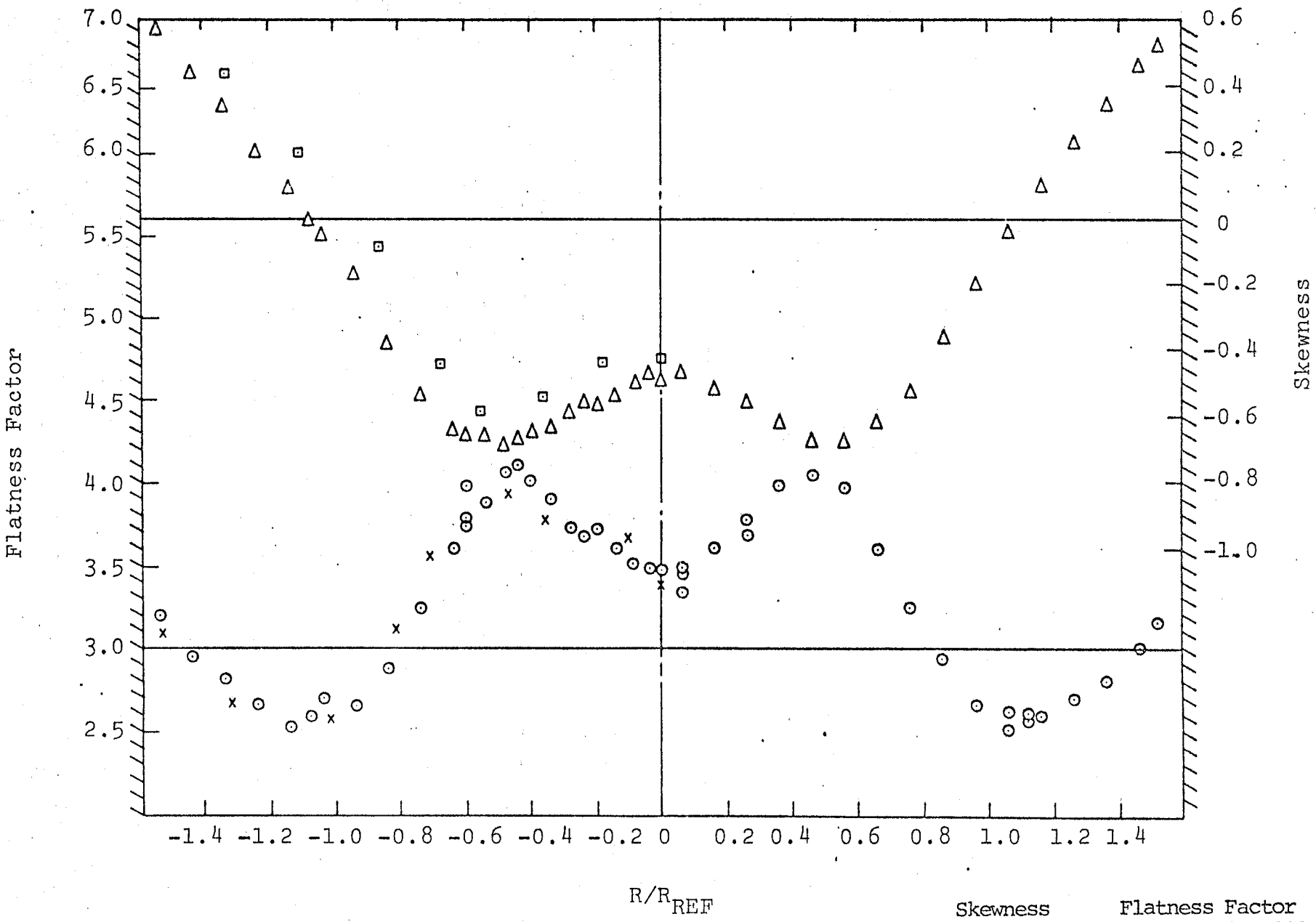

Figure 4.10 Skewness and Flatness Factor of u at Station 30

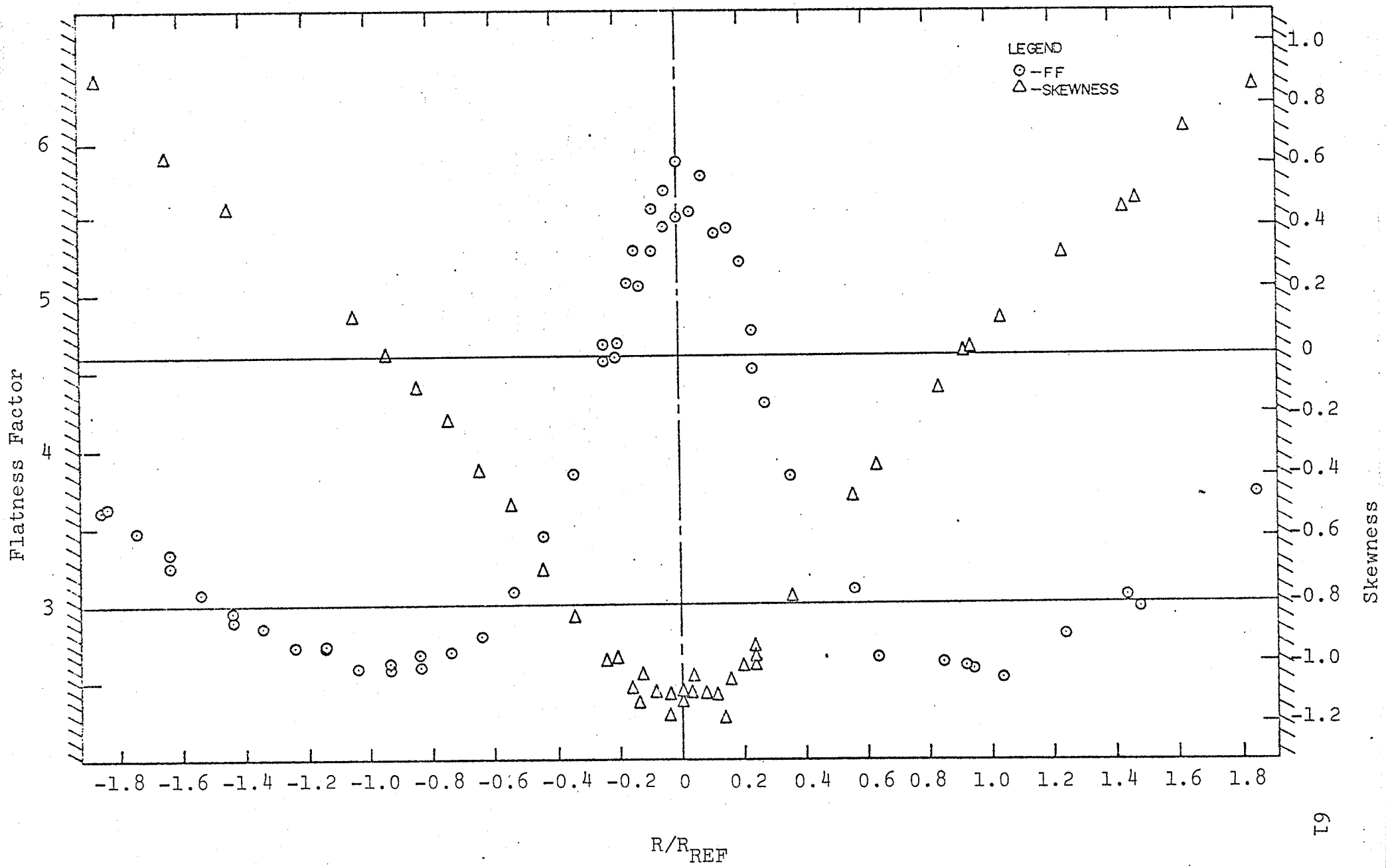

Figure 4.11 Skewness and Flatness Factor of u at Station 5. Re = 340,000

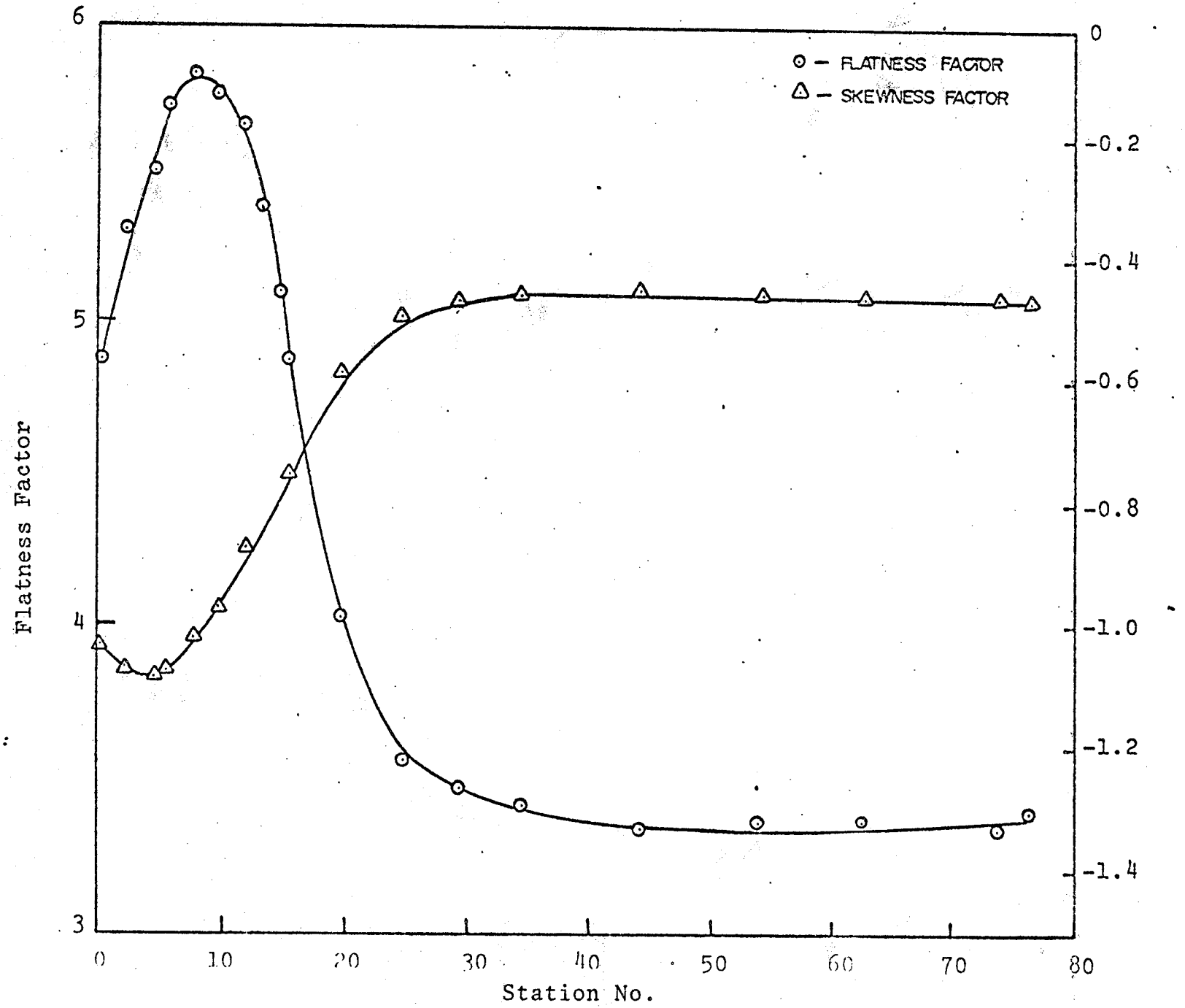

Figure 4.12 Skewness and Flatness Factor of u on the Centre Line.
Re = 340,000

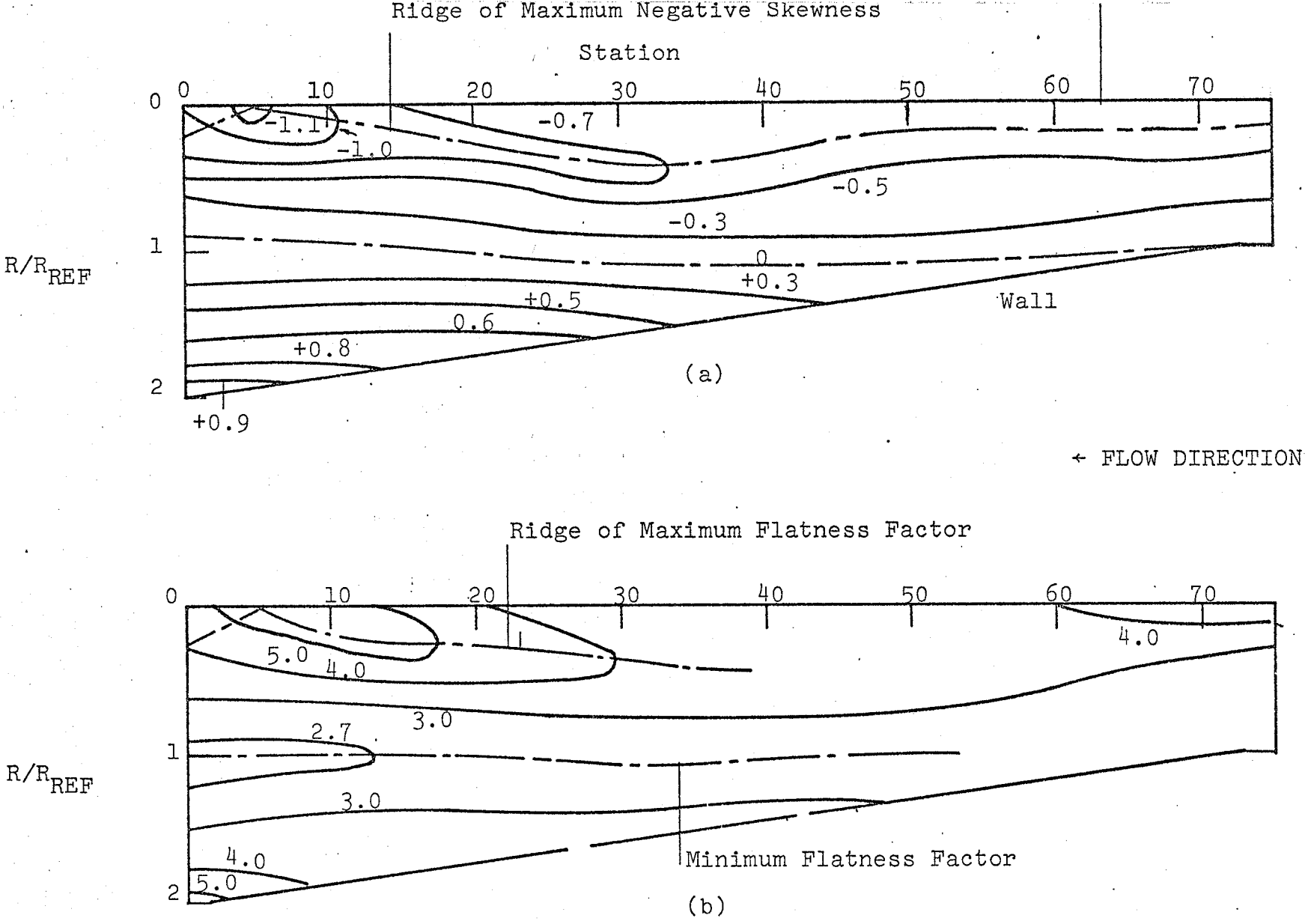

Figure 4.13 Iso-Skewness and Flatness Factor Contours of u. Re = 340,000

(a) Skewness
(b) Flatness Factor

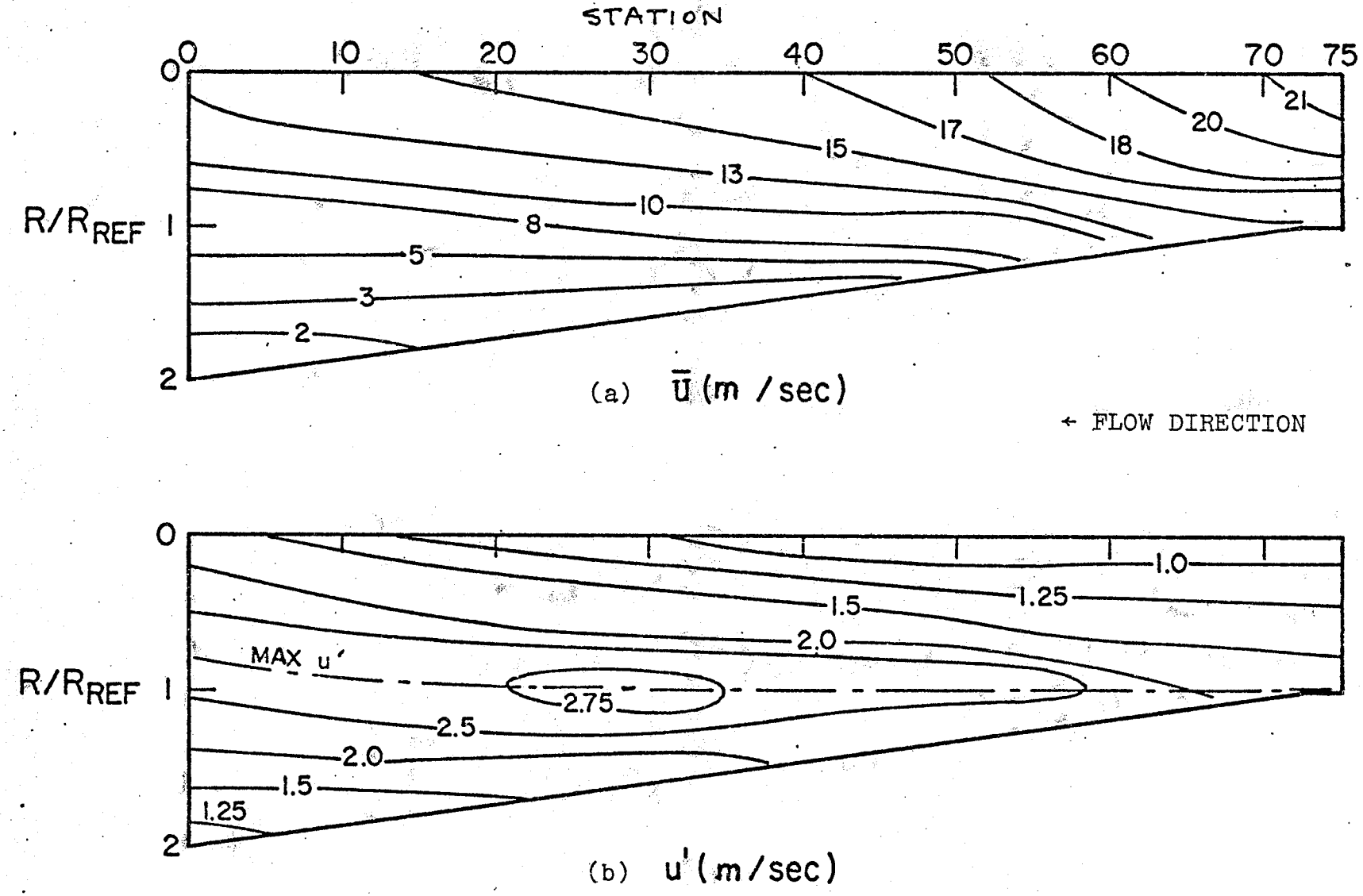

Figure 4.14 Contours of $\bar{U}$ and u'. Re = 137,000

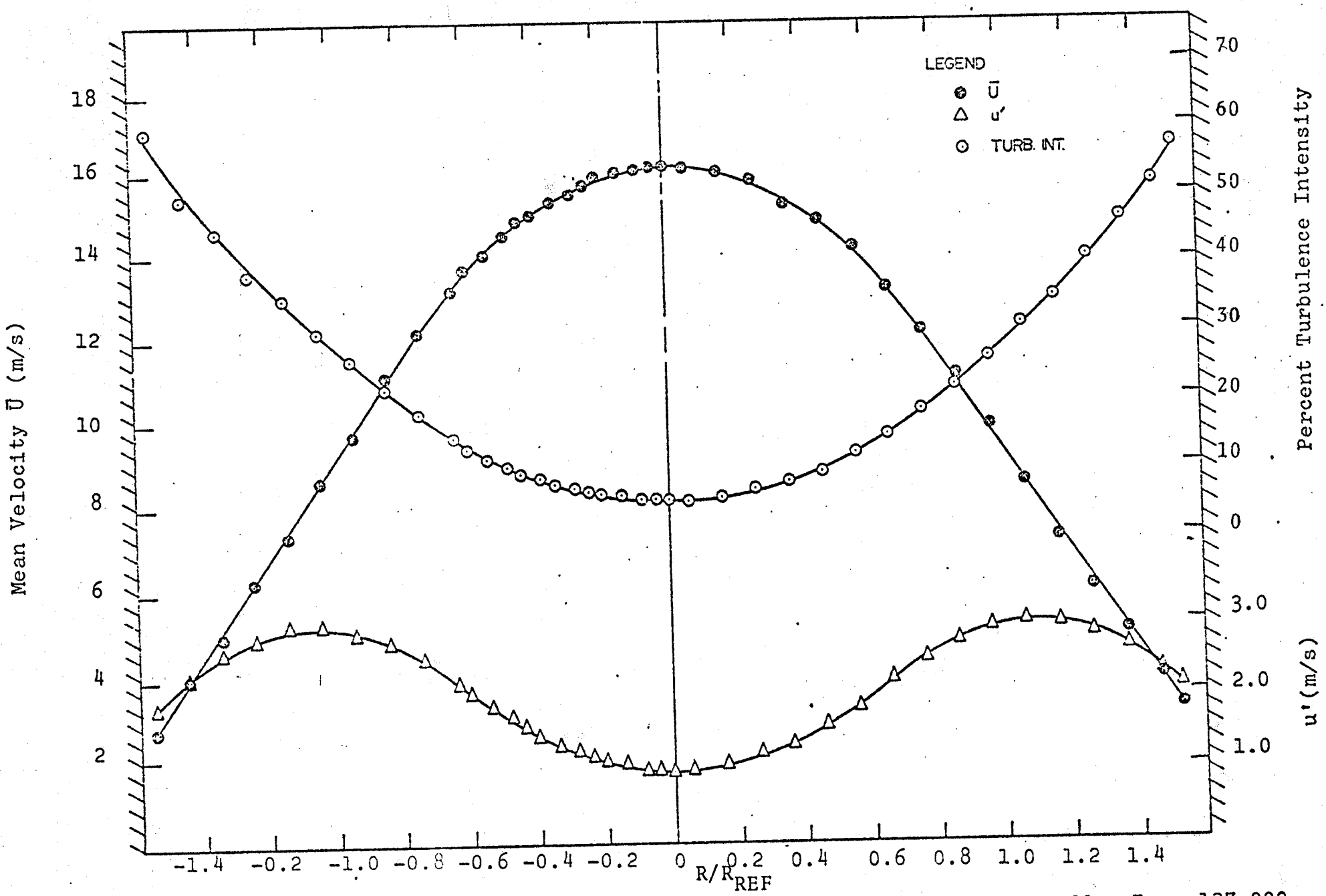

Figure 4.15 Distribution of Ū, u' and Turbulence Intensity at Station 30. Re = 137,000

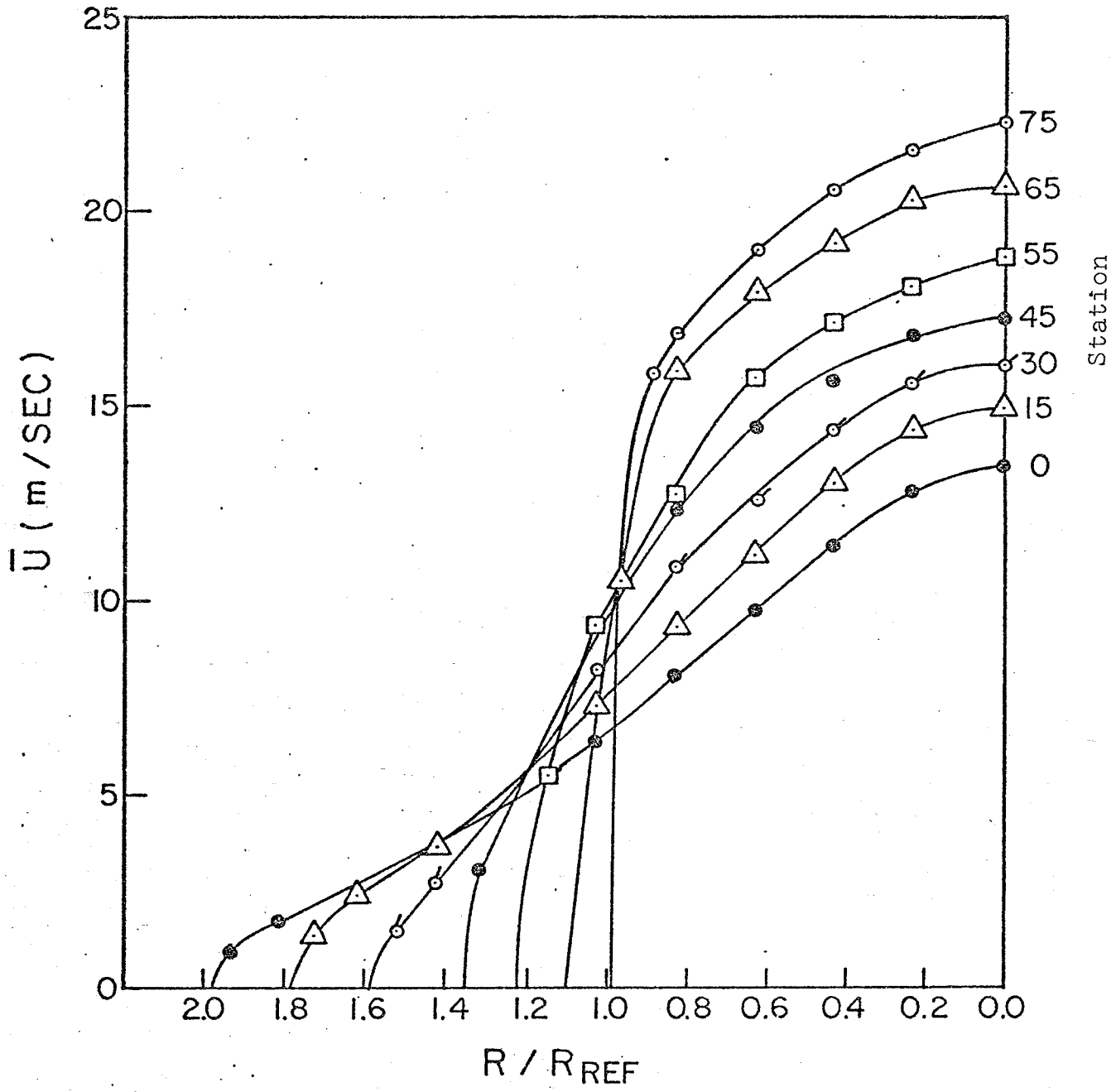

Figure 4.16 Mean Velocity Profiles. Re = 137,000

5.0 DETAILED EXPERIMENTS AT STATION 30

This chapter describes a number of experiments designed to give a more detailed picture of the turbulence structure at station 30. Where possible the results are compared to the boundary layer experiments of others in an attempt to show structure similarities which may exist between the two types of flow. All measurements were made at a Reynolds number of 137,000. In order to demonstrate down stream development, the truncated uv correlation measurements of Section 5.3 are also given at axial locations other than station 30.

5.1 Flow Parameters - Length Scales

Kolmogoroff's similarity theories postulate the existence of an inertial subrange if the integral length scale, L_f is much larger than the dissipation length scale η. Furthermore the turbulence Reynolds number R_λ is important in Kolmogoroff's modified theory. It is therefore useful to measure these and related quantities. Taylor's microscale λ was calculated from

$$\lambda^2 = \left[u'^2/\overline{(\partial u/\partial t)^2}\right]\bar{U}^2. \qquad 5.1$$

The mean dissipation $\bar{\varepsilon}$ was obtained from the isotropic relationship

$$\bar{\varepsilon} = 15\nu u'^2/\lambda^2,$$

and η by

$$\eta = (\nu^3/\bar{\varepsilon})^{1/4},$$

where ν is the kinematic viscosity.

The Kolmogoroff frequency f_k, was obtained from

$$f_k = \bar{U}/2\pi\eta.$$

To minimize the effect of high frequency anemometer noise a low pass filter is generally used in the measurement of $(\partial u/\partial t)^2$, required in Equation 5.1. This result is very sensitive to the filter cut-off frequency which is usually set to f_k. Since f_k is not known at the outset a value of 20 kHz was originally assumed and values obtained for $\lambda, \bar{\varepsilon}, \eta$ and f_k. Using this new value of f_k the measurements were repeated. Stable value of $\lambda, \bar{\varepsilon}, \eta$ and f_k were obtained after two such iterations. These quantities are plotted in Figure 5.1 and tabulated in Table 1.

The transverse integral length scale, L_g was calculated from,

$$L_g = \int_o^\infty R_{11}(0,y,0;0)dy,$$

R/R_{REF}	$\overline{U}$ m/s	u' m/s	λ mm	R_λ	$\overline{\epsilon}$ cm^2/sec^3	η mm	f_k KHZ	L_f mm	Lg mm	L_f/Lg	L_f/η
0	15.4	0.96	3.52	211	17.8×10^4	.123	19.9	43.0	7.9	5.44	349
0.236	15.1	1.17	3.84	281	22.2×10^4	.116	20.6	51.2	10.3	4.97	440
0.433	14.3	1.48	3.78	349	36.8×10^4	.102	22.2	46.5	12.2	3.81	453
0.630	12.5	1.97	3.88	477	61.9×10^4	.090	22.1	72.9	13.6	5.36	808
0.827	10.2	2.38	3.57	531	106.6×10^4	.079	20.6	64.1	14.0	4.58	814
1.024	7.7	2.51	3.04	477	163.2×10^4	.071	17.3	57.6	14.0	4.11	814
1.220	5.4	2.35	2.54	373	205.7×10^4	.067	12.8	40.4	12.2	3.31	605
1.398	3.3	1.79	1.90	213	211.9×10^4	.066	7.9	27.3	9.8	2.79	412
1.496	2.6	1.53	1.89	181	156.6×10^4	.071	5.7	22.3	9.3	2.40	312

TABLE 1

Distribution of various flow parameters at station 30 for Re = 137,000

where R_{11} was estimated by fitting an exponential function to the correlation coefficients (Figure 5.2) measured between probes spaced in the transverse direction.

The longitudinal integral length scale L_f was calculated from,

$$L_f = \bar{U} \int_o^\infty R_{11}(0,0,0;t)dt.$$

Here R_{11} is the autocorrelation of u. Time delay was obtained with a Lyric TR61-2 tape recorder (with moveable playback heads) and, as also for L_g, correlation coefficients were measured with a DISA 55D70 Correlator. The values of L_f and L_g are given in Table I, with L_f also shown in Figure 5.1.

At station 30 both integral scales L_f and L_g reach a maximum at $R/R_{REF} \simeq 0.8$. The ratio of the scales varies from 5.49 on the centre line to 2.40 near the wall. According to Comte-Bellot and Corrsin (1971) this ratio equals 2.0 for isotropic turbulence. The ratio L_f/η has a maximum near $R/R_{REF} \simeq 0.8$ where R_λ is also near maximum. This is consistent with the requirement (Tennekes and Lumley, 1972) that L_f/η should increase with R_λ.

5.2 Spectra of u

One-dimensional energy spectra were measured using

a KH3700 filter with bandwidth, $\Delta f/f_m = 0.43$. The spectra were normalized such that,

$$\int_0^\infty E_u(k_1)dk_1 = (u')^2$$

and non-dimensionalized by the small scale parameters v_k and η (Tennekes and Lumley, 1972, p. 267).

The results are shown in Figure 5.3. The universal character of the spectra at high wave-numbers compares favourably with the results given by Monin and Yaglom (1975, p. 491). For the present data, however, the spectra drop off somewhat faster at the high wave-numbers, possibly because the hot wires used in the present work were approximately 10η in length, thus reducing their high wave-number sensitivity. The spectra exhibit a -5/3 dependence for about one decade in agreement with Okwuobi and Azad (1973).

A useful characteristic of this type of spectrum normalization is that the low wave-number part of the spectrum increases more rapidly with decreasing wave-number as R_λ increases (Monin and Yaglom, 1975, p. 491). Thus it can be concluded from these spectra that the maximum value of R_λ occurs at ($R/R_{REF} \approx 1.02$), with minimum values occurring near the wall and on the centre line.

These conclusions are consistent with the results given in Figure 5.1.

5.3 Truncated uv Correlation

In an attempt to quantify the visualization results of Brodkey, Kline and their co-workers, Wallace et. al. (1972) sorted the contributions to the uv product into four categories depending on the signs of u and v. Thus,

$$\overline{uv} = \overline{u^- v^+} + \overline{u^+ v^-} + \overline{u^+ v^+} + \overline{u^- v^-}.$$

The four quantities on the right in the equation above are referred to as the truncated uv correlations. With each is associated a particular type of event with a name inspired by the results of the visualization studies. Thus, $\overline{u^- v^-}$ is non-zero when low (axial) momentum fluid is ejected away from the wall, hence the name ejection event. Similarly $\overline{u^+ v^+}$ is non-zero when high (axial) momentum fluid is swept toward the wall, hence the name sweep event. Associated with the remaining two quantities, $\overline{u^+ v^-}$ and $\overline{u^- v^+}$, are the so-called outward and wallward interactions respectively.

Wallace et al (1972) measured truncated uv correlations in a boundary layer and normalized the results with the

local value of $\overline{uv}$. Their results are reproduced in Figure 5.4. Using the circuit shown in Figure 3.6, the same quantities were measured in the diffuser at four stations, to show downstream development. The normalized results are shown in Figures 5.5 to 5.8. At station 75 (in the pipe) the trends (Figure 5.5) are identical to those of Wallace et al (1972) with the ejections larger than the sweeps in the outer region, $y^+ > 15$. For the present case no measurements were made in the inner region. Moving further downstream, the ejections remain larger than the sweeps for R/R_{REF} less than 1 but are less than the sweeps in the region where R/R_{REF} is approximately greater than 1. This region therefore corresponds to the boundary layer region, ($y^+ < 15$) where the sweeps are also larger than the ejections (Figure 5.4). Thus for the diffuser, the truncated uv correlation measurements are very similar to those of a boundary layer, if ($R/R_{REF} \simeq 1$) in the diffuser is made to correspond to ($y^+ \simeq 15$) in a boundary layer.

The non-normalized truncated uv correlation measurements are shown in Figures 5.9 to 5.12. These results are discussed further in Chapter 8.

5.4 Vorticity Measurements

Since high levels of fluctuating vorticity are characteristic of all turbulent flows a number of quantities relating to the longitudinal component of vorticity were measured using the four-wire vorticity probe described in Appendix A. The experimental results, given in Figure 5.13 show that the measured r.m.s. vorticity, ξ'(meas) increases from near 200 radians/sec on the centre line to over 800 radians/sec near the wall. The maximum rate of increase occurs approximately at $R/R_{REF} = 0.9$. As discussed by Willmarth (1975), fluctuating vorticity also increases sharply when approaching the wall of a boundary layer. Thus the trend for the diffuser is similar to that of a boundary layer.

Figure 5.13 also shows the isotropic values, ξ'(iso) computed from $\sqrt{5}\ u'/\lambda$ given by Batchelor (1960). This result is approximately twice the measured value, ξ'(meas) but with identical trend. Thus for this type of flow, the fluctuating longitudinal vorticity can be estimated from the simple relationship,

$$\xi' = u'/\lambda.$$

The flatness factor of ξ was also measured. It shows a broad maximum (Figure 5.13) at $R/R_{REF} \approx 0.4$ and also near

the wall. Similar trends exist for the flatness factor of $\partial u/\partial t$ (Figure 5.14) and the flatness factor of the transverse velocity difference (Figure 5.17). The significance of these similarities is discussed further in Chapter 8.

For the vorticity probe used, both ξ and u were simultaneously available. This prompted an investigation to show if any correlation existed between these quantities. As expected from symmetry considerations the cross-correlation $\overline{\xi u}$ was found to be very nearly zero throughout the station 30 profile. While the overall correlation is small or zero, its four components; i.e., the truncated correlations (as discussed in Section 5.3 for uv) will in general not be zero. Thus let

$$\xi u = \xi^- u^+ + \xi^+ u^+ + \xi^+ u^- + \xi^- u^-$$
$$= A + B + C + D = 0.$$

From axial symmetry A = - B and C = - D and only two independent quantities B and D say, need be considered. From these can be formed the ratios of non zero quantities,

$$\frac{\overline{\xi u^+}}{\overline{\xi u}} \equiv \overline{\xi^+ u^+}/(\overline{\xi^+ u^+} + \overline{\xi^- u^-}).$$

As shown in Figure 5.13 this quantity is less than 0.5 over most of the flow indicating that large longitudinal

vorticity, of either sign correlates better with low (axial) momentum fluid than with high momentum fluid. Near the wall ($R/R_{REF} > 1.35$) the reverse appears true with high vorticity correlating better with the high momentum fluid.

5.5 Skewness and Flatness Factor of $\partial u/\partial t$

The skewness and flatness factor of $\partial u/\partial t$ were measured at station 30 with the results shown in Figure 5.14. For all the measurements the signal u was first passed through a low-pass filter with the cut-off frequency set to f_k. Trends, taken from the boundary layer experiments of Ueda and Hinze (1975)* are also shown for comparison. A y^+ value of 15 in the UH data is set to correspond to $R/R_{REF} \simeq 1.1$ since in both cases this is the approximate position of maximum turbulence intensity.

Monin and Yaglom (1975) discuss the variation of the skewness S, and FF of $\partial u/\partial t$ with R_λ. From this discussion S is expected to vary as $R_\lambda^{3/16}$ and FF as $R_\lambda^{1/2}$, assuming the universal constant $\mu = 0.5$. Thus both S and FF are

*Henceforth often referred to as UH.

expected to increase with R_λ. For turbulence with R_λ less than 1000 the trend for S is reversed as shown by UH. They have summarized the results of several research groups who have made similar measurements in essentially shear-free flows. Their summary is repeated in Figure 5.15 along with results of the present work for comparison.

UH give the following explanation for their boundary layer data. At $y^+ \simeq 15$ the bursting sequence is dominated largely by the sweep events resulting in an occasional large increase in u with time ($\partial u/\partial t > 0$). Thus the skewness and flatness factor of $\partial u/\partial t$ are increased. Furthermore the increased FF cannot be attributed to increased R_λ which decreases in this region. Further from the wall, at $y^+ > 20$ where both ejection and sweep events are important the FF decreases whereas R_λ remains constant.

For the diffuser (Figure 5.14) at ($R/R_{REF} < 0.6$) the FF of $\partial u/\partial t$ is approximately the same as in the outer region of a boundary layer. However at ($R/R_{REF} \simeq 1.0$) the FF shows a dip, somewhat opposite to the boundary layer case which shows a maximum value at $y^+ \simeq 15$. For ($R/R_{REF} > 1$) the FF of $\partial u/\partial t$ increases rapidly, and very close to the wall even surpasses the maximum value reached in the boundary layer at $y^+ \simeq 15$. Referring to the FF data in Figure 5.15 the two FF values above the line correspond to

measurements made near the wall while the cluster of three values for largest R_λ correspond to measurements for which ($R/R_{REF} \approx 1$). Thus only on and near the centre line do the FF of $\partial u/\partial t$ correspond to that of a shear-free layer with the same R_λ.

For the diffuser the skewness of $\partial u/\partial t$ remains approximately constant across the entire station 30 profile (Figure 5.14) with no similarity to the trend shown for the boundary layer. As shown in Figure 5.15 it is also approximately equal to that of a shear-free layer with the same R_λ.

5.6 Skewness and Flatness Factor of the Transverse Velocity Difference

The skewness and flatness factor of $u_1 - u_2$ were measured at station 30. u_1 and u_2 were the fluctuating components of the streamwise velocity measured at two points separated in the transverse direction, with u_1 closer to the wall.

The results for various probe separations are shown in Figure 5.16 and 5.17. For a homogeneous flow the skewness should be zero, but was in fact always negative for the diffuser, with a peak at ($R/R_{REF} \approx 0.4$), a valley at ($R/R_{REF} \approx 1.0$) and becoming more negative again as the

wall is approached. The flatness factor measurements show a similar trend, with the value increasing significantly with decreased probe spacing.

It is interesting to speculate on the significance of these results in terms of the bursting concept. Consider for example the case where the two probes are positioned at $R/R_{REF} \approx 0.4$. As shown in Figure 5.11 this region is dominated by ejection events consisting of low momentum fluid ejected from the direction of the wall towards the centre line. For many of such events the velocity of the fluid passing probe 1 will temporarily be reduced more than that of probe 2, because probe 1 is closer to the wall and therefore closer to the origin of the low momentum fluid. Thus $u_1 - u_2$ will be negative and the average of many such events will result in increased negative skewness and flatness factor.

5.7 Flatness Factor Measurements of Narrow-band Filtered Signals - Intermittency of $\partial u/\partial t$

The flatness factor of the narrow-band filtered u fluctuations was obtained by first passing the u signal through a narrow-band filter ($\Delta f/f_m = 0.43$) and then measuring the flatness factor using the circuit in Figure 3.4. The large flatness factor values obtained near the wall at high filter frequencies are the result of repeated measurements based on 100 second averages.

The results (Figure 5.18) show an increase in FF with filter frequency, f_m/f_k thus showing increased spottiness of the fine structure, a property of all turbulence.

More important, in the present case is the maximum value of the FF which increases sharply as the wall is approached. This result is shown in Figure 5.19 which also shows the intermittency factor, γ, of $\partial u/\partial t$ measured with the circuit shown in Figure 3.8. There is an obvious relationship between the maximum FF of the narrow-band filtered u signal and the intermittency factor of $\partial u/\partial t$. Conversely this result also suggests that if the maximum FF of the narrow-band filtered u signal is less than about 25, then $\partial u/\partial t$ is not intermittent.

It is interesting to compare these maximum FF results for the diffuser with the results obtained by UH in a

boundary layer. They have found this maximum to equal about 20 at $y^+ = 332$ and about 65 at $y^+ = 5.01$. Thus for a boundary layer the maximum narrow-band filtered FF also increase sharply when approaching the wall.

UH suggest that for the boundary layer the in-rush and out-flow are effective far from the wall, thus doubling the spatial density of bursts and reducing the flatness factor. Near the wall only the in-rush phase will be effective, with a corresponding reduction of bursts and an increase in flatness factor. The exact nature of the flow for a boundary layer has been studied in great detail with the aid of flow visualization and much information is available on how the bursting cycle proceeds through the various phases. One cannot readily extrapolate these results to the case of a diffuser with its adverse pressure gradient. For the diffuser, however, there is also a relatively wide region ($R/R_{REF} > 1.1$) analogous to the boundary layer with $y^+ \leq 15$ for which the intermittency of the fine structure is very large.

5.8 Spectra of $(\partial u/\partial t)^2$

To measure these spectra the signal, $\partial u/\partial t$, was first squared using the squaring circuit shown in Figure 3.4. The spectra were then measured with a KH 3700 filter

($\Delta f/f_m = 0.43$) and a Disa 55D35 r.m.s. voltmeter. Following UH, the spectral distribution $E_{\phi\phi}$ (where $\phi = (\partial u/\partial t)^2$) was plotted in the non-dimensional form $u^{*2}E_{\phi\phi}/2\pi\nu E_\infty$ (where $E_\infty = \int_o^\infty E_{\phi\phi}df$). At station 30 the friction velocity, u^* was calculated to be 0.116 m/sec by extrapolating to the wall the sum of the viscous shear, and the Reynolds stress, using the equation,

$$u^{*2} = \nu\partial U/\partial y + \overline{uv}.$$

The results are shown in Figure 5.20. At all radial locations the high frequency end of the spectra collapse with a single slope. For R/R_{REF} less than 1 this slope is approximately maintained for the lower frequencies. Nearer the wall however ($R/R_{REF} \geq 1$), the slopes at the lower frequencies become more negative. From these results it would thus appear that this region has characteristics similar to that of the buffer region for a boundary layer where UH also found a dual-sloped spectrum for $(\partial u/\partial t)^2$.

As discussed in Chapter 2, the slope of spectrum of $(\partial u/\partial t)^2$ equals μ-1 in the inertial subrange. The slope of the collapsed spectra in Figure 5.20 was estimated as -0.56 giving a value of 0.44 to the "universal" constant μ. Values ranging from 0.4 to 0.85 have been reported by various authors (Ueda and Hinze 1975, p. 142).

5.9 Probability Densities of U, Conditioned on Fine Structure

Repeated observation of the u signal by oscilloscope suggested the existence of a very definite relationship between the high frequency components of u and the positive excursions of u as a whole. To quantify these observations the conditional probability density of U was measured with I(t), the two-state intermittency signal of $\partial u/\partial t$ used as the conditioning signal. The results, given in Figures 5.21 to 5.24 show that fine-structure activity coincides more with positive u, while fine-structure inactivity coincides more with negative u. Since $\partial u/\partial t$ was used as the indicator of fine structure the above effect was observed only where $\partial u/\partial t$ was intermittent ($R/R_{REF} > 0.8$).

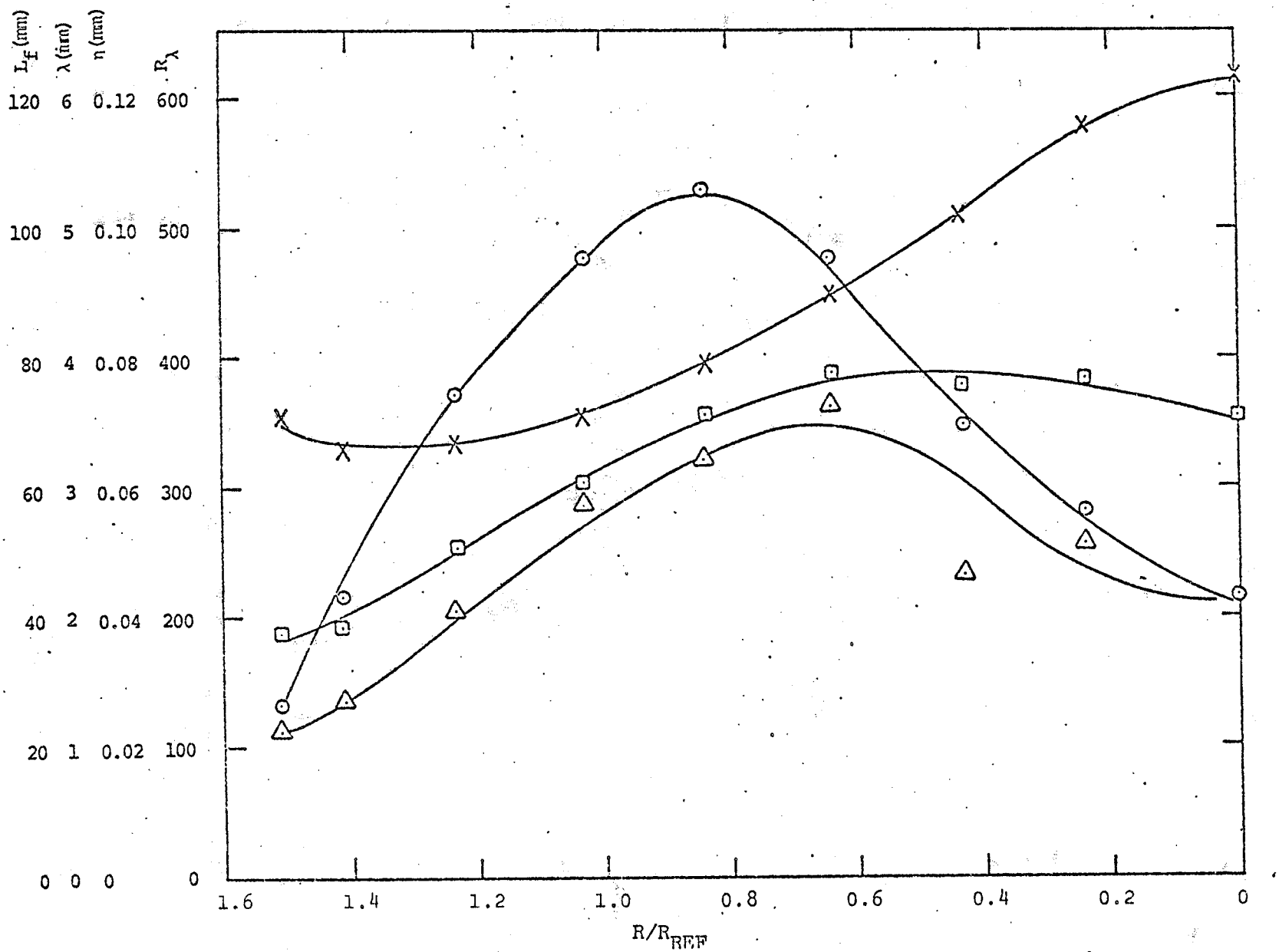

Figure 5.1 Distribution of R_λ, λ, L_f, and η at Stá. 30. ⊙ R_λ; ⊡ λ; △ L_f; × η.

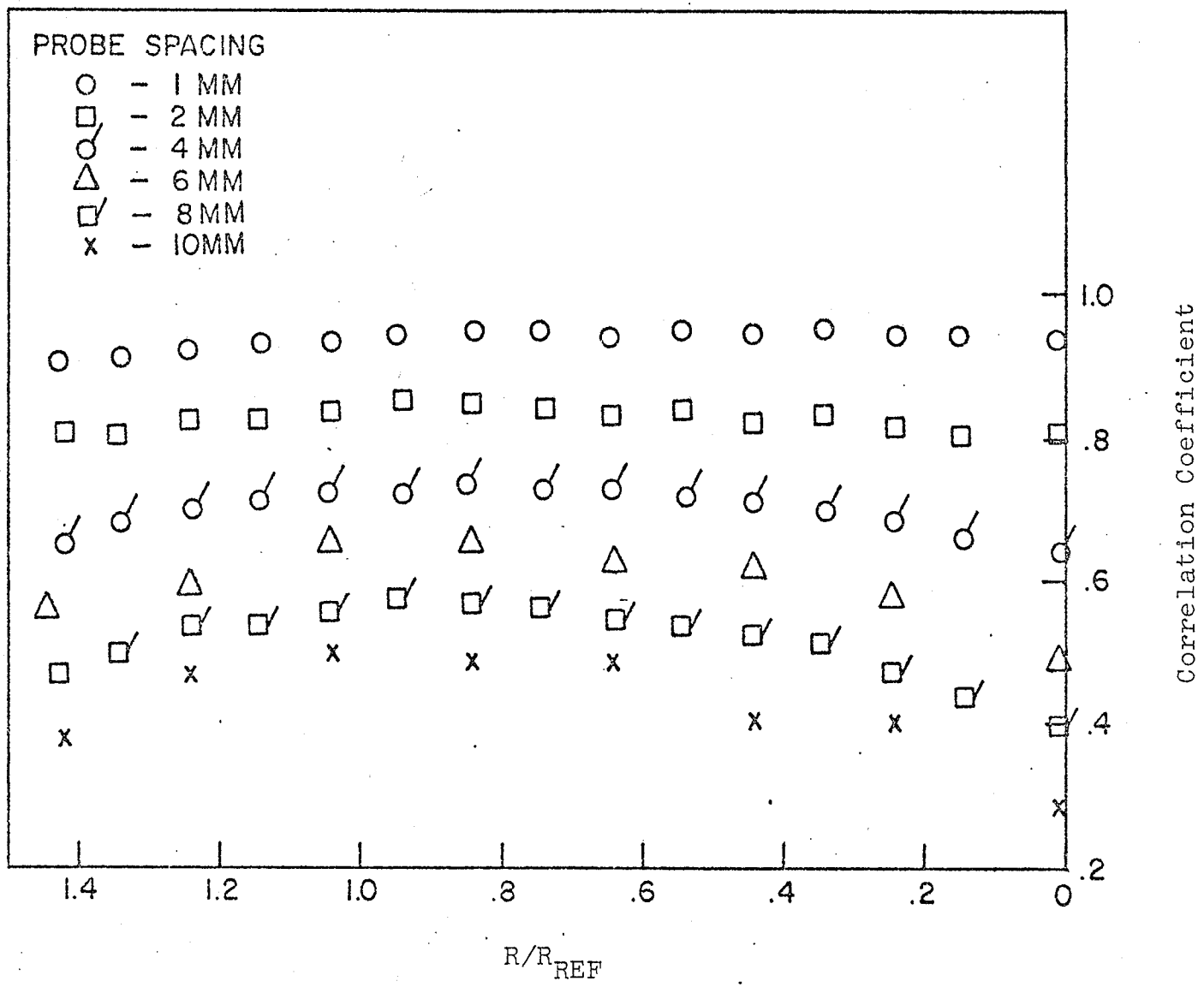

Figure 5.2 Distribution of $R_{11}(0,y,0;0)$ at Station 30.

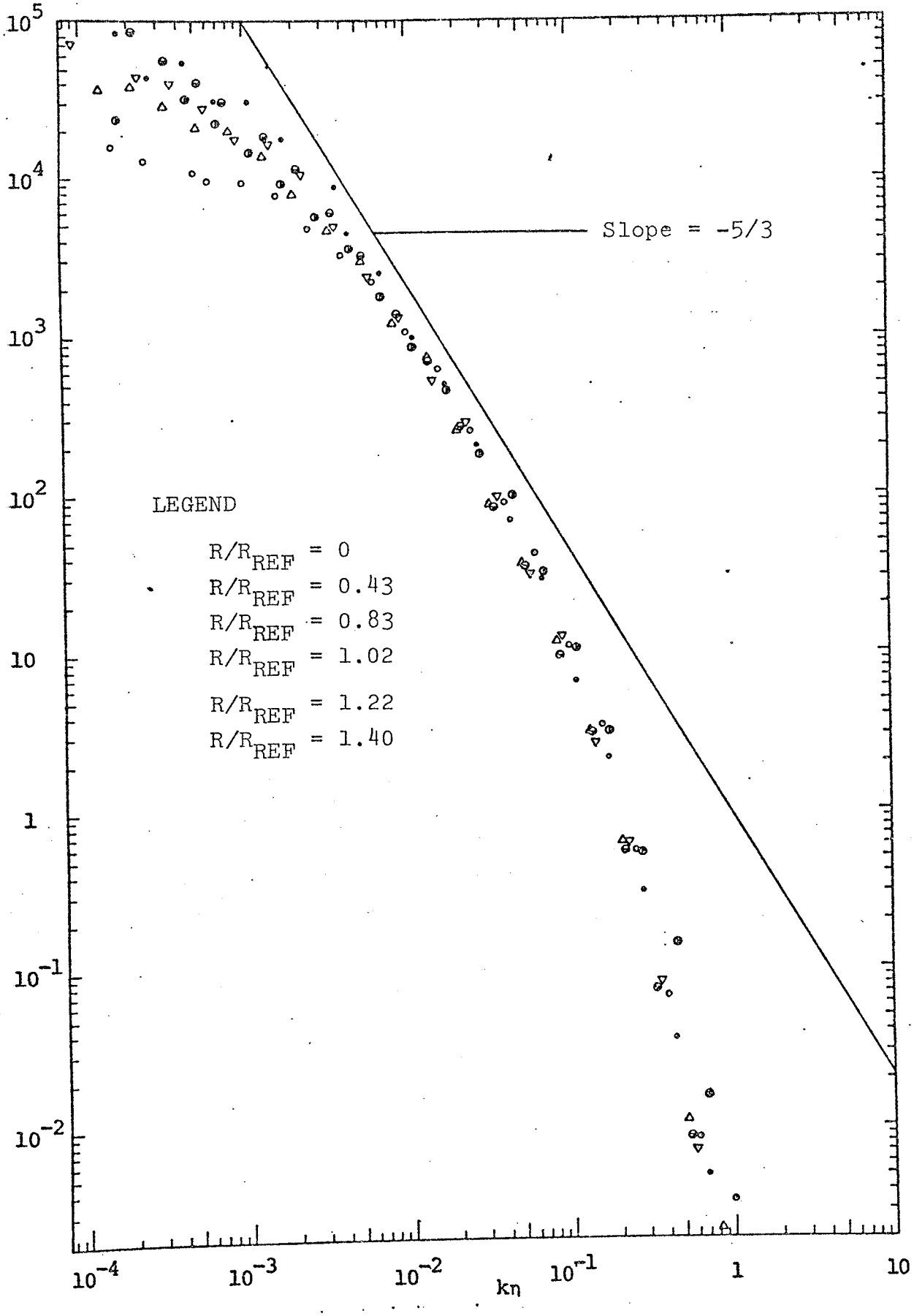

Figure 5.3 Normalized Spectra of $E_u/v_k^2\eta$ at Station 30.

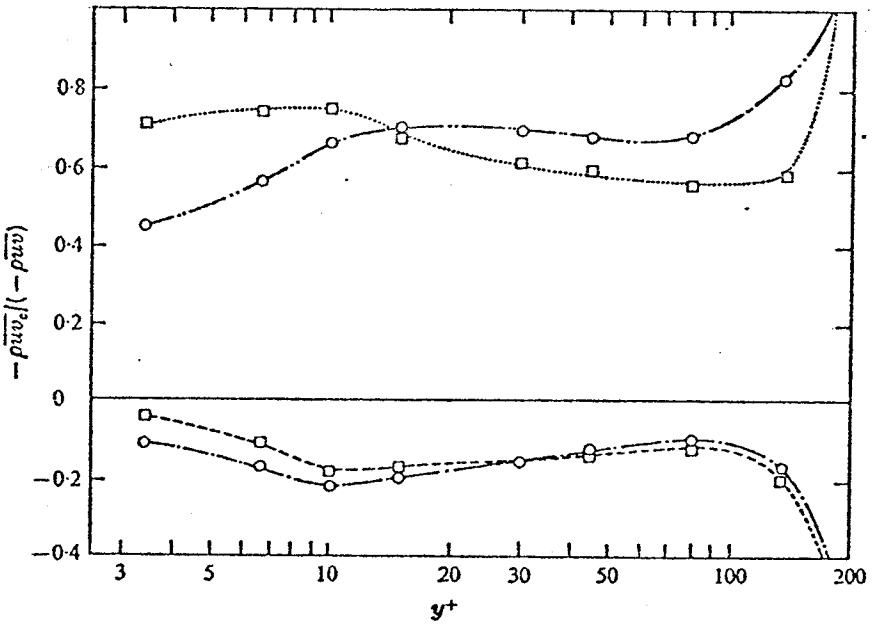

Figure 5.4 Non-dimensional truncated uv correlations for a boundary layer.

..... sweep —·—·— ejection
— — — interaction (wallward)
—·—·— interaction (outward)

(From Wallace, J.M., Eckelmann, H. and Brodkey, R.S., J. Fluid Mech. (1972) 55, part 1, p. 45).

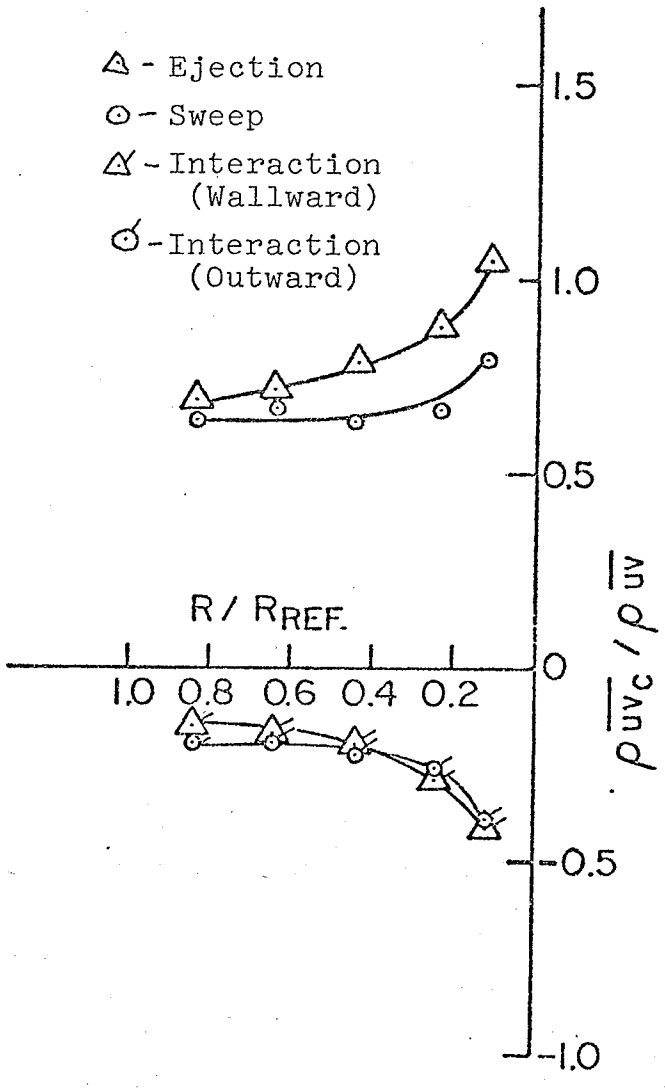

Figure 5.5 Normalized truncated uv correlations at Station 75.

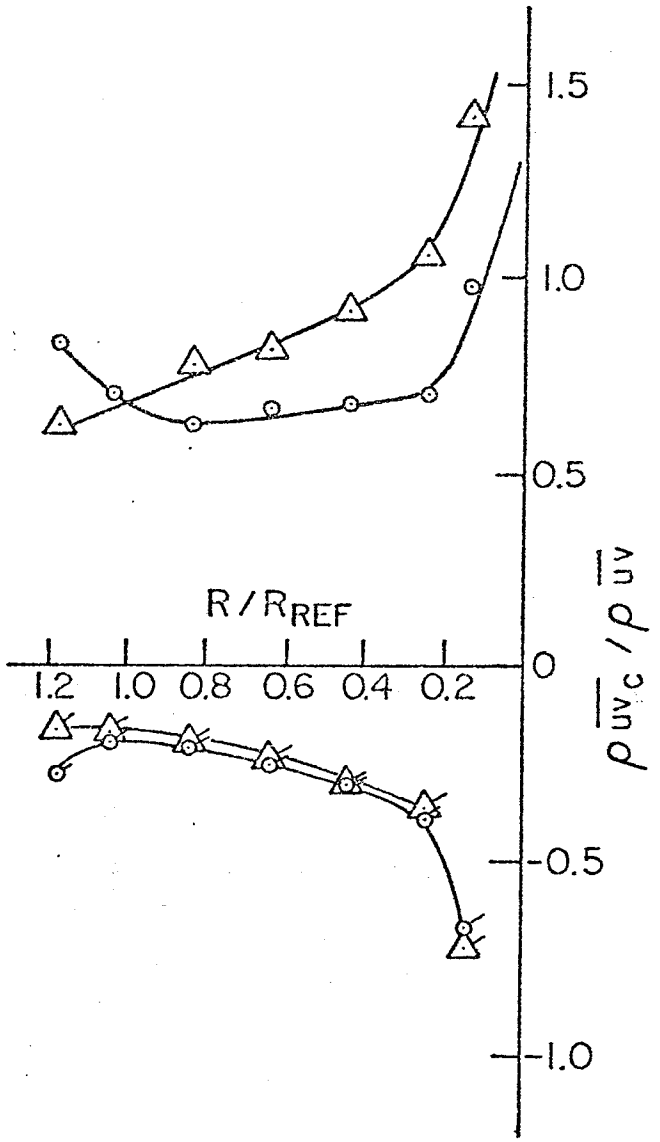

Figure 5.6 Normalized truncated uv correlations at Station 55. Symbols same as Figure 5.5.

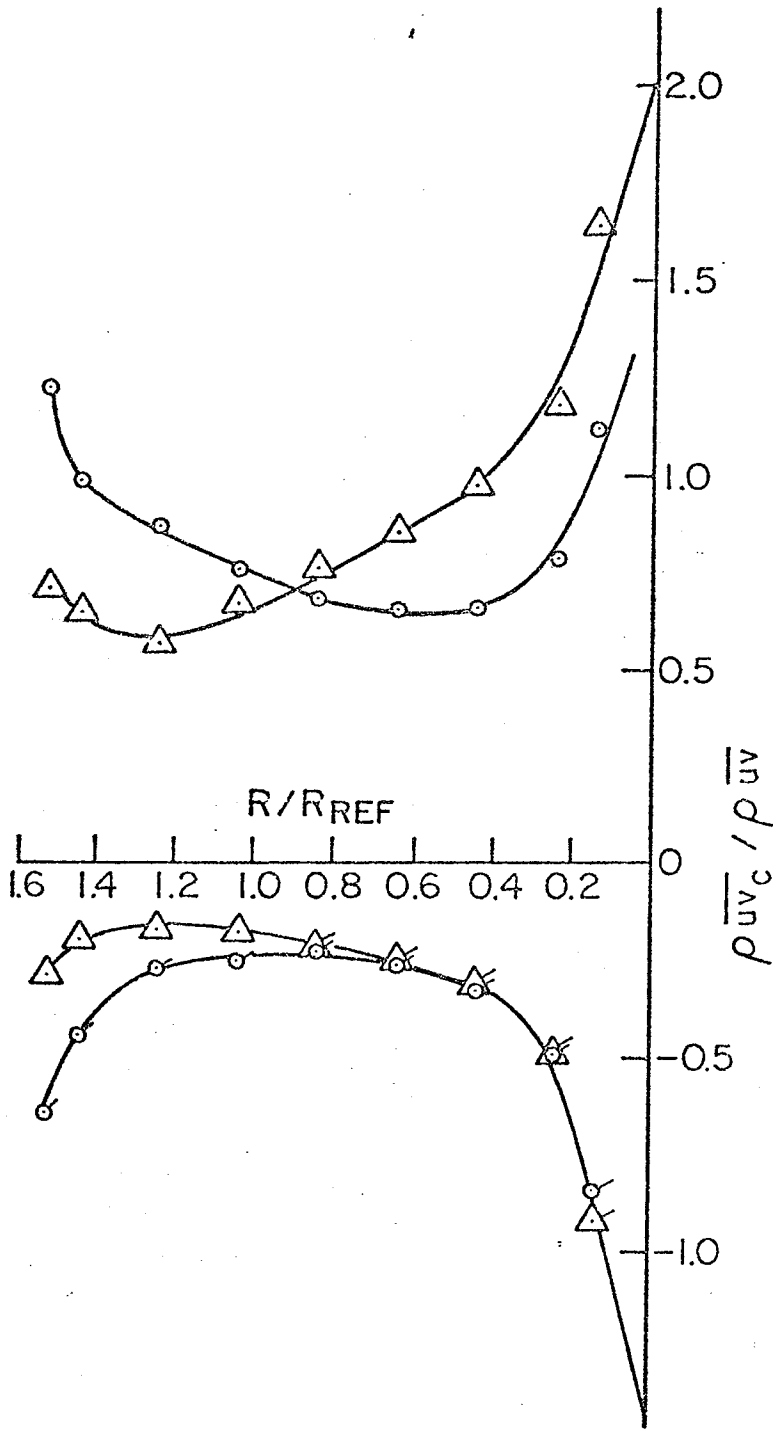

Figure 5.7 Normalized truncated uv correlations at Station 30. Symbols same as Figure 5.5.

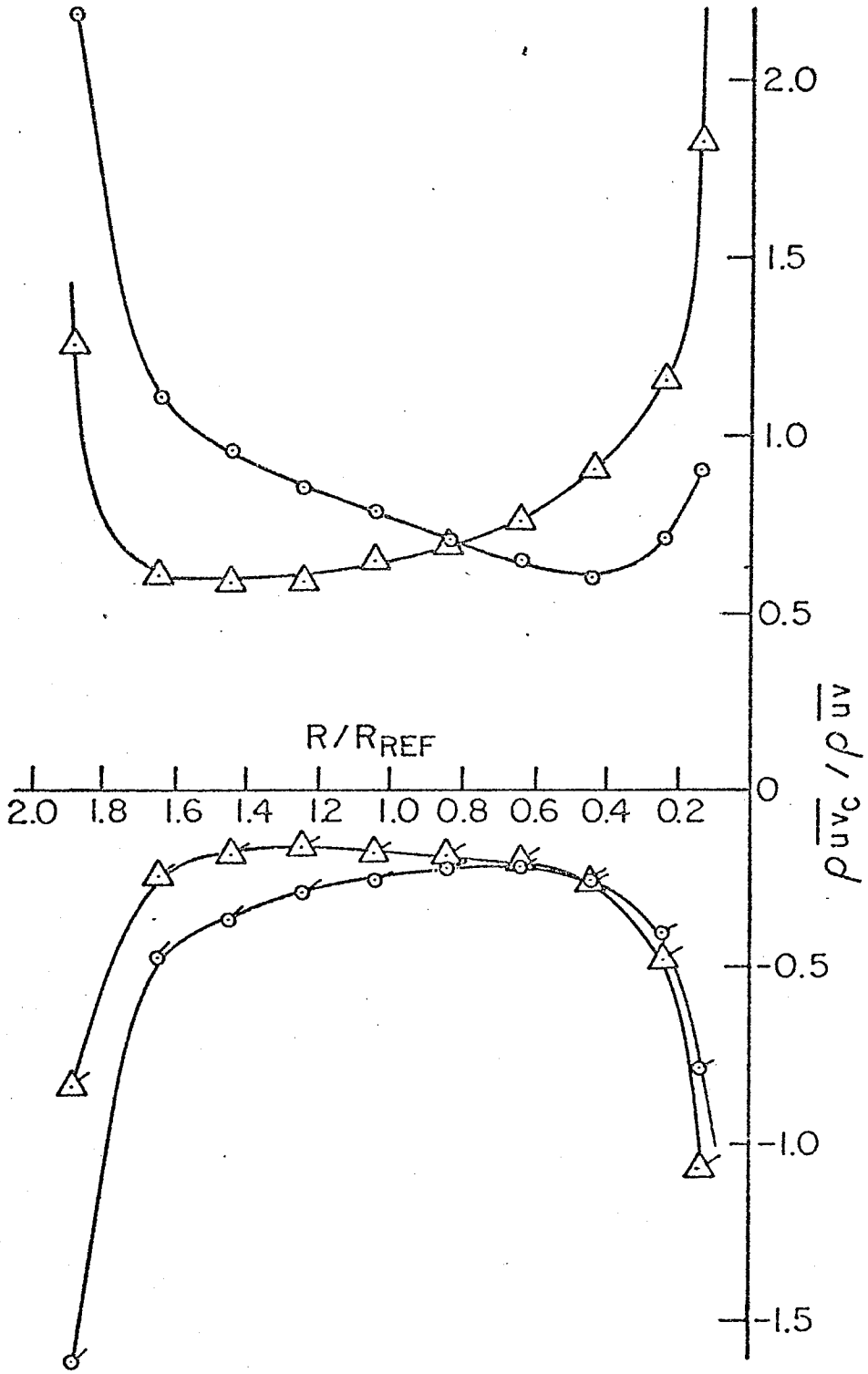

Figure 5.8 Normalized truncated uv correlations at Station 5. Symbols same as Figure 5.5.

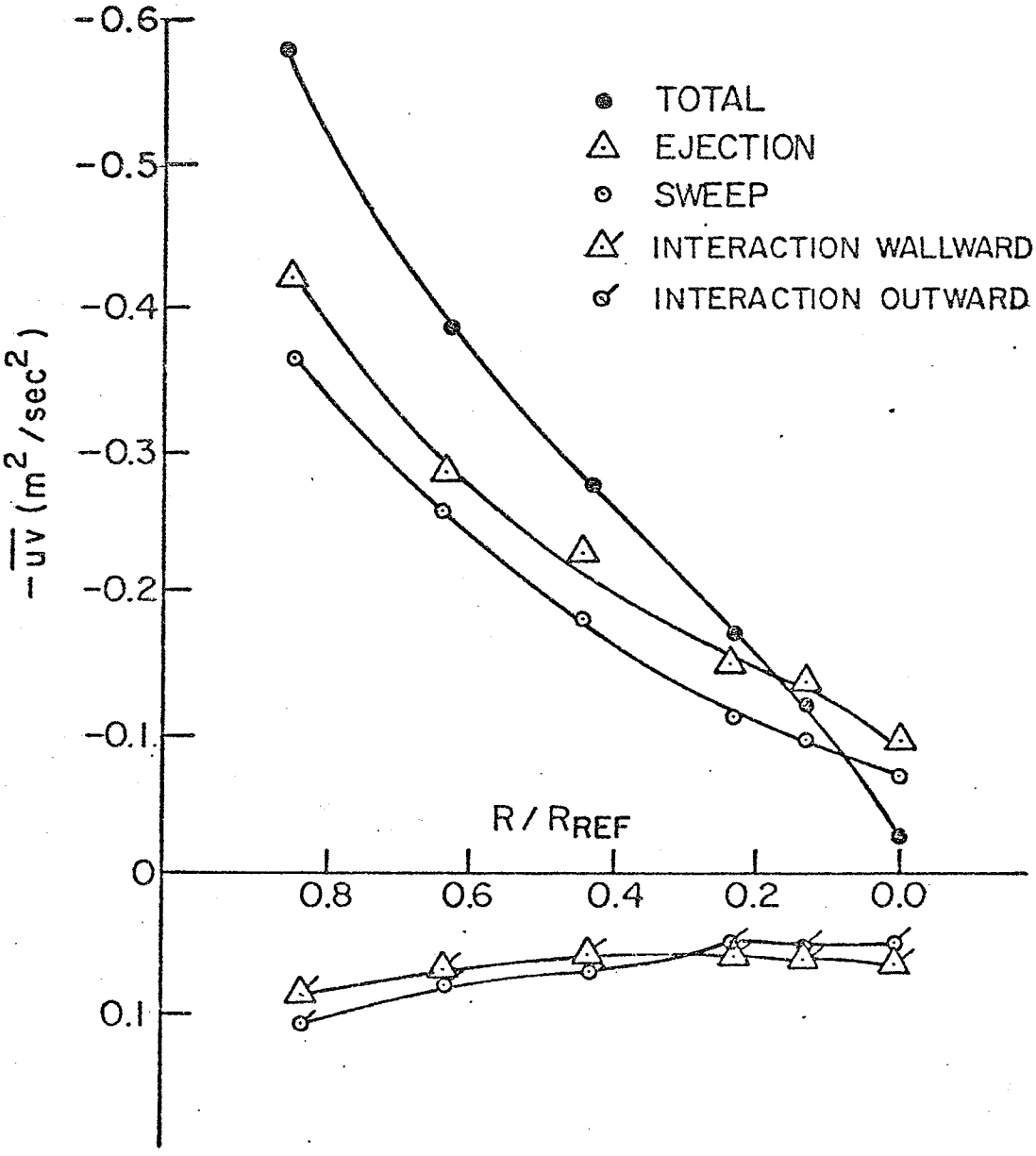

Figure 5.9 Truncated uv correlations at Station 75.

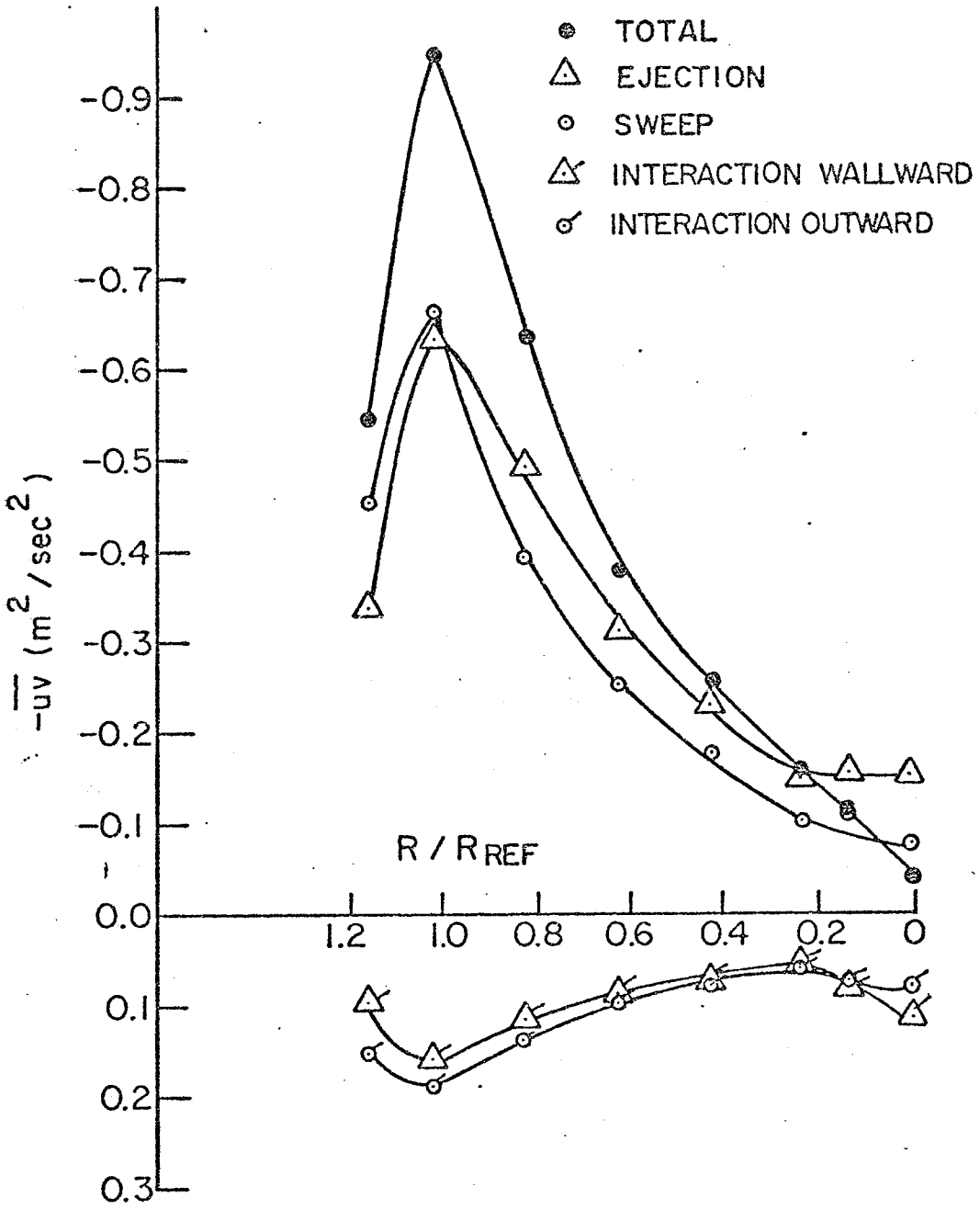

Figure 5.10 Truncated uv correlations at Station 55.

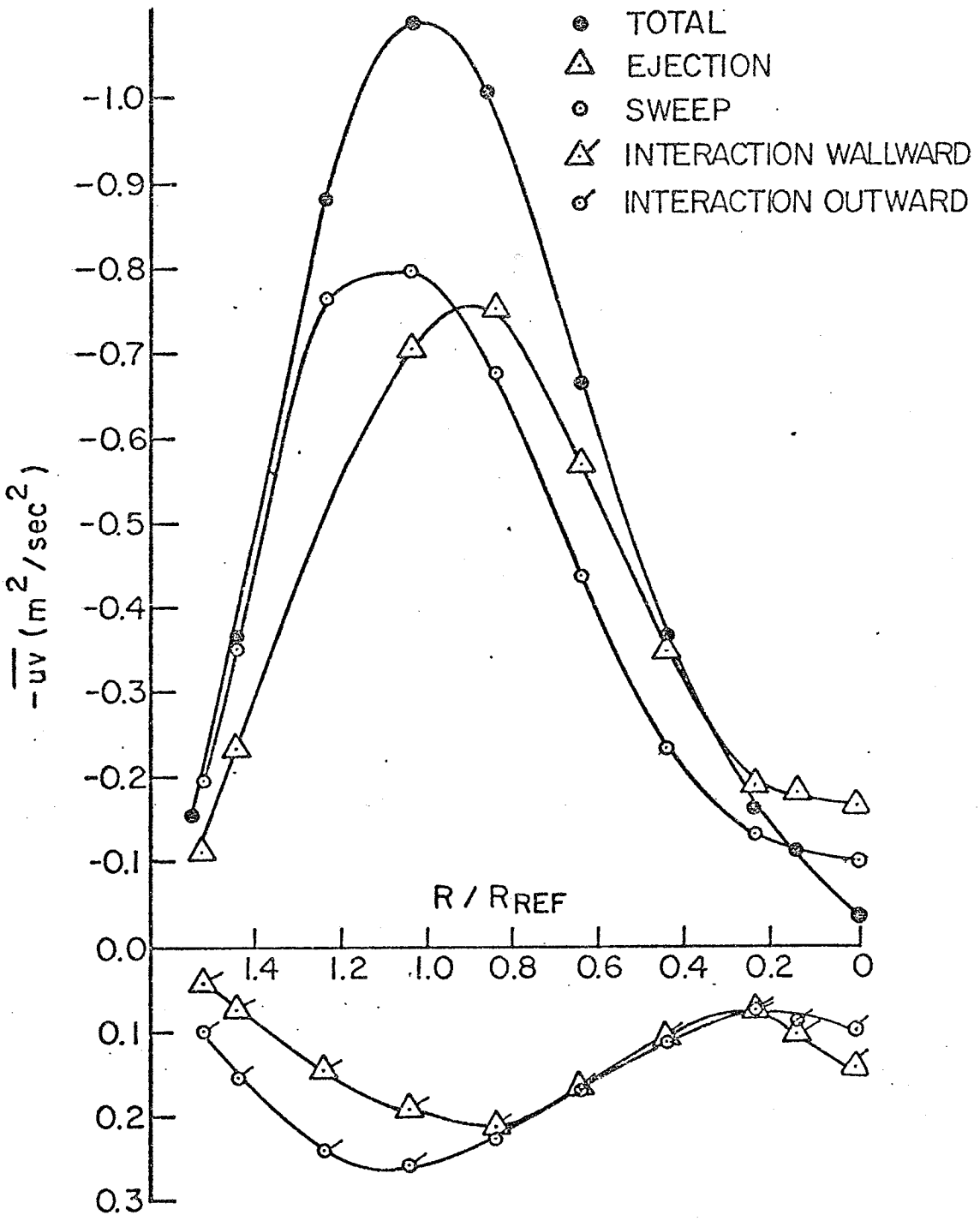

Figure 5.11 Truncated uv correlations at Station 30.

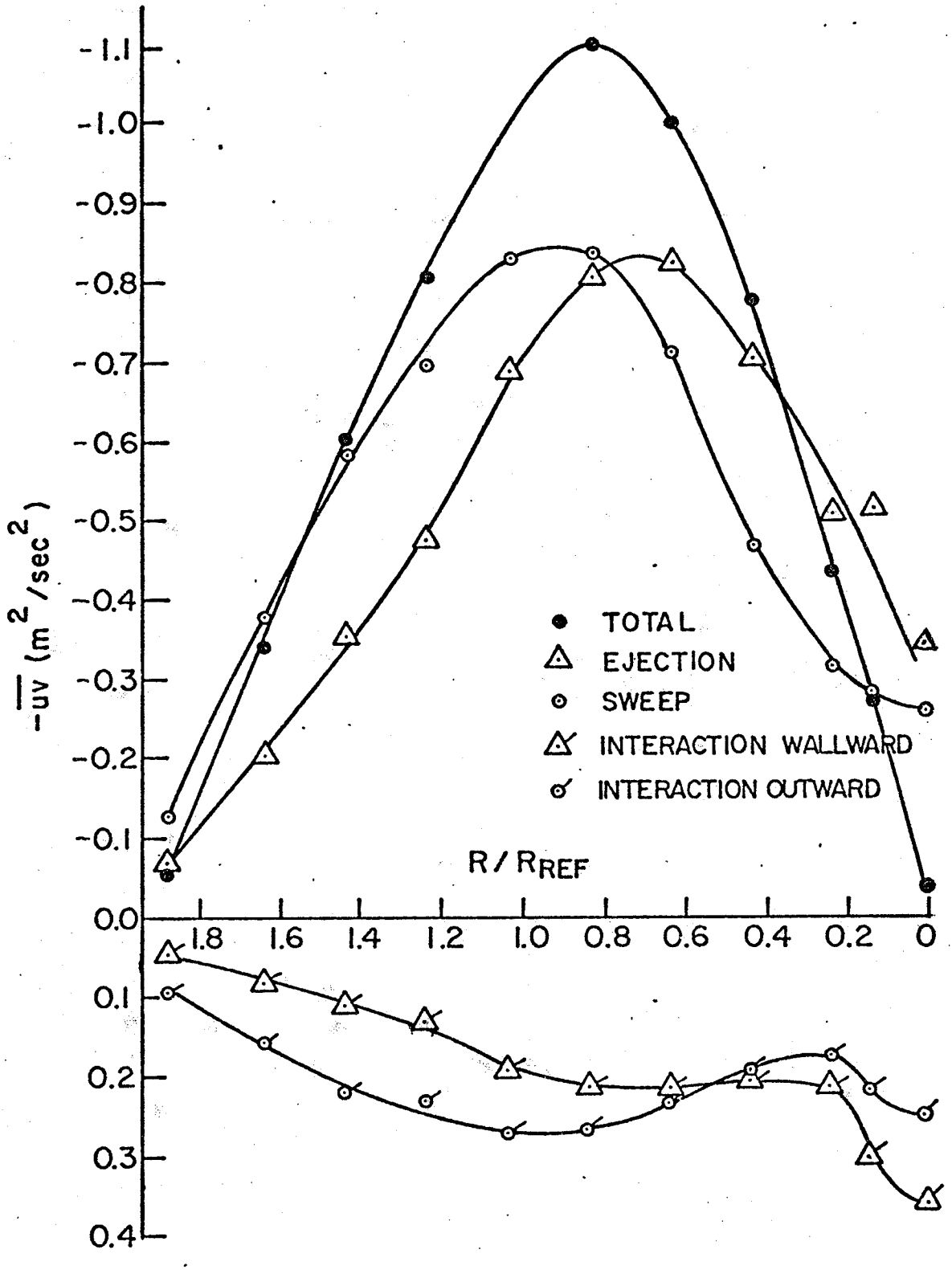

Figure 5.12 Truncated uv correlations at Station 5.

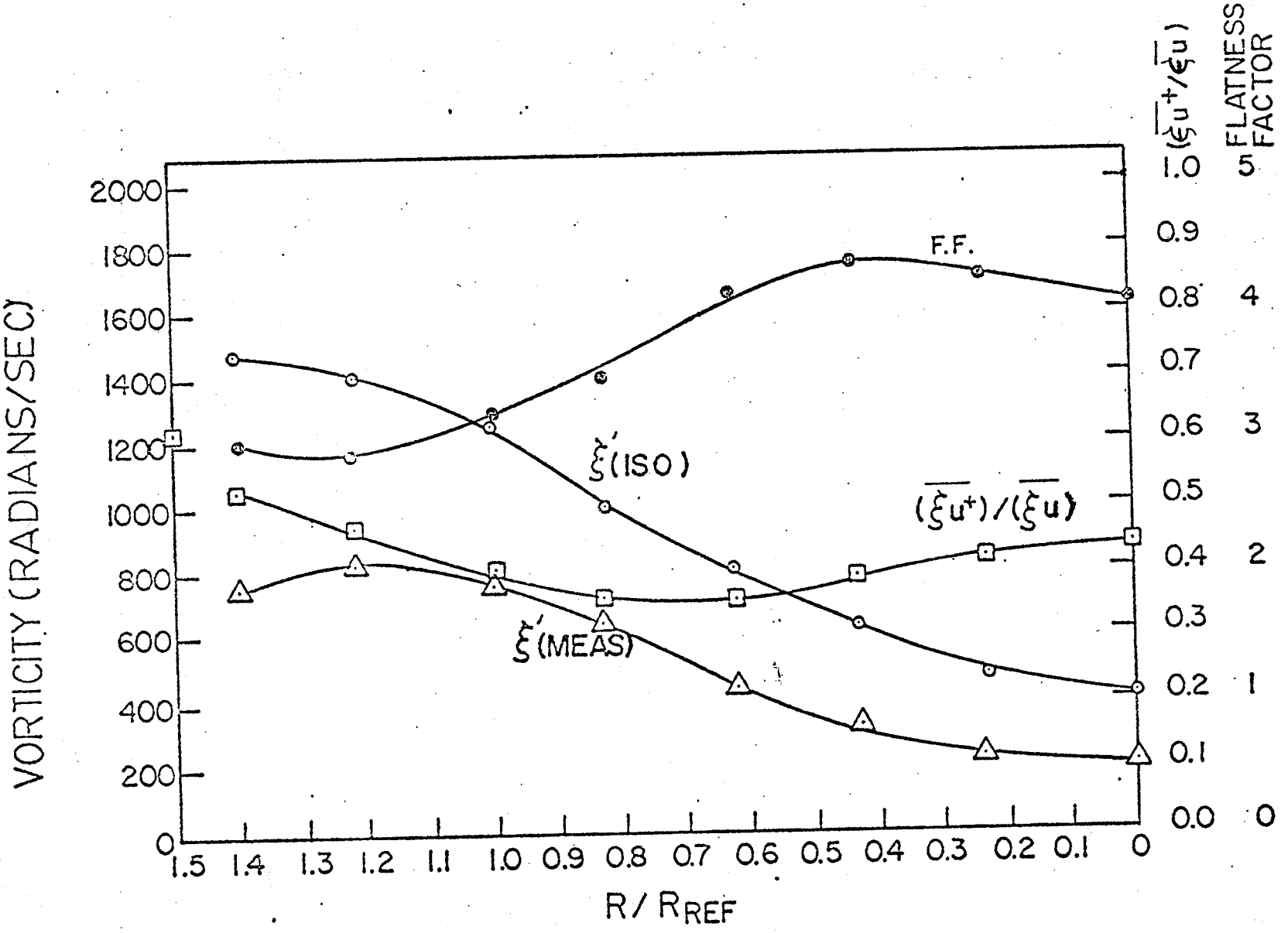

Figure 5.13 Vorticity measurements at Station 30.

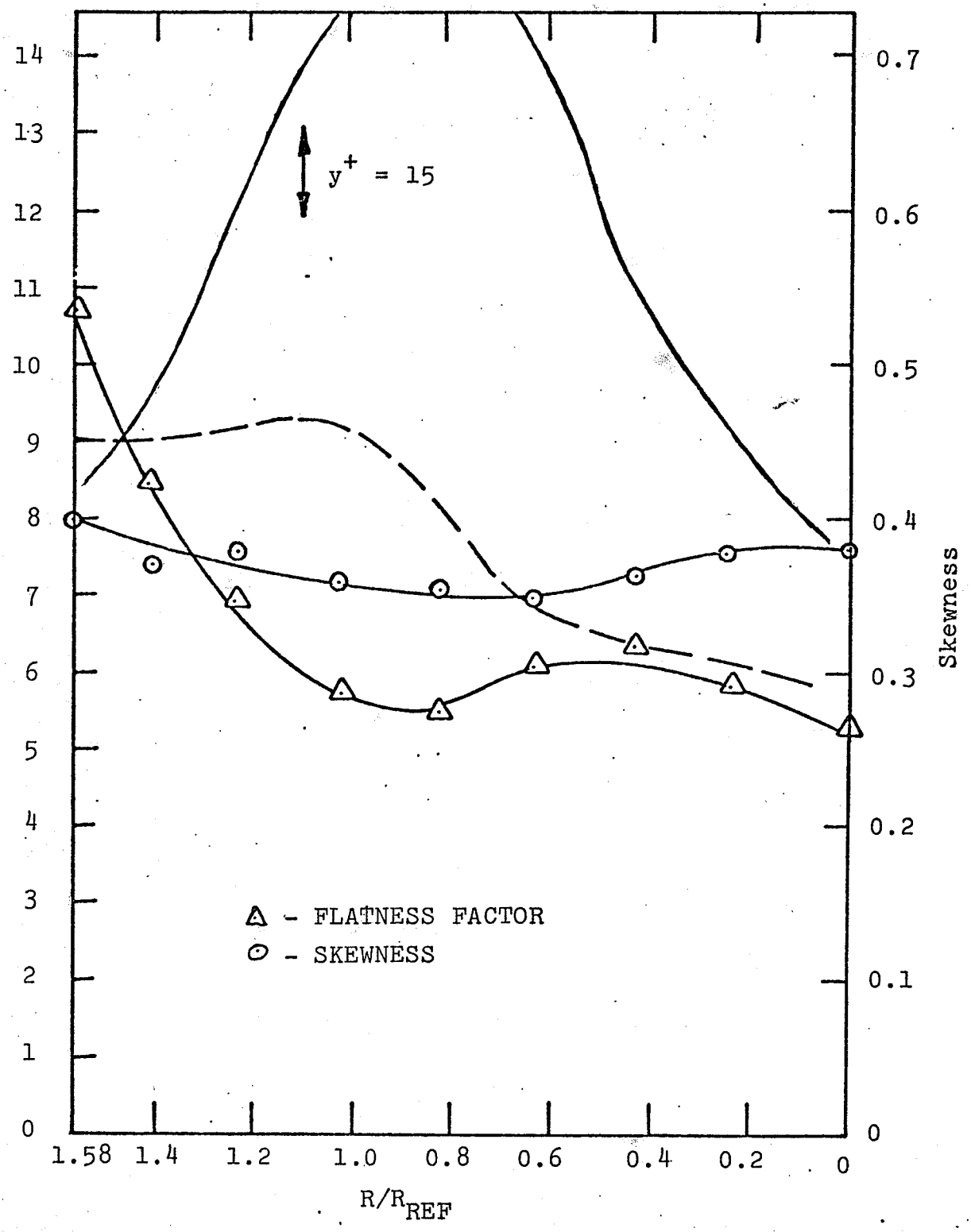

Figure 5.14 Skewness and flatness factor of $\partial u/\partial t$ at Station 30.
Trends for a boundary layer: Ueda and Hinze (1975) Skewness ————————
Flatness Factor — — — —

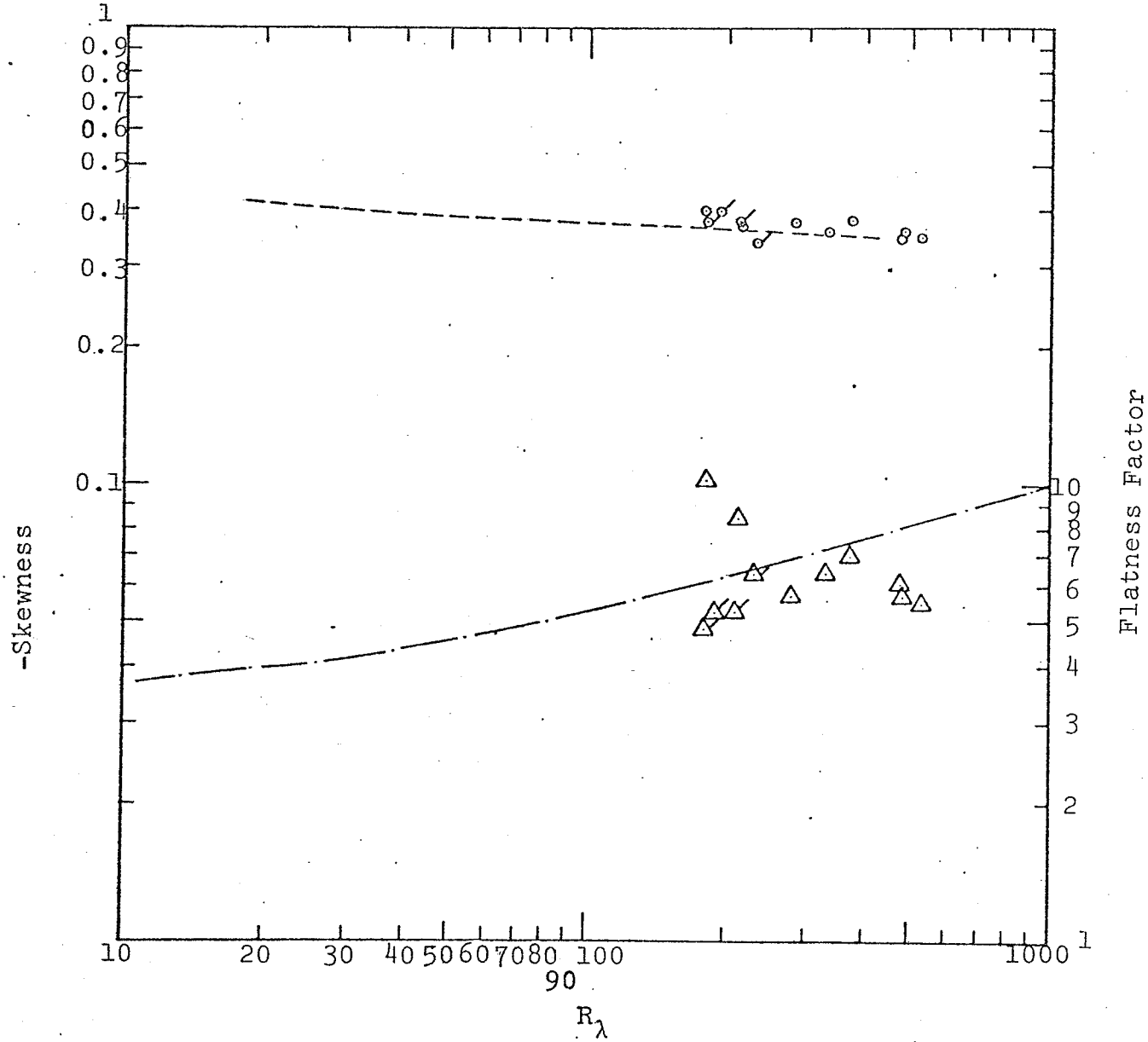

Figure 5.15 Skewness and flatness factor of $\partial u/\partial t$ vs. R_λ.

(a) Skewness: station 30, ⊙ ; center line, ⊙/.
Ueda and Hinze (1975): — — —

(b) Flatness Factor: station 30, △ ; center line △/
Ueda and Hinze (1975): — · — · —

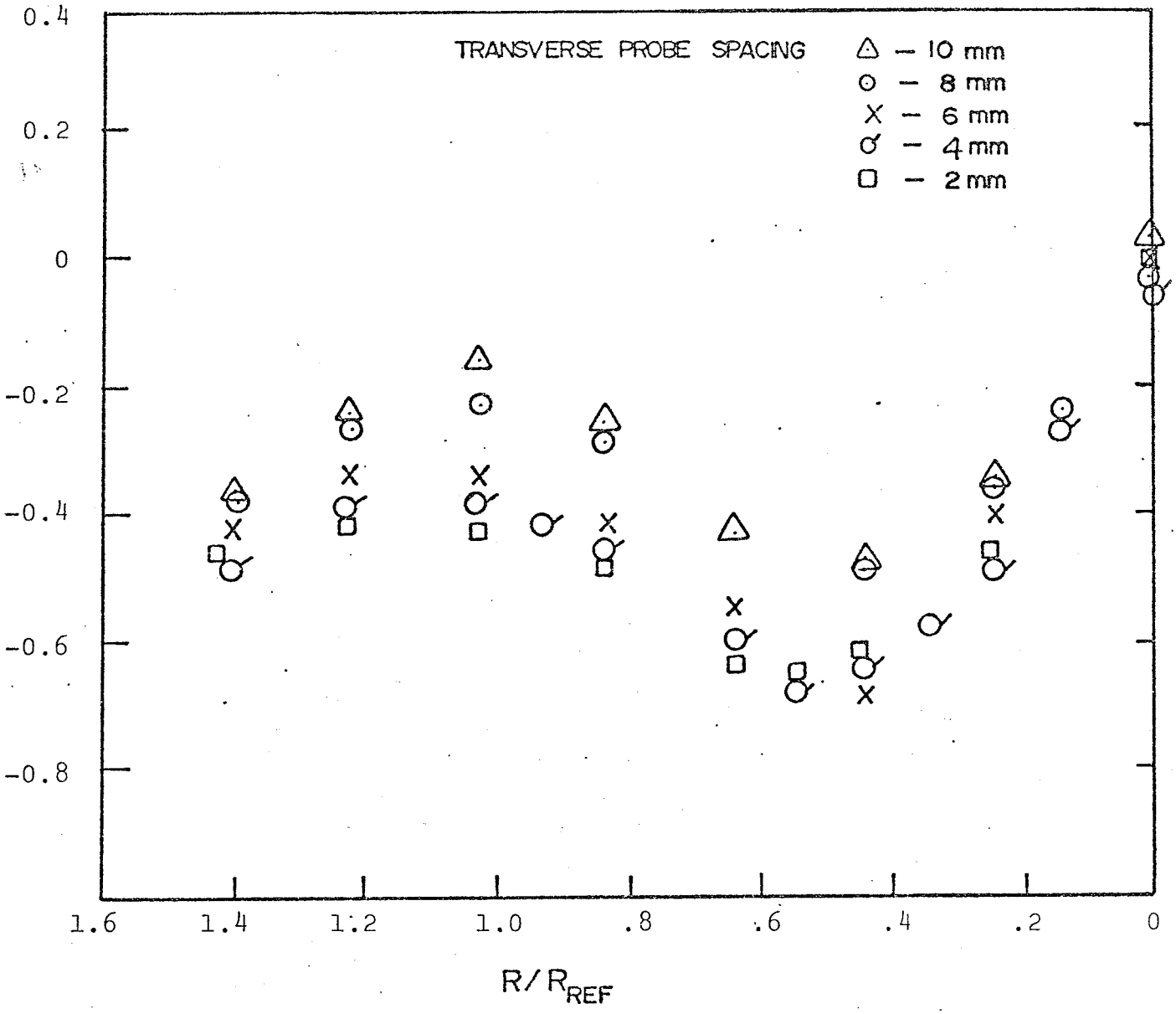

Figure 5.16 Skewness of the transverse velocity difference at Station 30.

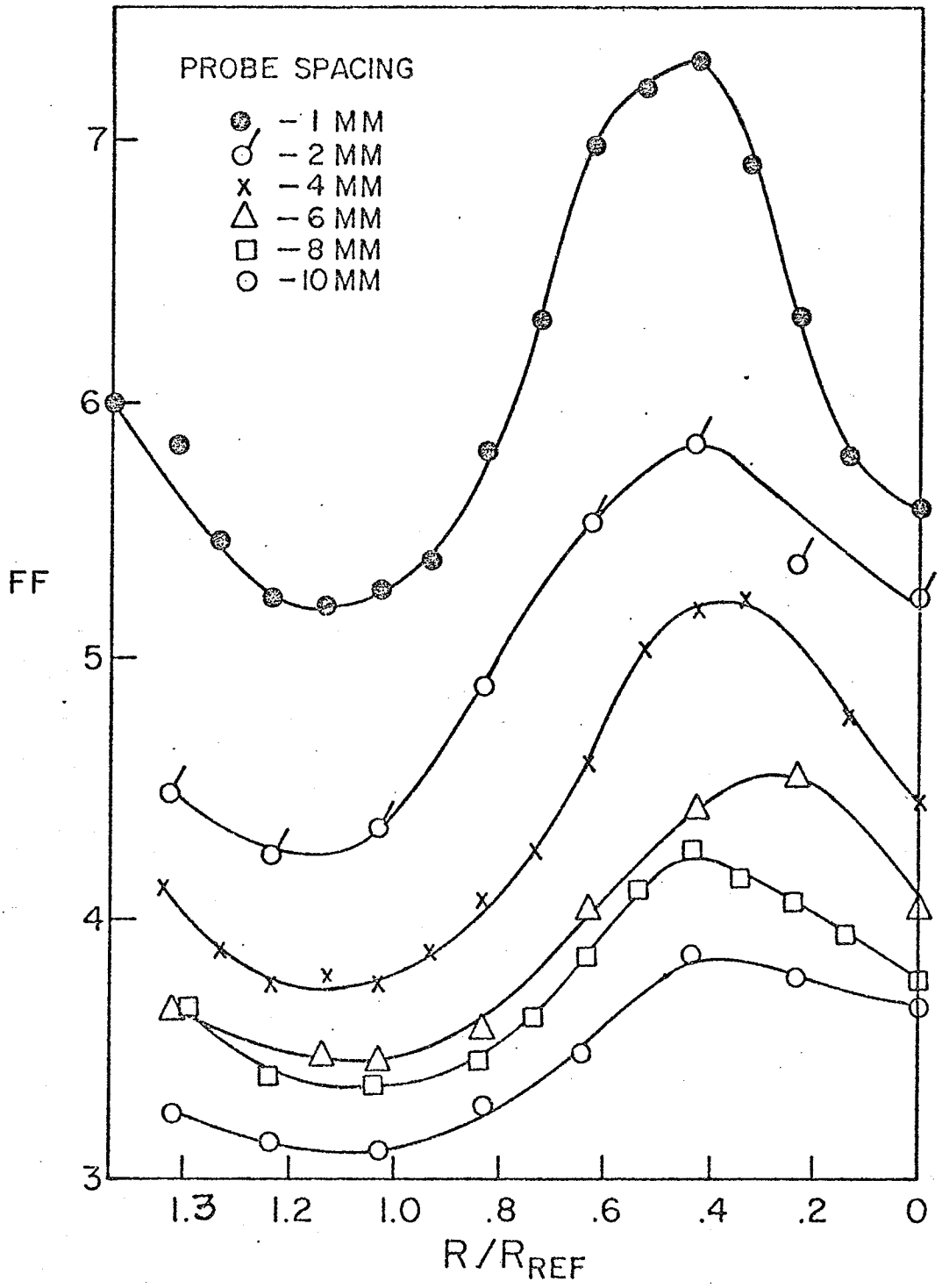

Figure 5.17 Flatness factor of the transverse velocity difference at Station 30.

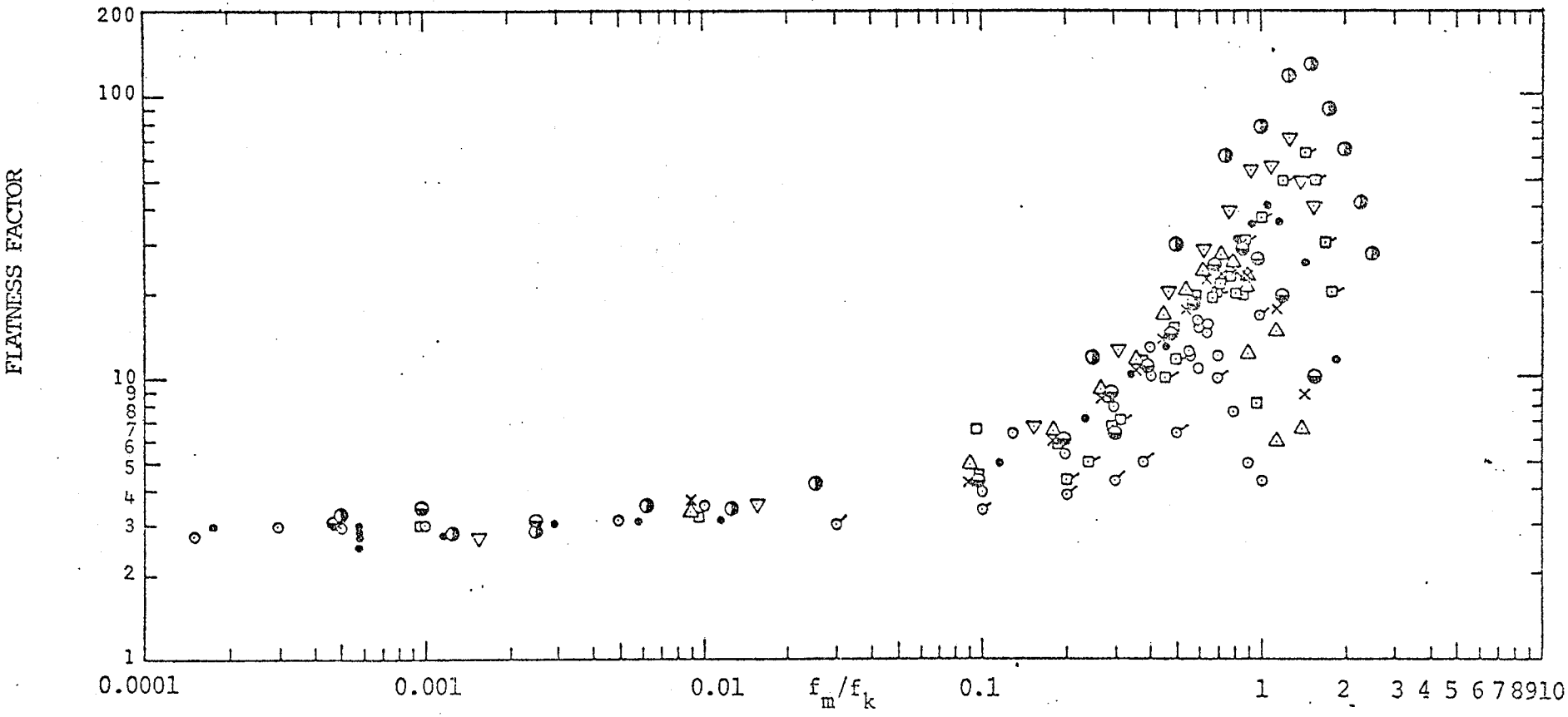

Figure 5.18 Flatness factor of narrow-band filtered u.
Kuo and Corrsin (1971), $\Delta f/fm = 0.52$, $R_\lambda = 86.5$, 110 and
Ueda and Hinze (1975), $\Delta f/fm = 0.24$, $R_{e\delta} = 35{,}500$, $y+ = 334$
Ueda and Hinze (1975), $\Delta f/fm = 0.24$, $R_{e\delta} = 35.500$, $y+ = 5.01, 21.0$

Present Results: Re = 137,000 - Sta. 30.
R/R_{REF}: 0, ⊙ ; 0.236, □ ; 0.433, △ ;
0.630, × ; 0.827, ⊖ ;
1.024, • ; 1.220, ▽ ;
1.398, ◑ .
$\Delta f/f_m = 0.43$

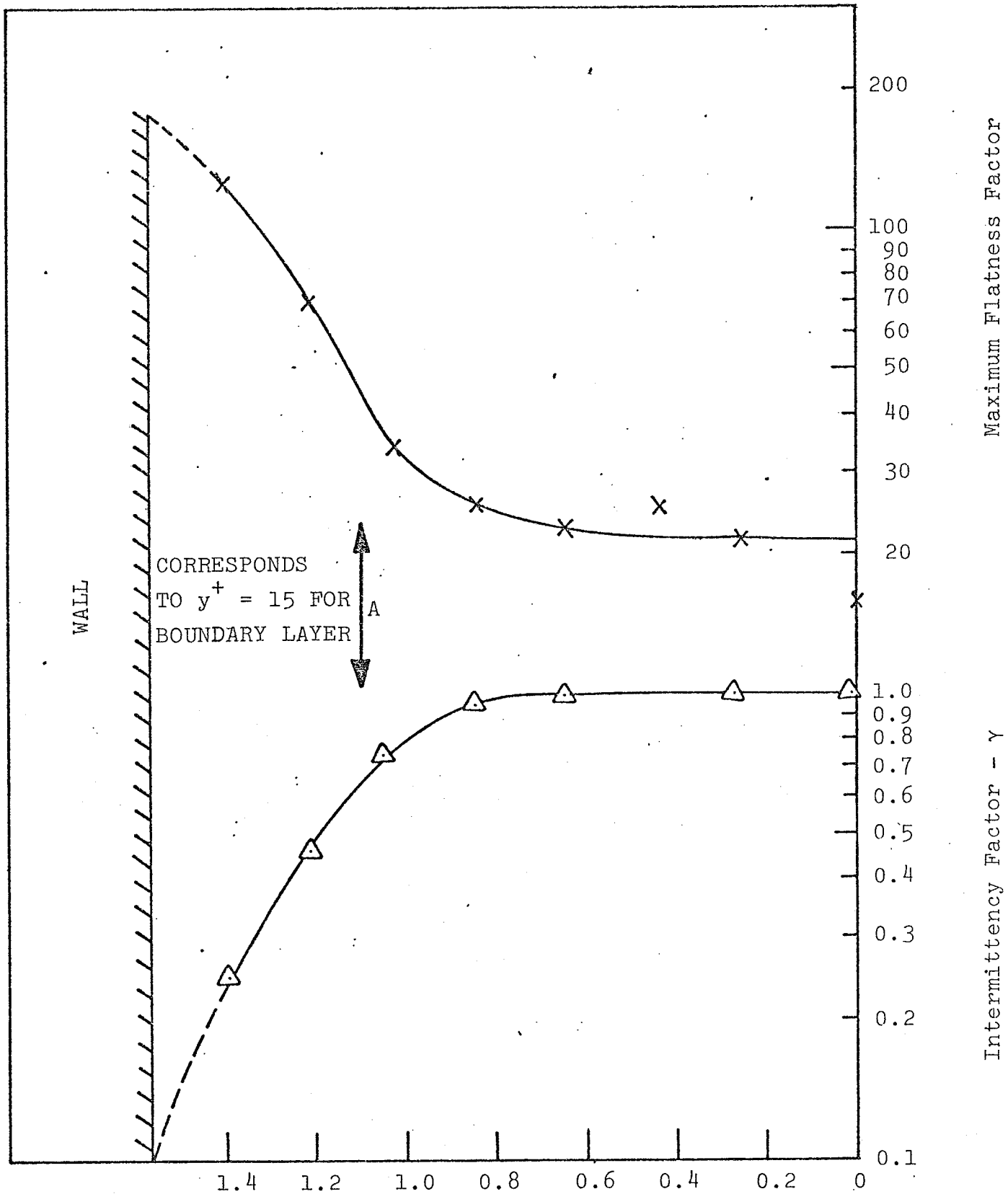

Figure 5.19 Maximum FF of narrow-band filtered u and intermittency factor of $(\partial u/\partial t)$ at Station 30.

× - Flatness factor
△ - Intermittency factor

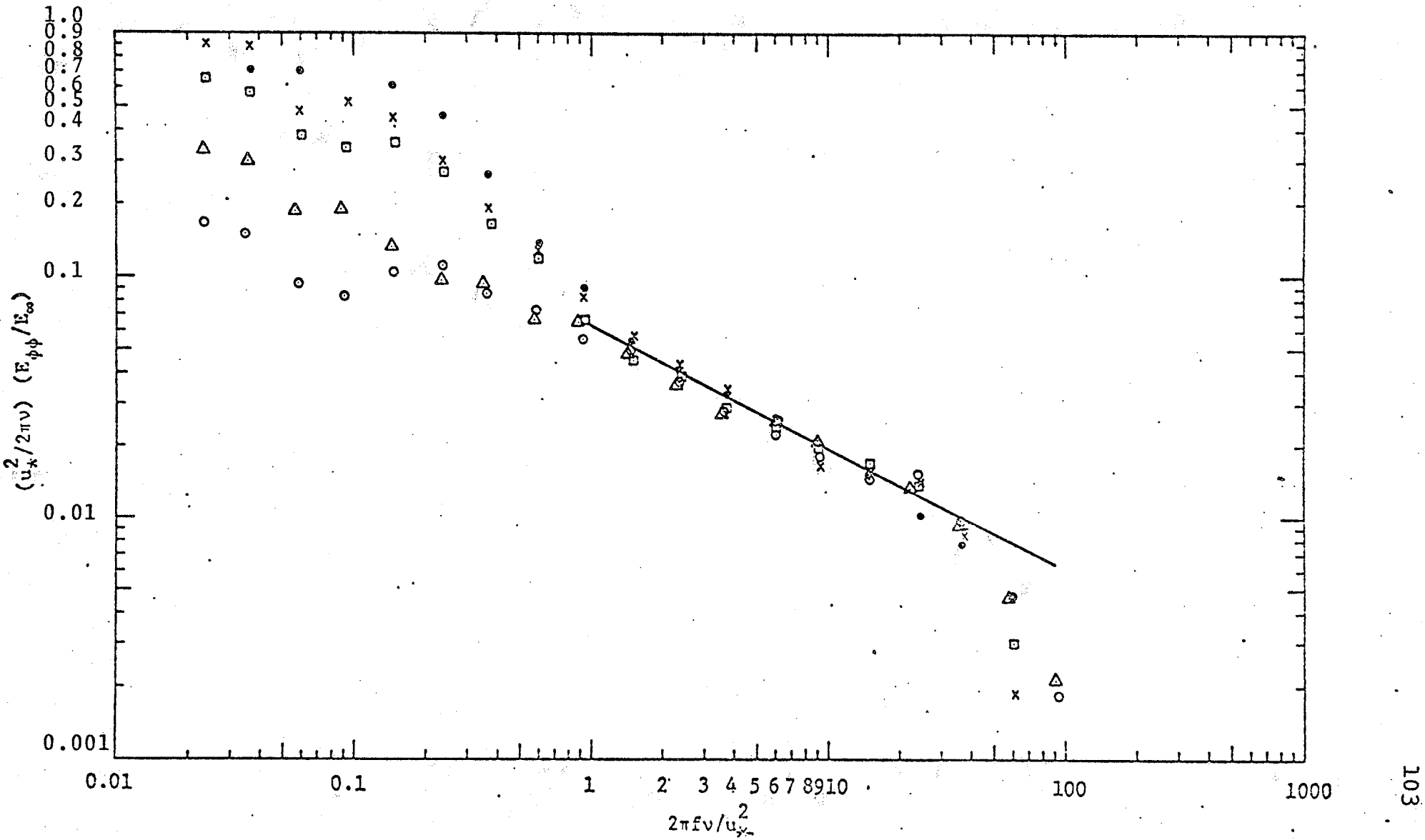

Figure 5.20 Non-dimensional spectra of $(\partial u/\partial t)^2$ at Station 30.

R/R_{PEP}: 0, ⊙ ; 1.024, △ ; 1.220, □ ; 1.398, × ; 1.496, ○ .

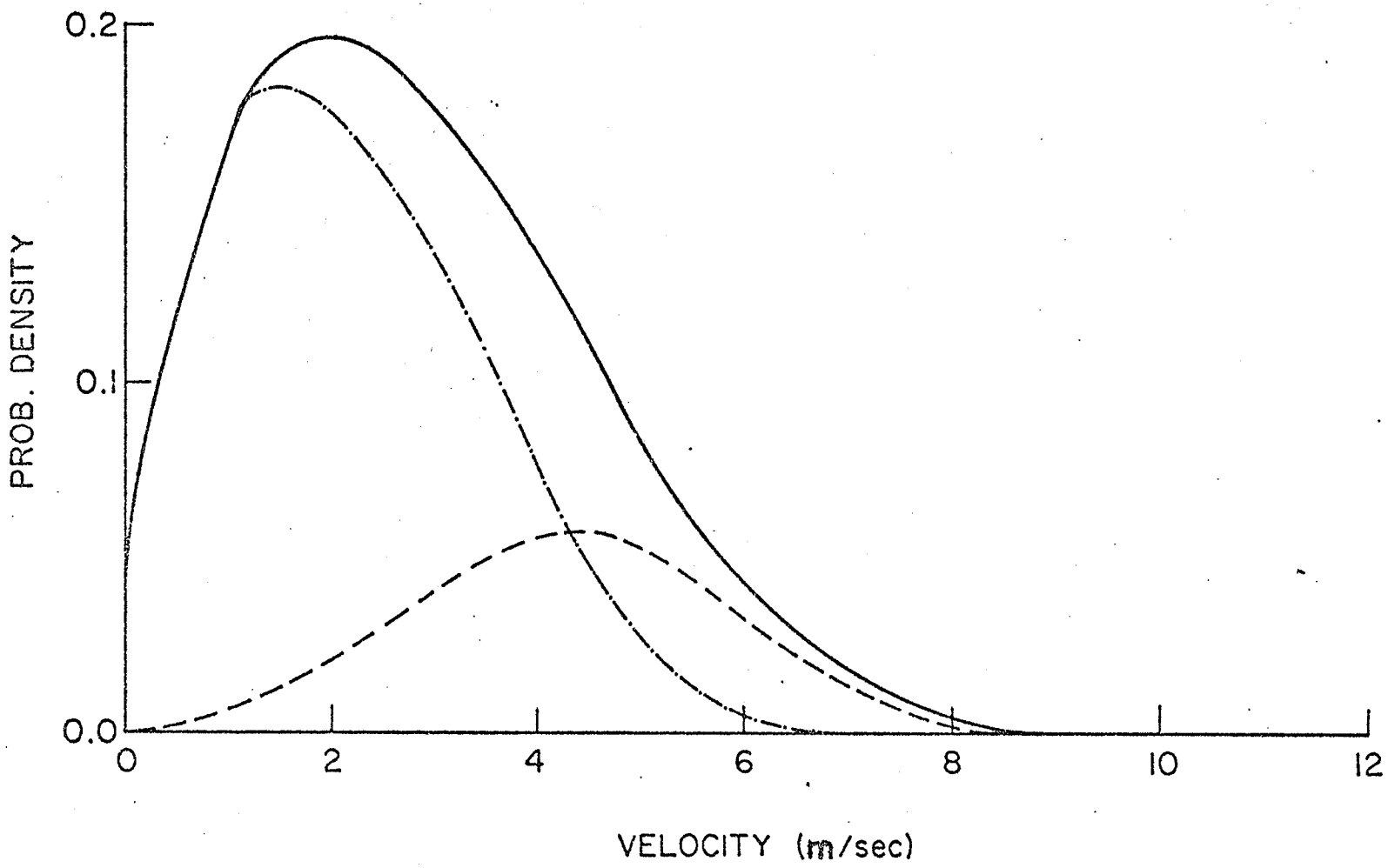

Figure 5.21 Conditional probability density functions of U at Station 30. R/R_{REF} = 1.41, γ(of $\partial u/\partial t$) = 0.26.

Total ——
Fine Structure Active — · — —
Fine Structure Inactive — — · — — —

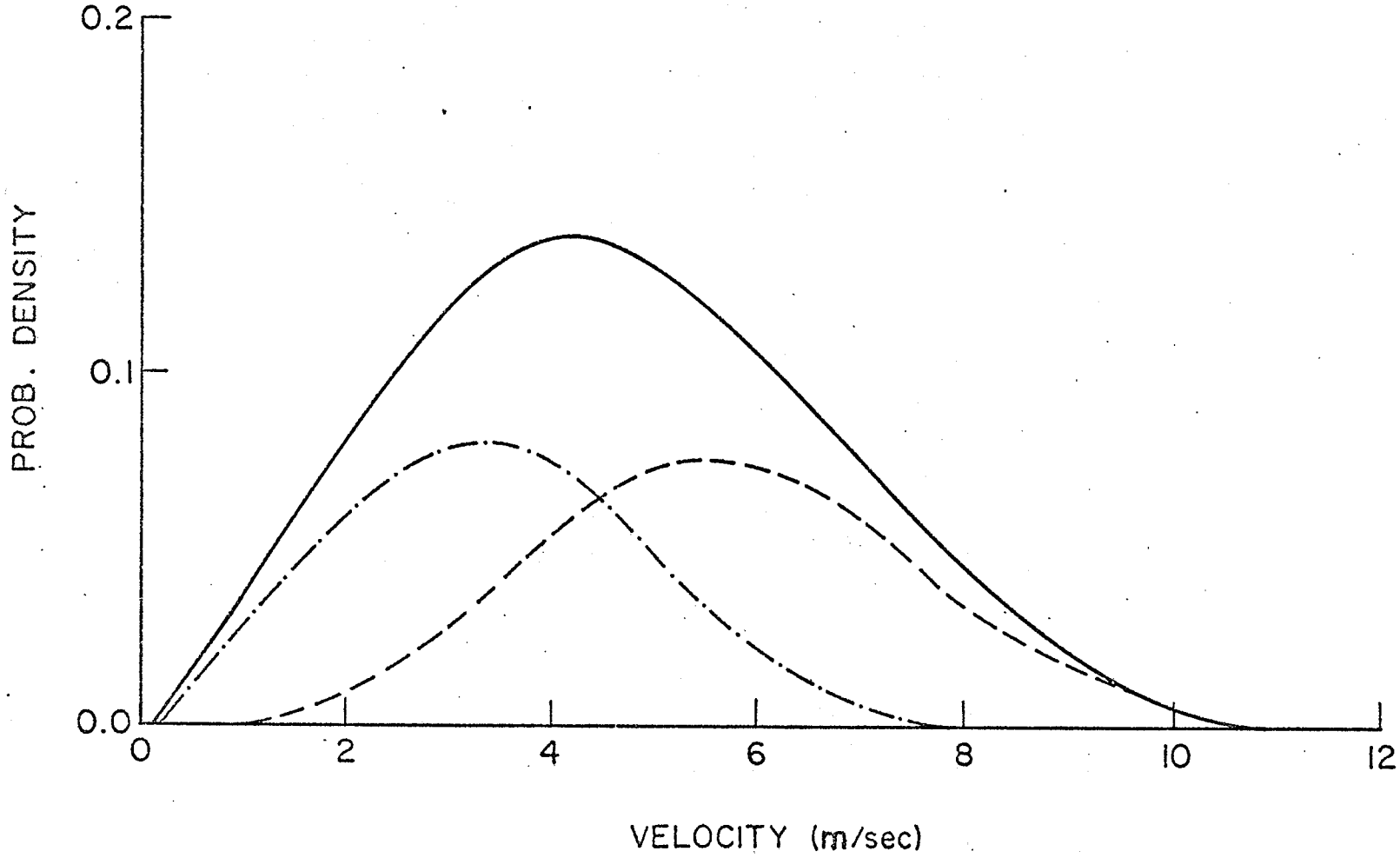

Figure 5.22 Conditional probability density functions of U at Station 30. R/R_{REF} = 1.23, γ(of $\partial u/\partial t$) = 0.47

Total ————————
Fine Structure Active — — — —
Fine Structure Inactive ——-——— —

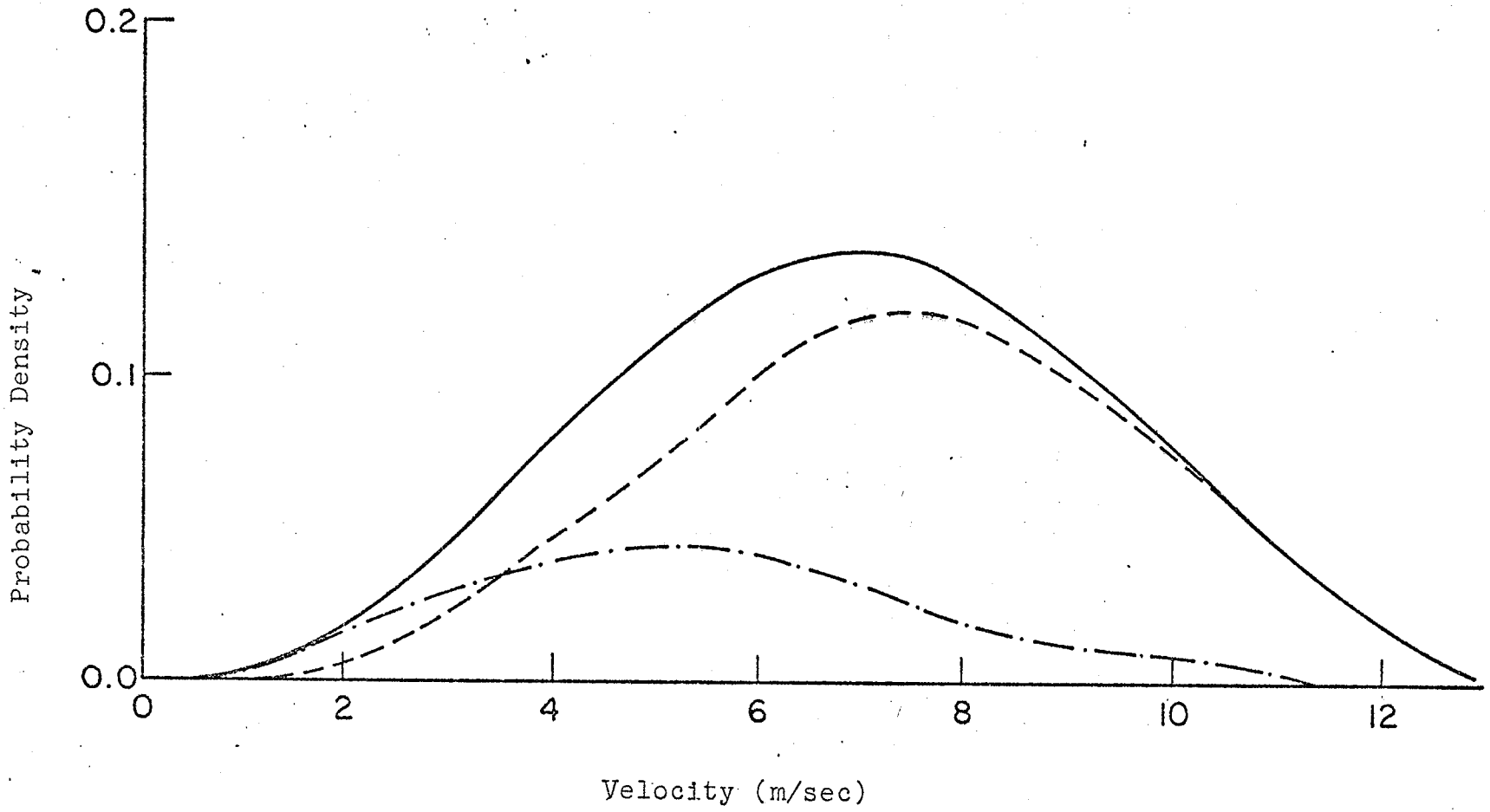

Figure 5.23 Conditional probability density functions of U at Station 30. R/R_{REF} = 1.03, γ(of $\partial u/\partial t$) = 0.74.

Total ———
Fine Structure Active — — —
Fine Structure Inactive —·—·—

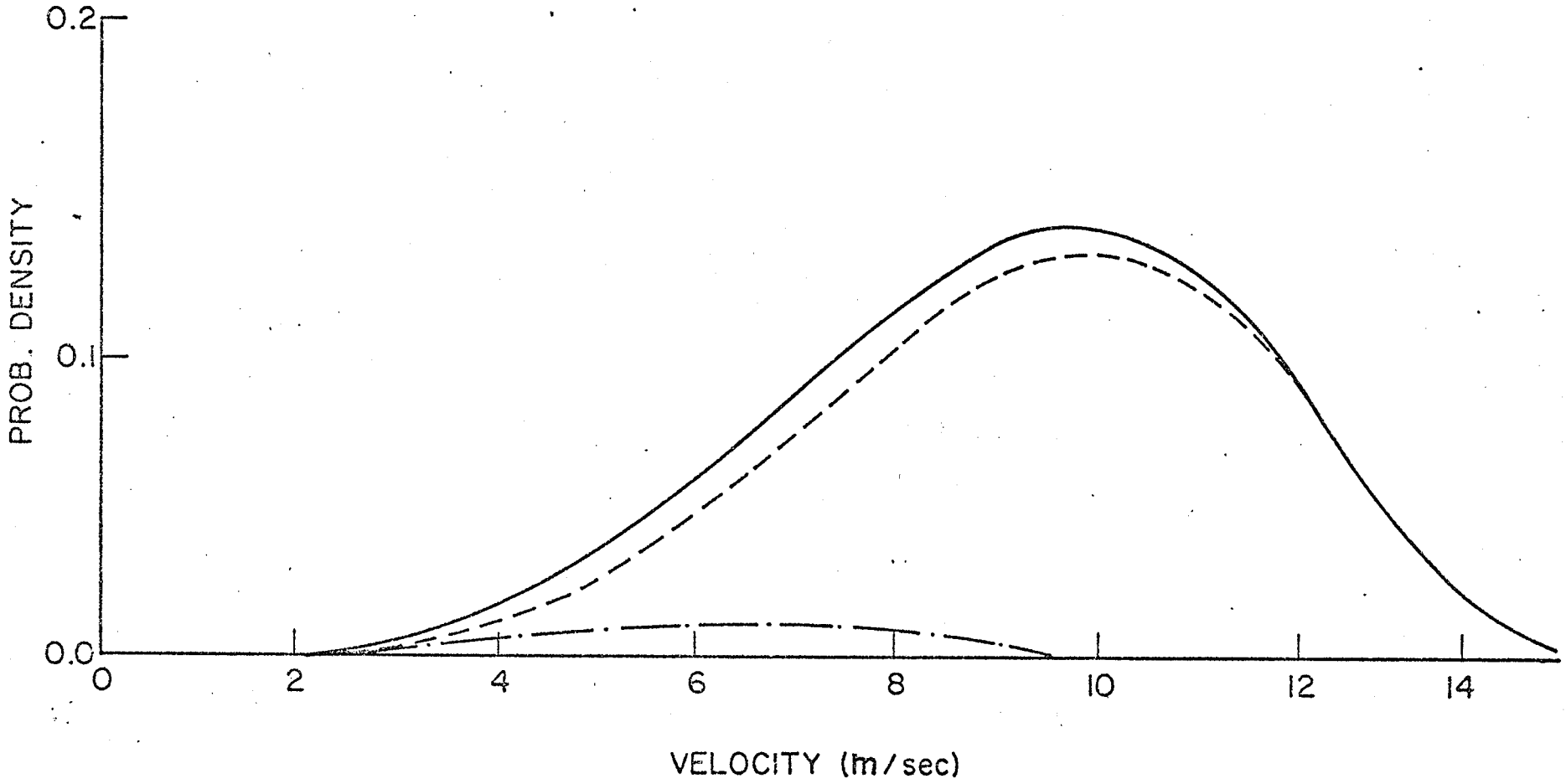

Figure 5.24 Conditional Probability Density Functions of U at Station 30. R/R_{REF} = 0.84, γ(of $\partial u/\partial t$) = 0.90.

Total ——
Fine Structure Active — — —
Fine Structure Inactive —·——·—

6.0 STRUCTURE FUNCTIONS EXPERIMENTS

A non-normalized structure function of order n is defined by $\overline{(u_1 - u_2)^n}$ where u_1 and u_2 are the fluctuating components of the velocities in the main flow direction measured at different positions in space. They are usually normalized by the Kolmogoroff velocity scale, v_k. As discussed in Chapter 2, the structure functions can be used to indicate the existence and extent of an inertial subrange.

Van Atta and Chen* (1970) have measured longitudinal structure functions in the atmosphere at various distances over an ocean surface. For the present work both longitudinal and transverse structure functions were measured up to the fourth order at station 30, with Re = 137,000. Since the third and fourth order structure functions are related to skewness and flatness factor measurements, data and discussion concerning these quantities are also given.

6.1 Experimental Procedure

The experiments, described in this chapter required two signals, defined by,

$$\Delta_{xr} \equiv u(x + r) - u(x),$$

and

$$\Delta_{yr} \equiv u(y + r) - u(y).$$

*Henceforth often referred to as VC.

Δ_{xr} (or the longitudinal velocity difference) is the difference of u, measured at two points in space with longitudinal separation r, and zero separation in the remaining axes. The separation was simulated using a time delay, t (provided by the Lyric TR 61-2 tape recorder with moveable playback heads) and Taylor's hypothesis in the form $r = \bar{U}t$. To obtain this quantity only a single hot-wire probe was required.

Δ_{yr} (or the transverse velocity difference) is the difference of u, measured at two points with transverse separation, r, and no separation along the remaining axes. In this case the dual probes described in Chapter 3 were used. They provided a maximum transverse separation of 10 mm. Here, as for Δ_{xr}, the difference was obtained with a DISA 55D26 signal conditioner in the "subtract" mode.

The non-normalized second order structure functions, $D_{LL}(r)$ and $D_{NN}(r)$ were obtained by measuring the mean square values of Δ_{xr} and Δ_{yr} respectively with a DISA 55D35 rms voltmeter. The skewness and flatness factor of Δ_{xr} and Δ_{yr} were measured with the circuit shown in section 3.4. The skewnesses are abbreviated $S_{\Delta x}$, and $S_{\Delta y}$ respectively and the flatness factors, $F_{\Delta x}$ and $F_{\Delta y}$ respectively.

The remaining structure functions were calculated from,

$$D_{LLL} = S_{\Delta x} \cdot D_{LL}^{1.5}$$

$$D_{LLLL} = F_{\Delta x} \cdot D_{LL}^{2}$$

$$D_{NNNN} = F_{\Delta y} \cdot D_{NN}^{2}$$

6.2 Experimental Results

6.2.1 Flatness Factor and Skewness of the Longitudinal Velocity Difference

Compared with the results of VC, as shown in Figure 6.1, $F_{\Delta x}$ for the diffuser is less than that of atmospheric turbulence but greater than that of grid turbulence. Furthermore, it decays to the gaussian value of 3 for r/η at least 2 orders of magnitude less than is the case for atmospheric turbulence.

According to the "constancy of skewness" theory, discussed in Chapter 2, the skewness, $S_{\Delta x}$ should be constant in the inertial subrange. In the present case (Figure 6.2) this skewness is approximately constant with a value of -0.25 for $50 < r/\eta < 200$. By comparison, the atmospheric turbulence data of VC show a much larger range of r/η with constant skewness, indicating a correspondingly larger inertial subrange. For the grid turbulence,

the skewness data of VC shows no constant region thus indicating no inertial subrange.

6.2.2 Skewness and Flatness Factor of the Transverse Velocity Difference

These quantities are also discussed in section 5.6. They are replotted here as a function of the non-dimensional probe separation r/η. As shown in Figure 6.3 the flatness factors, $F_{\Delta y}$ essentially all collapse onto a single line with a slope of -0.255. The skewness, $S_{\Delta y}$ given in Figure 6.4 show no tendency to collapse.

6.2.3 Structure Functions

Structure functions, up to the fourth-order, are given in Figures 6.5 to 6.9. With the exception of those taken nearest the wall (at $R/R_{REF} = 1.4$, shown as solid circles) all of the structure functions tend to collapse onto a single line for the approximate range, $20 < r/\eta < 200$. Within this range the longitudinal second-order structure functions (Figure 6.5) follow the theoretical (Chapter 2) two-thirds law; the fourth-order structure function (Figures 6.8 and 6.9) the theoretical four-thirds law, and the longitudinal third-order structure functions

(Figure 6.7), the more specific theoretical law $D_{LLL}/v_k^3 = -0.8\ r/\eta$. For the transverse second-order structure functions (Figure 6.6) the slope in the range, $20 < r/\eta < 200$ was measured to be 0.854 as opposed to the theoretical two-thirds value. No reason for this difference can be offered.

For $r/\eta < 20$, all of the structure functions start decreasing more rapidly with decreasing r/η. For the second-order structure functions, the slopes in this region are approximately 2 as shown in Figures 6.5 and 6.6. While these slopes are appropriate for $r/\eta << 1$, (Monin and Yaglom 1975, p. 353) they already become evident in the present case for $r/\eta < 20$ as noted above. This effect can possibly be attributed to the hot-wires which were about 10η in length and hence insensitive to eddies much smaller than 10η.

6.3 Discussion of Results

Except possibly near the wall, the structure function measurements generally indicate the existence of an inertial subrange. In several cases (Figures 6.5, 6.6 and 6.9) the data near the wall also has the proper slope but does not collapse onto the theoretical line followed more or less by the other data. The transverse structure function results of Figures 6.6 and 6.9 also

suggest that the maximum transverse probe separation (10mm) was not sufficient at all locations to completely cover the inertial subrange.

For eddies of size r to be part of the inertial subrange it is necessary that $\eta << r << L_f$, implying that the inertial subrange will be largest where L_f/η is also largest. All of the data show a largest inertial subrange for $R/R_{REF} = 0.827$ and 1.024. As shown in Table I, these are also the locations of maximum L_f/η.

The results, generally show the extent of the inertial subrange to be about one decade, a fact also established by the spectra measurements of section 5.2. This result is also consistent with the discussion of Tennekes and Lumley (1972), p. 272, who suggest that the extent of an inertial subrange is usually about two decades less than L_f/η, which approaches 10^3 in the present case. Not surprisingly for the diffuser, the inertial subrange is much less than that found by VC in the atmosphere. Their second order structure function measurements followed the two-thirds law for $80 < r/\eta < 20{,}000$; indicating the existence of an inertial subrange for more than two decades.

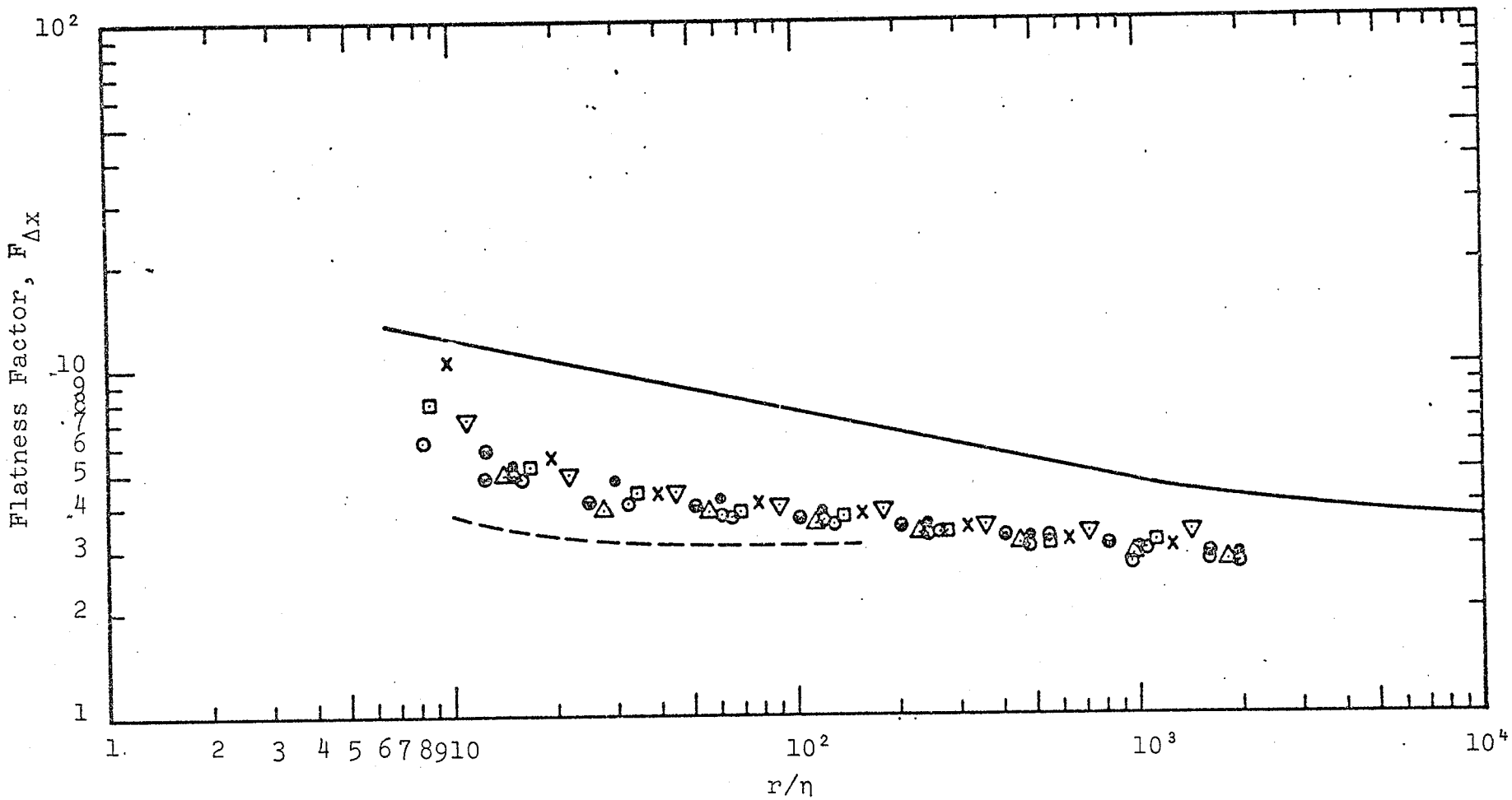

Figure 6.1 Flatness Factor of longitudinal velocity difference at Station 30.

R/R_{REF}: 0, ⊙ ; 0.236, ⊡ ; 0.433, X ; 0.630, ▽ ;
0,827, ◒ ; 1.024, △ ; 1.220, ⊙ ; 1.398, ●

Van Atta and Chen (1970); Atmospheric Turbulence ————
Grid Turbulence — — —

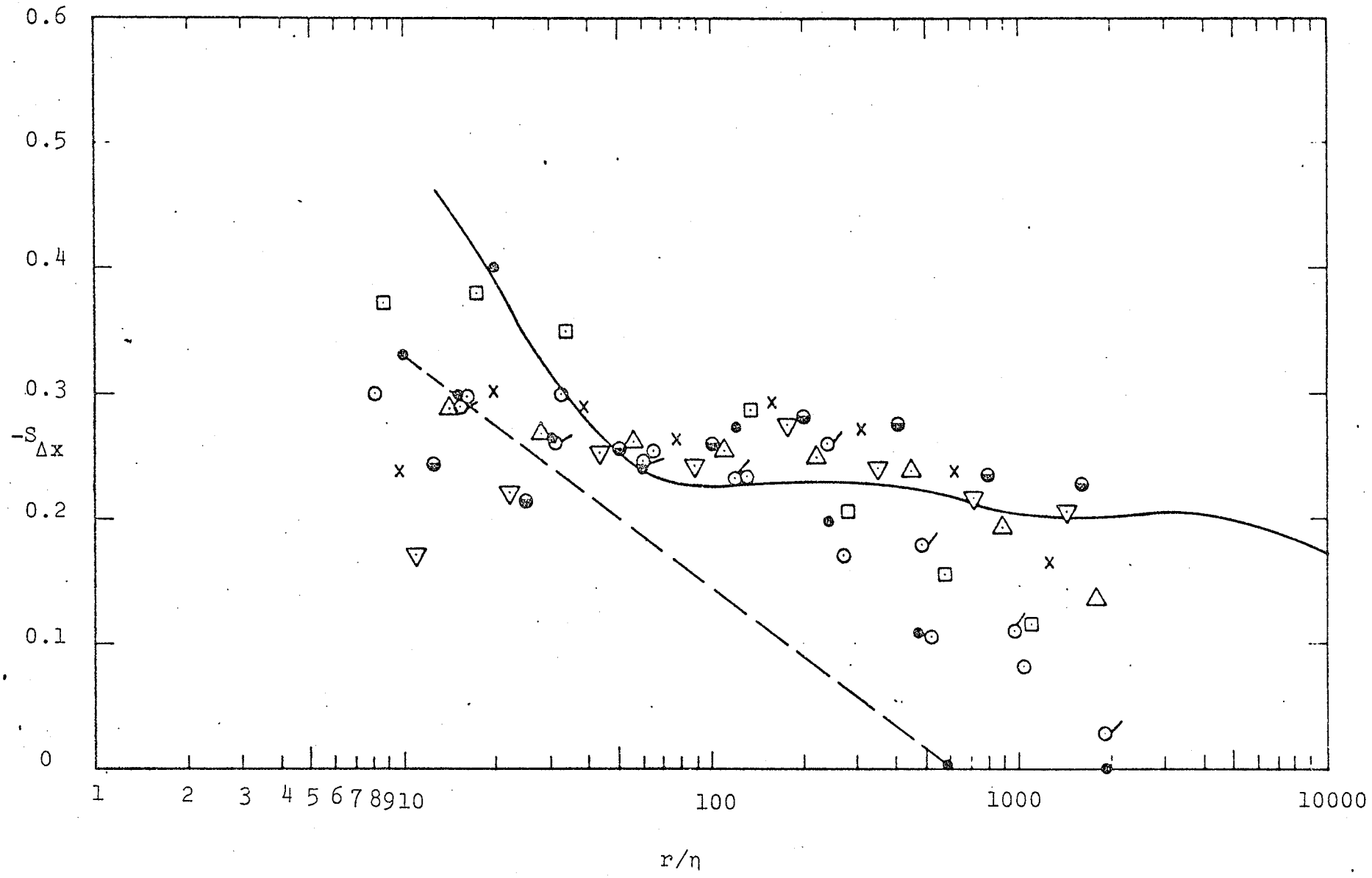

Figure 6.2 Skewness of longitudinal velocity difference at Station 30. Symbols are the same as in Figure 6.1

Van Atta and Chen (1970); Atmospheric Turbulence ———
Grid Turbulence — — —

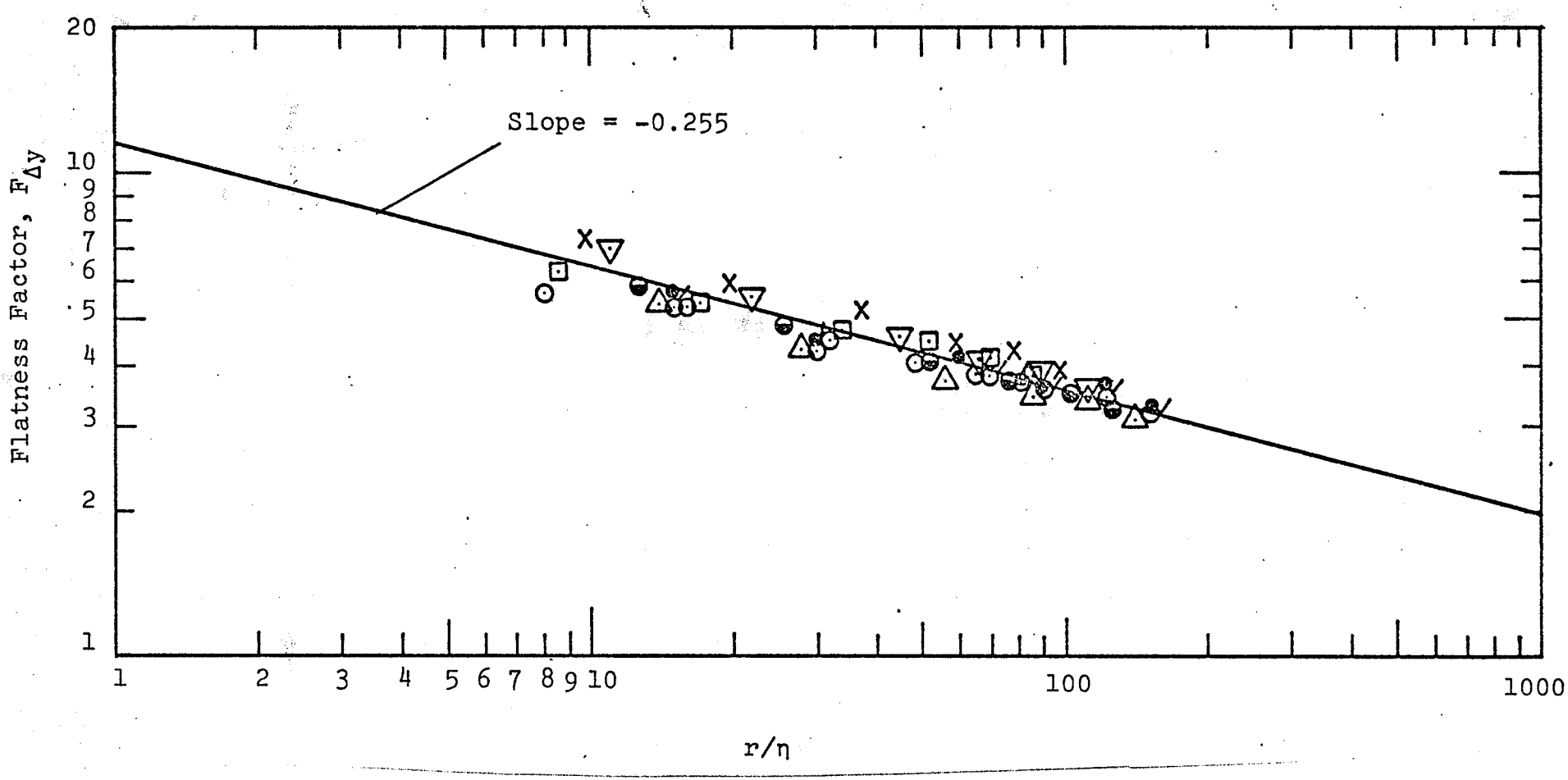

Figure 6.3 Flatness factor of transverse velocity difference at Station 30. Symbols are the same as in Figure 6.1

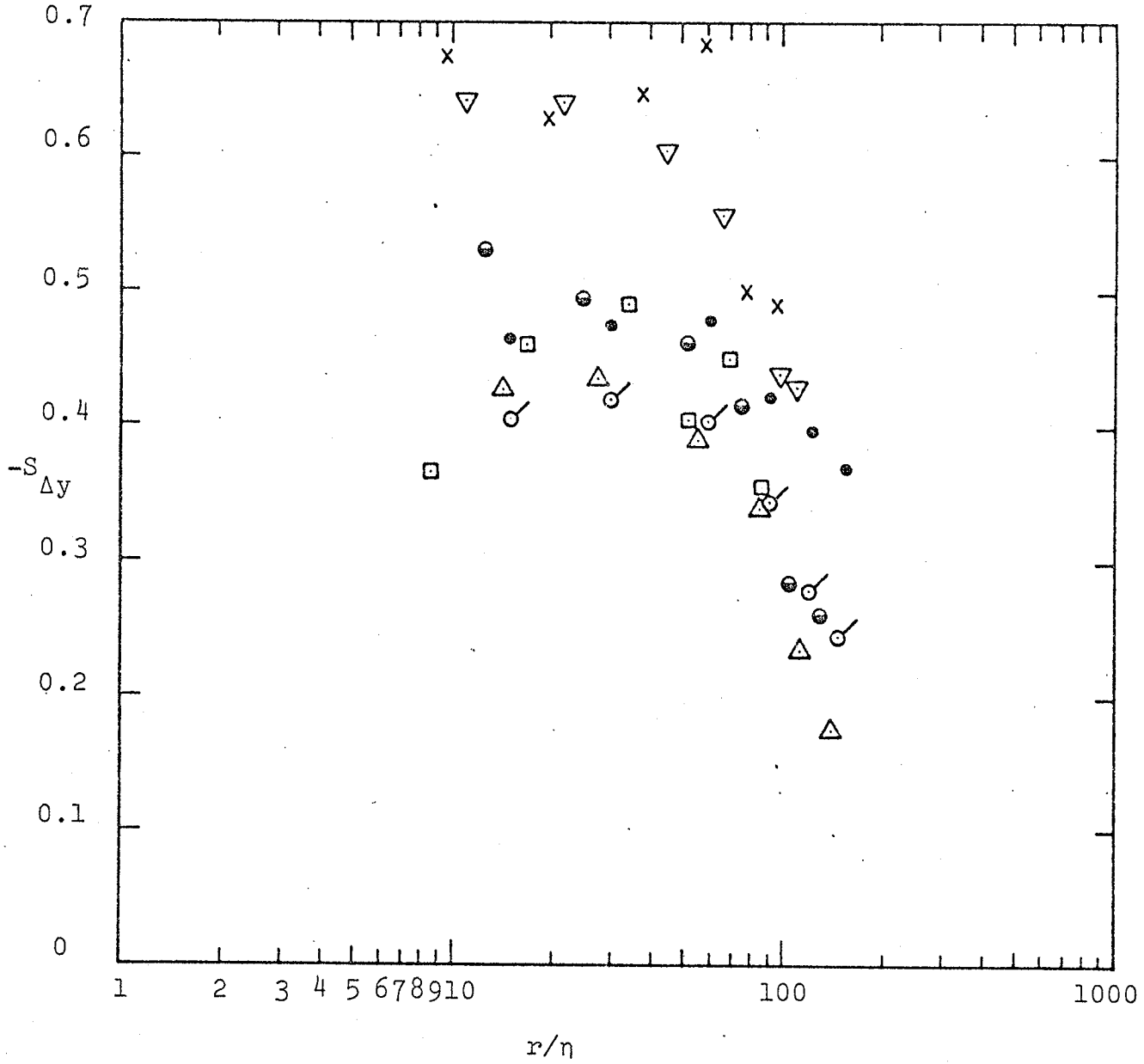

Figure 6.4 Skewness of transverse velocity difference at Station 30. Symbols are the same as in Figure 6.1

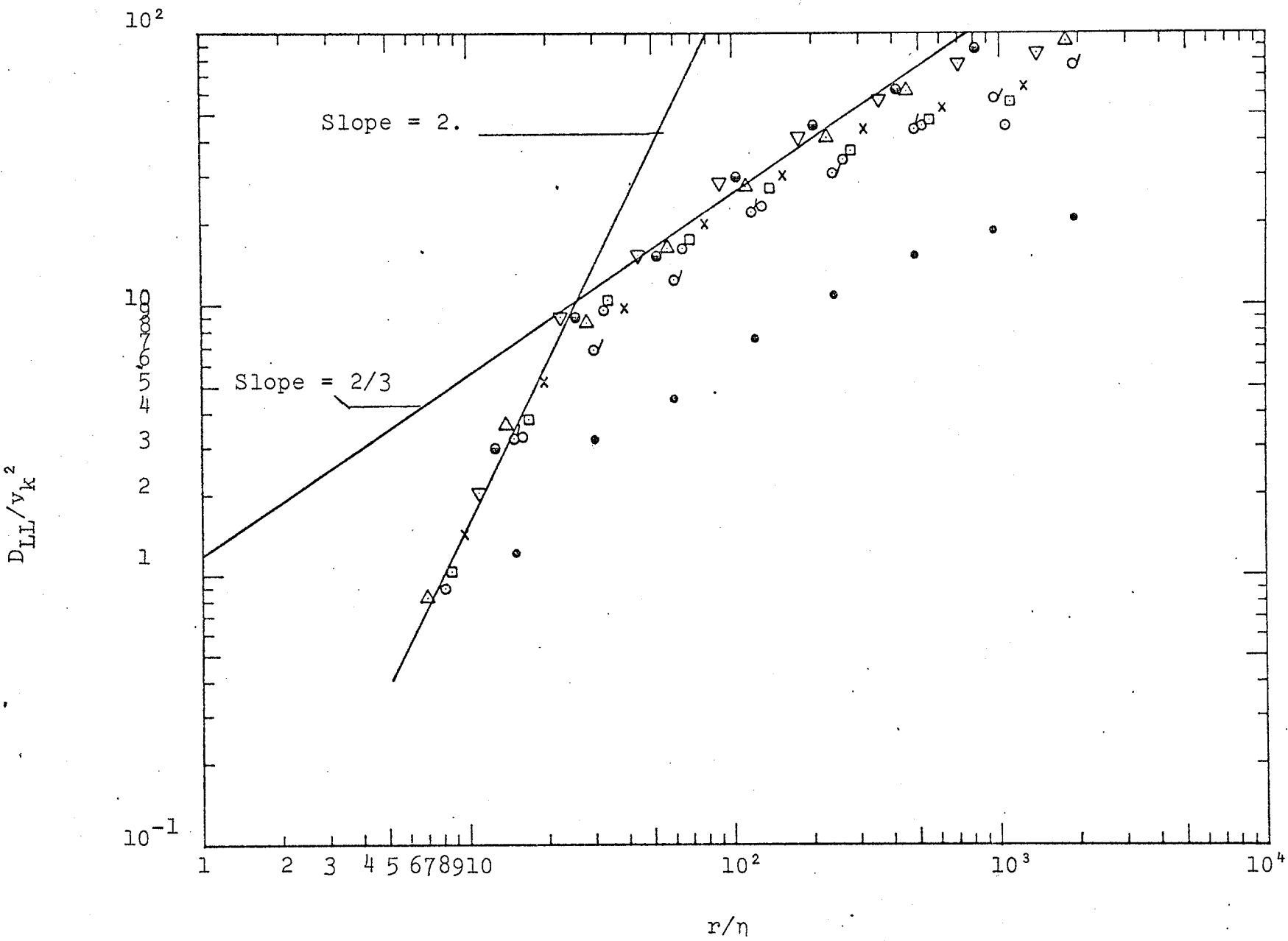

Figure 6.5 Longitudinal second-order structure functions at Station 30. Symbols are the same as in Figure 6.1

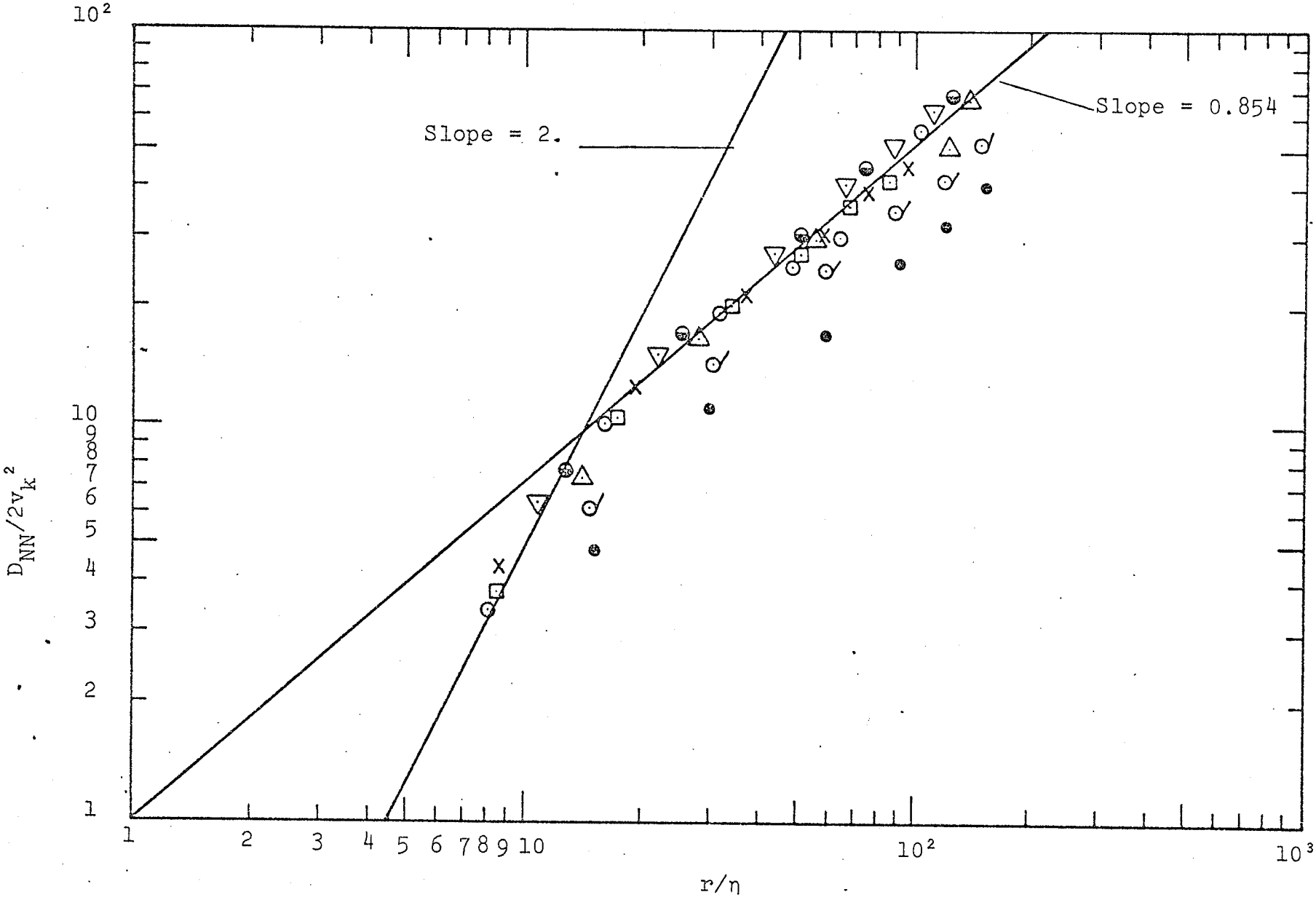

Figure 6.6 Transverse second-order structure functions at Station 30. Symbols are the same as in Figure 6.1

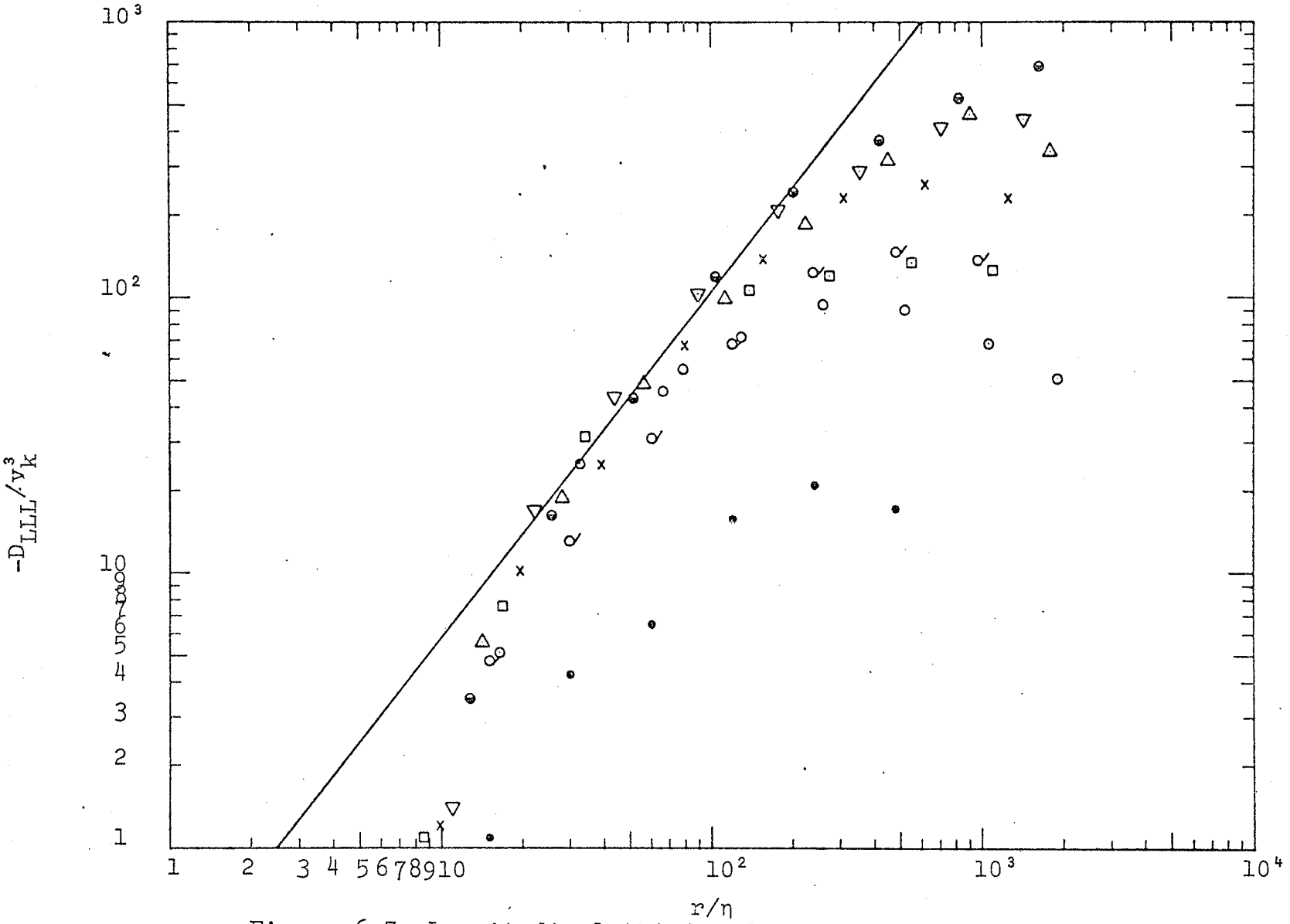

Figure 6.7 Longitudinal third-order structure functions at Station 30. Symbols are the same as in Figure 6.1

$D_{LLL}/v_k^3 = -0.8\ r/\eta$ ————————

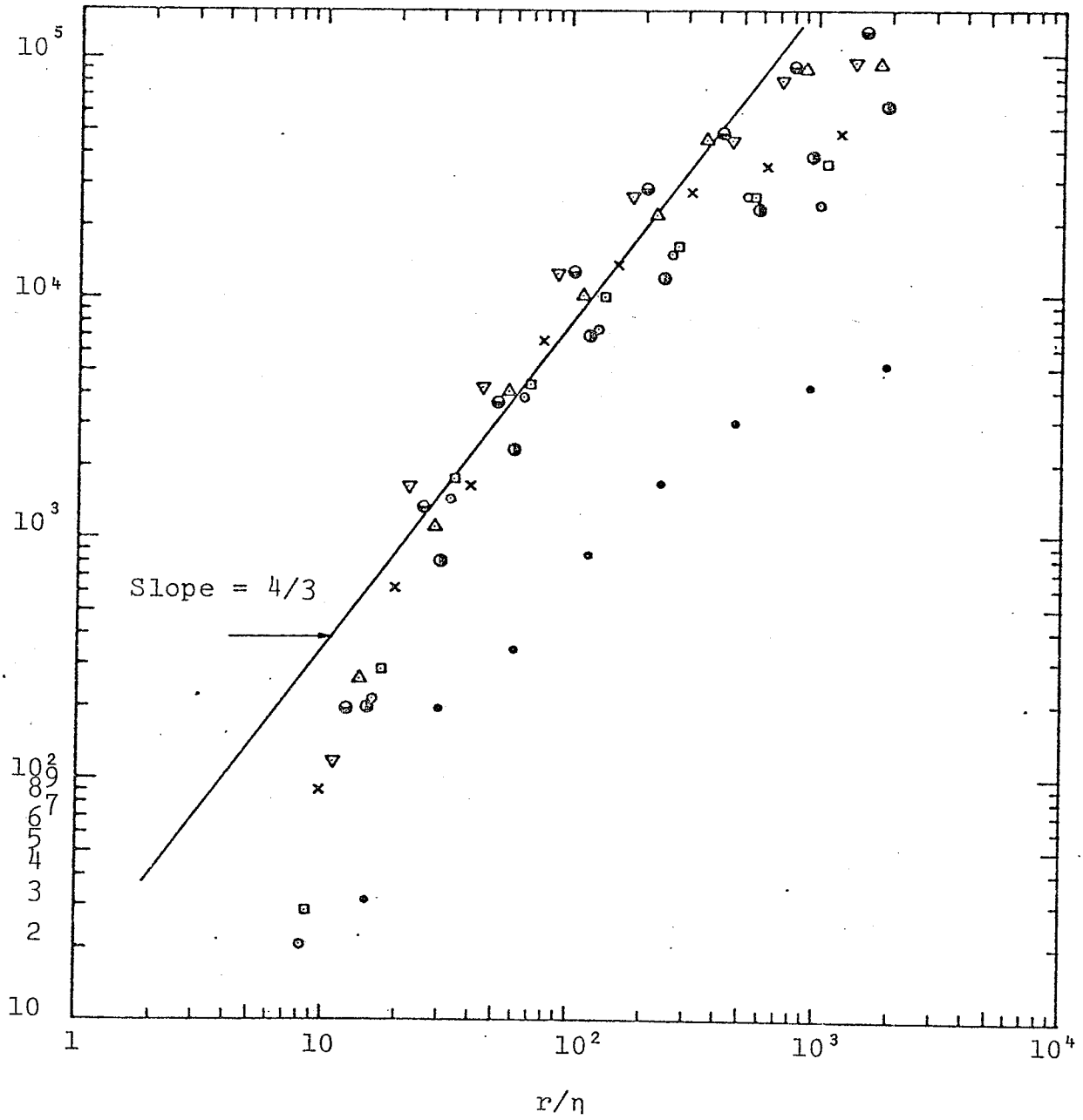

Figure 6.8 Longitudinal fourth-order structure functions at Station 30. Symbols are the same as in Figure 6.1

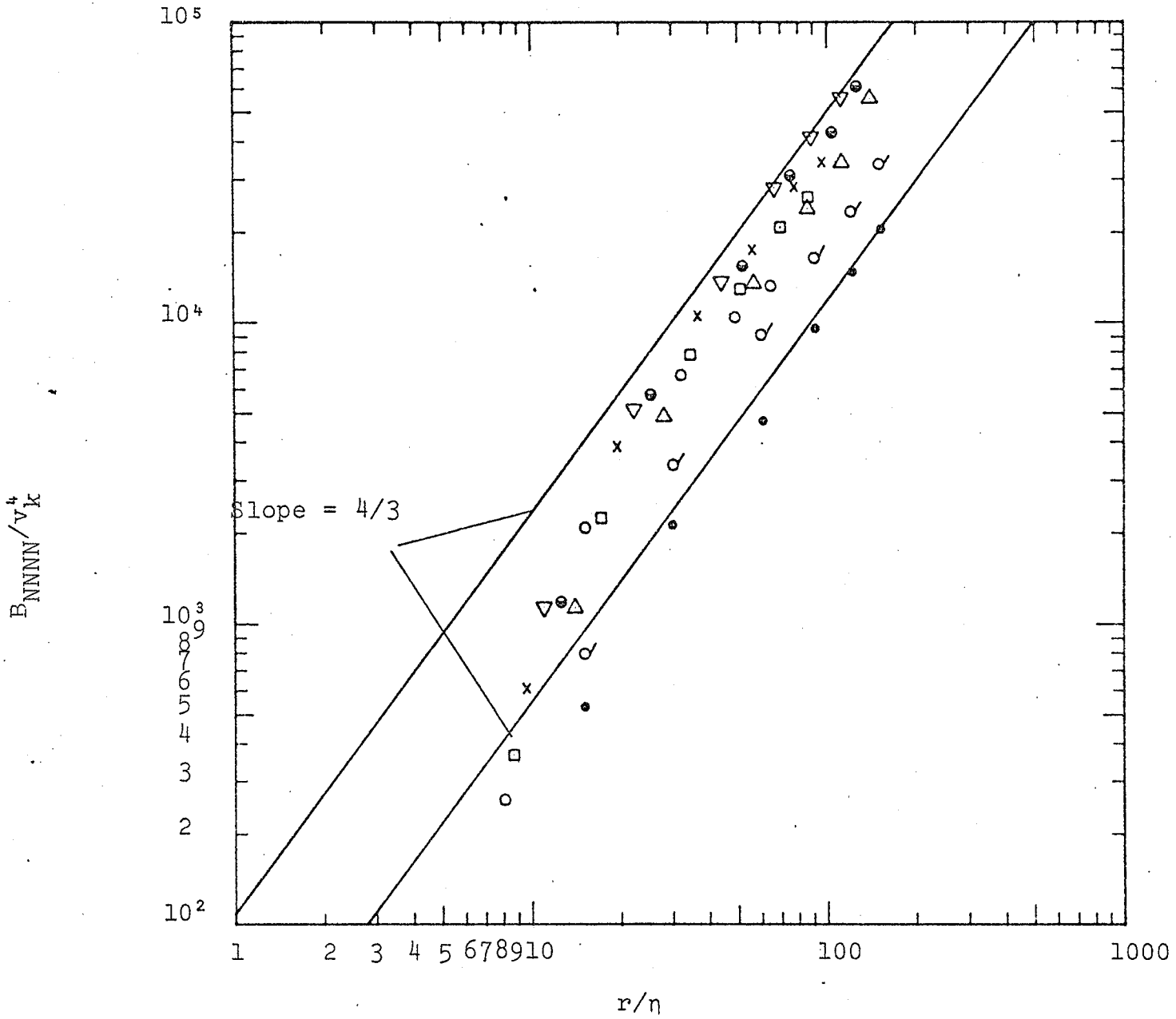

Figure 6.9 Tranverse fourth-order structure function at Station 30. Symbols are the same as in Figure 6.1

7.0 EXPERIMENTS USING AN ENVELOPE DETECTOR

An important property of all turbulence is the spotty nature of the fine structure. Near the wall of a boundary layer this spottiness is further increased by large local shear due to the bursting process.

A number of experimenters have studied the fine structure of turbulence using narrow-band filters. Rao et al (1971) have assumed that for shear flow each "burst" of high activity from the output of a narrow-band filter corresponds to a burst of energy production. By manually counting these bursts from paper-chart recordings they found a time scale, (the mean time between bursts), which was constant across the boundary layer ($y^+ > 15$), and scaled on the outer variables; i.e., the b undary layer thickness and free stream velocity. A similar technique was used by Ueda and Hinze (1975) who found the mean time between bursts to be twice as large in the viscous sublayer as for $y^+ > 40$.

The manual counting techniques described above are always subject to a certain amount of arbitrariness since it is often difficult to decide what is a burst and what is not. It was therefore decided to study some statistical properties of narrow-band filtered signals by forming the envelope of such signals. The envelope characterizes only a narrow-band of frequencies, or wave-numbers, thus

all of its statistical properties can be obtained as a function of frequency, or wave-number. Furthermore, the envelope experiments are unique. There are no "arbitrary" adjustments or decisions similar to those required in setting up an intermittency detector or in manually counting the mean time between bursts.

Three important fine-structure properties of turbulence are:

a) the average linear dimension of the fine-structure bursts, L_A,

b) the average spacing between the fine-structure bursts, L_B,

c) the degree of spottiness, characterized by the intermittency factor, γ.

Since $L_B = L_A/\gamma$, the present work concentrates on measuring L_A and γ; the former by analyzing the frequency spectra of the envelope, the latter by analyzing flatness factors and probability distributions.

7.1 The Envelope of a Gaussian Signal

As a preliminary experiment the envelope of a gaussian (or white noise) signal was formed at three arbitrary frequencies, 1.25, 5 and 12.5 kHz. This signal

was obtained from a prototype noise generator which was thoroughly tested to insure that its probability density was normal, and frequency spectrum flat within 3 db from 10 Hz to beyond 30 kHz.

The envelope detector has already been described in Chapter 3. Figure 7.1 shows a block diagram of the experimental set-up. The white noise was fed into a narrow-band filter with bandwidth $\Delta f/f_m = 0.43$. For these experiments the midband frequency of the filter f_m, is called the envelope frequency F_E. The filtered signal was then fed into the envelope detector and the spectrum of the envelope measured with a second narrow-band filter and an r.m.s. voltmeter.

Figure 7.2 shows the spectra. As for all these measurements the vertical scales are normalized by the lowest frequency value and the horizontal scale by F_E. When thus normalized it is readily seen that the envelope spectra of gaussian signals are well described by the emperical relationship,

$$G(f/F_E) = \frac{1}{1 + (3.26\ f/F_E)^3} \qquad (7.1)$$

7.2 The Envelope of Narrow-band Filtered u

For each of four radial positions at station 30 (with Re = 137,000) the narrow-band envelope of u was formed (Figure 7.1) at four frequencies. The radial positions were:

a) Near the wall (R/R_{REF} = 1.43).

b) Near the radial position of maximum u' (R/R_{REF} = 1.04).

c) In the core region (R/R_{REF} = 0.403).

d) On the centre line (R/R_{REF} = 0).

Since the basic interest was in fine-structure the envelope frequencies F_E were selected, starting from the centre of the inertial subrange (500 Hz) to well into the dissipation region (12.5 kHz). The selected frequencies are identified at the bottom of Figure 7.3 which shows frequency spectra of u for each of the four radial locations.

7.2.1 Spectra and Autocorrelations

Preliminary inspection of the spectrum of an envelope obtained near the wall at F_E = 12.5 kHz, suggested that it might be considered as a sum of two spectra, as shown in Figure 7.4a. In this case the autocorrelation function of the envelope f(t), also revealed a rapid decrease near zero time delay, followed by a much slower

delay to zero with increased time delay (Figure 7.4b). These results suggested that the envelope consisted of two components, one with a relatively long time scale τ_1, called the large scale component, and the other, with a relatively short time scale τ_2, called the small scale component. These scales are properties of the envelope which already represents a narrow-band of wave-numbers, and must not be confused with similar terminology used to describe large and small eddies.

For the envelope just described the autocorrelation f(t), was assumed to be of the form,

$$f(t) = A_1 e^{-|t|/\tau_1} + A_2 e^{-|t|/\tau_2}, \qquad (7.2)$$

for all t and with $A_1 + A_2 = 1$.

Taking the Fourier transform of 7.2 gives the spectrum,

$$S(f) = \frac{2A_1\tau_1}{1 + (2\pi f\tau_1)^2} + \frac{2A_2\tau_2}{1 + (2\pi f\tau_2)^2} \qquad (7.3)$$

While equations 7.2 and 7.3 are characterized by the same four parameters, A_1, A_2, τ_1 and τ_2, it was decided to proceed further using the spectral method. The envelope spectra for each radial position and envelope frequency are shown in Figures 7.5 to 7.8 with the universal gaussian envelope spectrum also shown for comparison. Only

frequencies below F_E are considered.

Two important features of these spectra are:

a) As the envelope frequency decreases (corresponding to lower wave-numbers or larger eddies) the dual nature of the spectrum diminishes and approaches the universal gaussian spectrum.

b) As distance from the wall increases the dual nature diminishes further and is almost non-existent on the centre line for any of the envelope frequencies.

For the envelope spectra, the most interesting parameters are the delay time τ_1 and τ_2. These were estimated numerically using Powell's method (Box, Davies and Swann, 1969) of non-linear optimization, which selected the parameters such as to minimize the sum of squared errors between equation 7.3 and the spectral data.

Length scales L_1 and L_2 for various envelope frequencies F_E, and probe positions are shown in Figure 7.9. These were obtained by multiplying the time scales τ_1 and τ_2 by the local mean velocity $\bar{U}$. The data show that as the envelope frequency increases from the centre to the top of the inertial subrange the length scale of the large-scale component increases whereas the length scale of the

small component decreases. In the dissipation region both components decrease with increasing envelope frequency.

7.2.2 Probability Distribution, Intermittency, Flatness Factor and Skewness

To obtain intermittency information concerning the envelope, probability distribution measurements were made. For a gaussian signal the envelope has a Rayleigh distribution (Middleton; 1960). To show how intermittency factor and probability distribution are related it is useful to consider a gaussian signal chopped on and off with duty cycle γ. The intermittency factor of the resultant signal is also γ. The probability density of the envelope of such a signal will have an impulse of strength $1 - \gamma$ at the origin followed by a Rayleigh probability density function but with area equal to γ. The probability distribution will thus have a step jump from 1 to γ at the origin, then decreasing monotonically to zero. The intermittency factor is thus obtained by extrapolating the probability distribution to the vertical axis. This is summarized quantitatively in Figure 7.4c.

Probability distributions for the envelopes e(t), are shown in Figures 7.10 to 7.13. A logarithmic

vertical scale has been used since this results in long straight line segments readily extrapolated to the vertical axis giving the intermittency factor. The γ values thus obtained are plotted in Figure 7.14 and compared with the γ values obtained by feeding the envelopes directly into the intermittency detector as shown in Figure 7.1. The results show that the unambiguous technique of probability distribution extrapolation produces results very comparable to those obtained using the intermittency detector.

The FF of the filtered envelope was measured by first feeding the envelope through a narrow-band filter ($\Delta f/f_m = 0.43$) as shown in Figure 7.1. The results are shown in Figures 7.15 to 7.18. For each envelope, the γ value, obtained by using the intermittency detector is also indicated. The flatness factor and skewness of the unfiltered envelope were also measured with the results shown in Figure 7.19. These results generally show increased values toward the wall.

7.3 Discussion of Results

In the previous section it was determined that the envelopes of narrow-band filtered u generally have a dual structure; i.e., are characterized by two length scales.

It has thus far not been possible to determine the physical significance of each length scale and the tentative assumption will be that the linear dimension of the fine-scale structure is actually represented by the large length scale. The small length scale is thus assumed to play only a secondary role, possibly related to that electronic formation of the envelope and not really related to the turbulence itself.

Under these assumptions it is interesting to determine $L_B (= L_A/\gamma)$, where L_A is now the large length scale L_1, and γ the intermittency factor, taken from Figure 7.14. Only the results at $R/R_{REF} = 1.41$ are considered where γ is generally less than unity. These results are summarized in the following table.

L_1(mm)	γ	$L_B = L_1/\gamma$(mm)	F_E(Hz)
9.91	0.17	54.06	12,500
25.94	0.56	46.32	5,000
16.28	0.80	20.35	2,000
6.96	1.0	6.9	500

They generally show that for envelopes found in the dissipation region (F_E = 5 and 12.5 kHz) the length scale L_B, remains approximately constant, but decreases rapidly with decreasing frequency in the inertial subrange. Thus, when manually counting the mean-time between bursts, these results would suggest that the centre frequency of the

narrow-band filter should be set in the dissipation region.

It is interesting to investigate the relationship between the intermittency factor γ, and the flatness factor of the narrow-band filtered envelopes given in Figures 7.15 to 7.18. For γ values less than 1.0 the flatness factor of the filtered envelopes shows a peak value at a frequency less than F_E. Thus it appears that the existence of such a peak indicates the existence of intermittency. Figure 7.20 shows the relationship between these quantities. It is approximately linear and suggests the interesting prospect of replacing intermittency measurements with (more straightforward) flatness factor measurements.

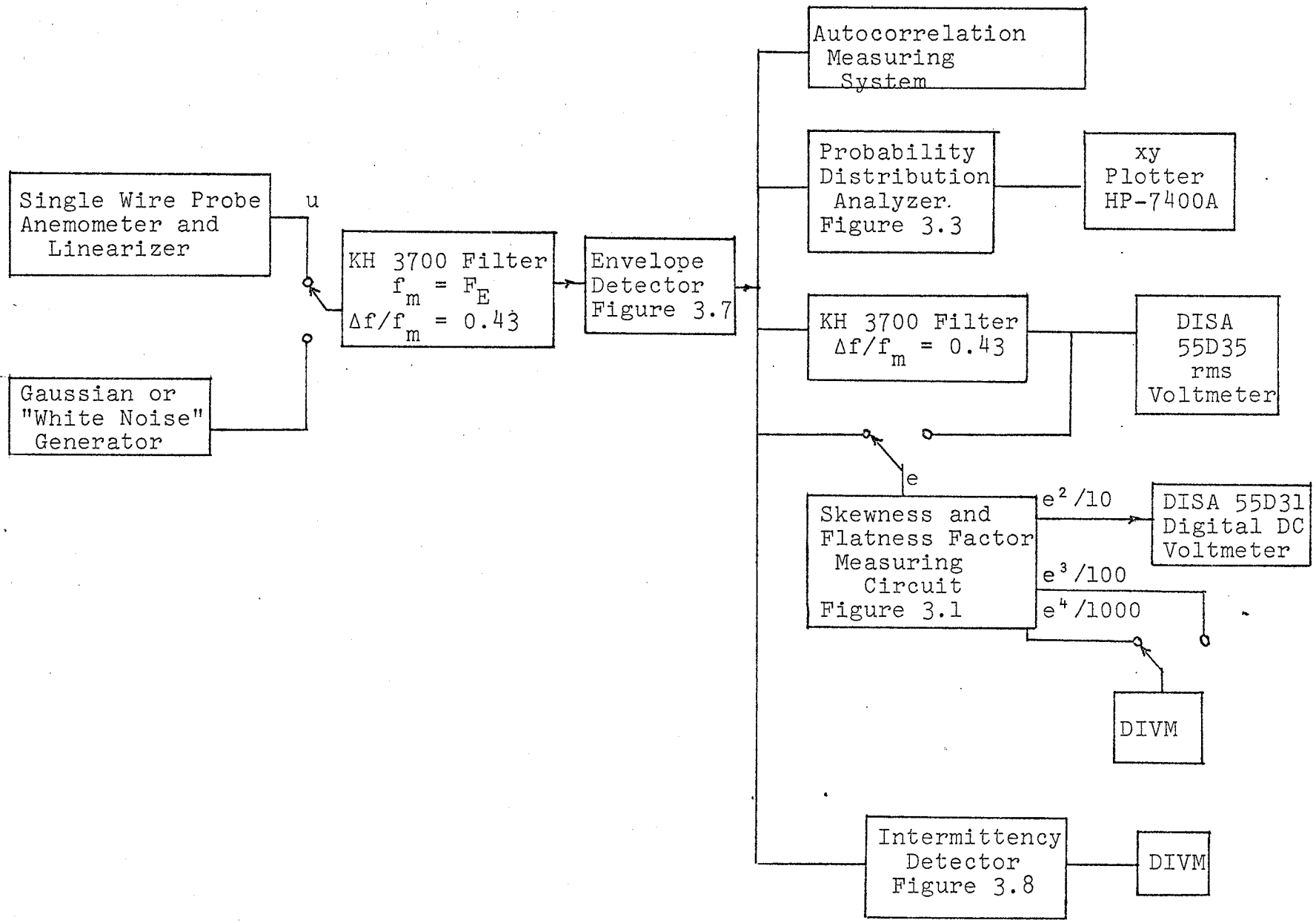

Figure 7.1 Block diagram of equipment for envelope experiments

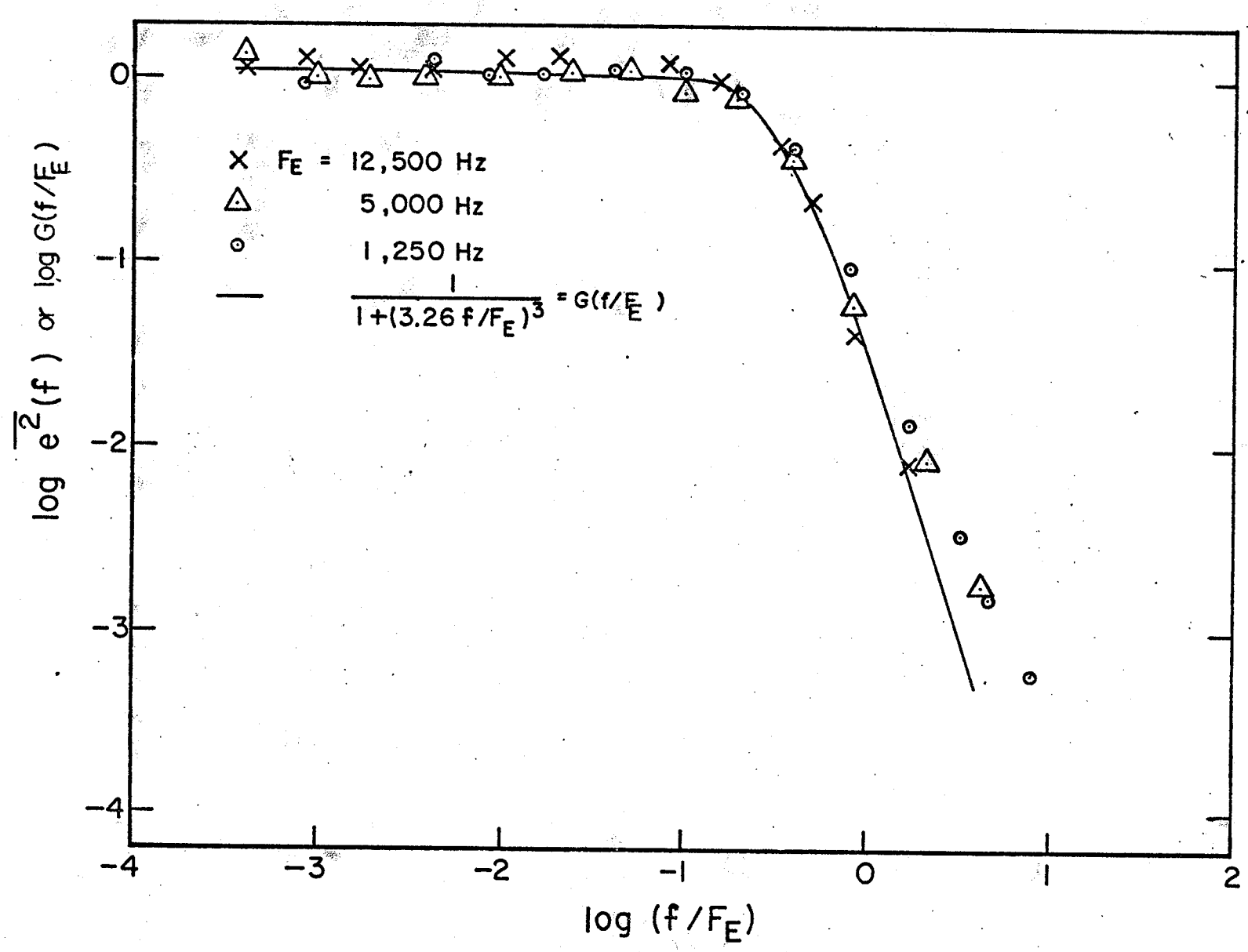

Figure 7.2 Envelope spectra for Gaussian signals (White noise)

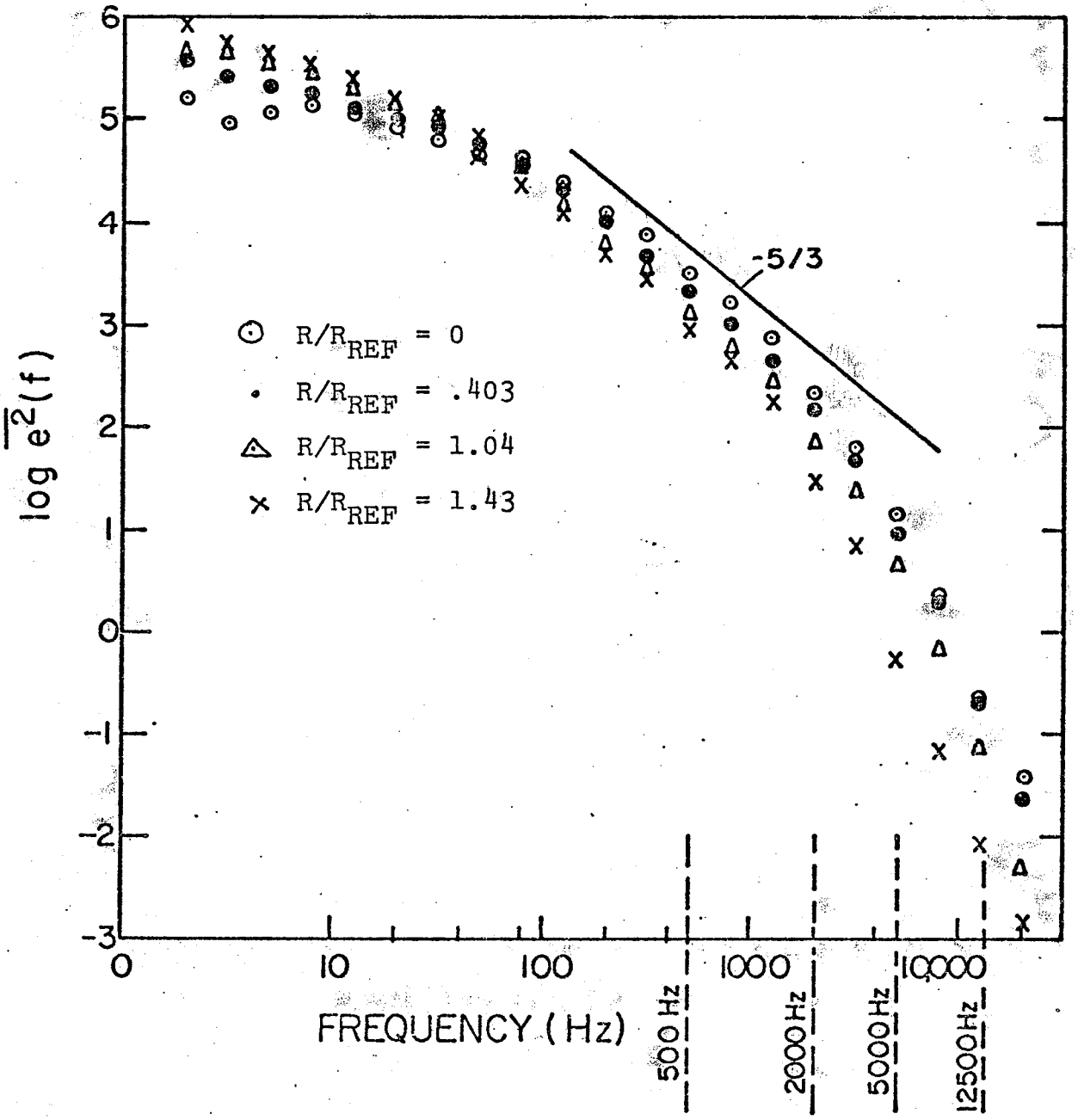

Figure 7.3 Frequency spectra of u at Station 30

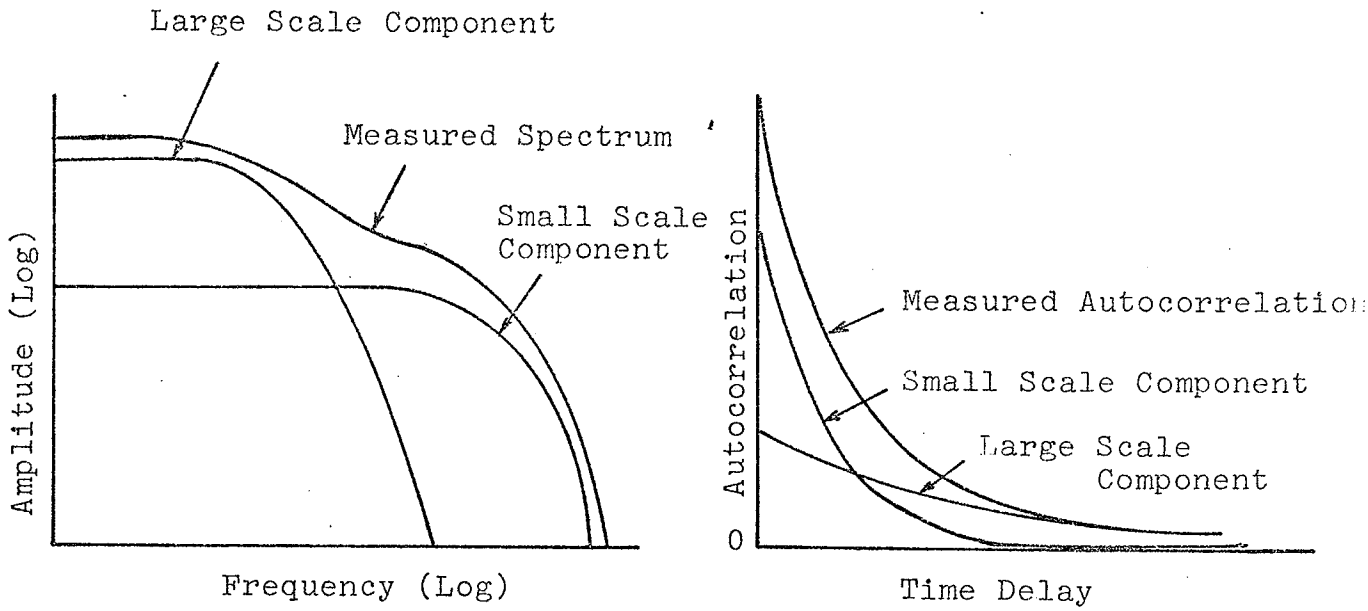

(a) Spectrum

(b) Autocorrelation

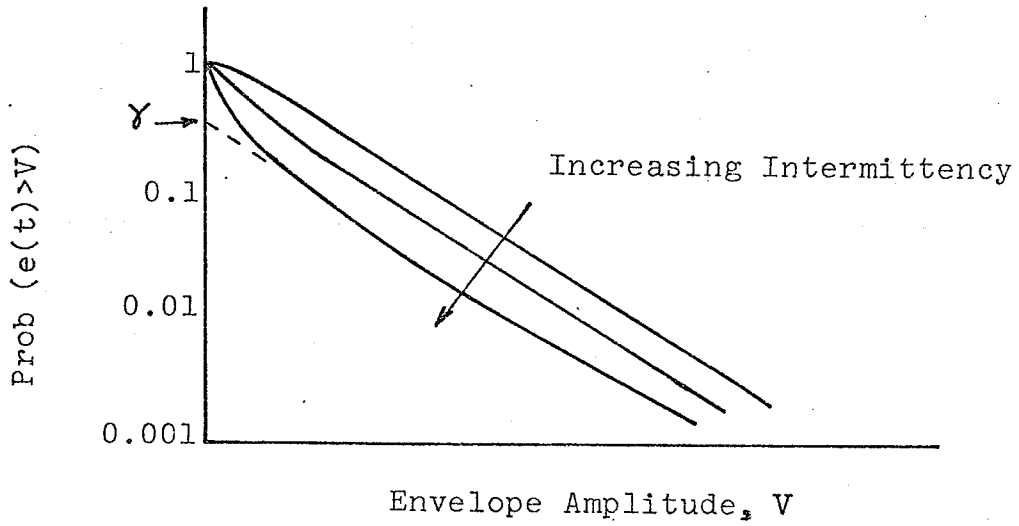

(c) Probability Distribution

Figure 7.4 Some statistical properties of the envelope

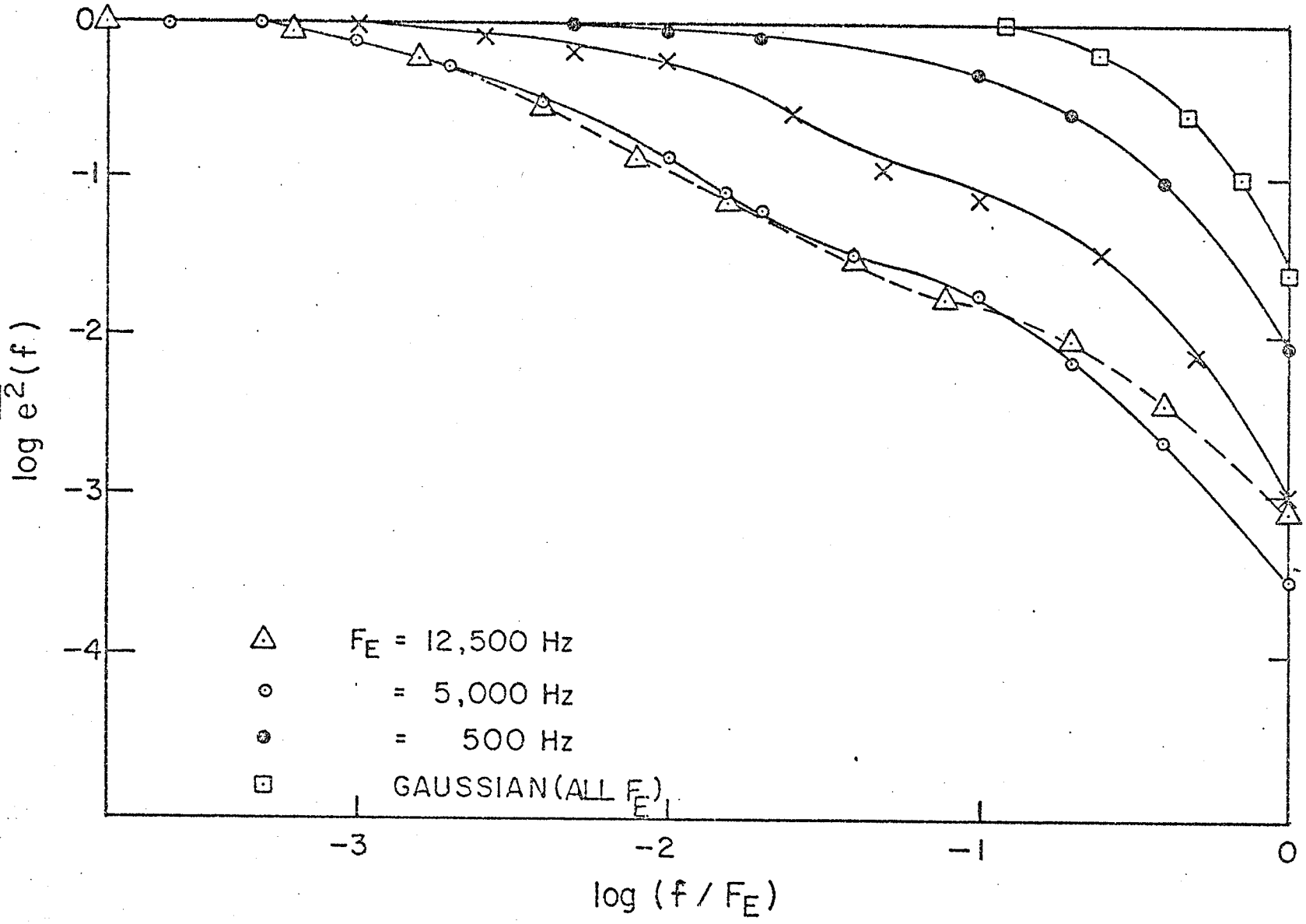

Figure 7.5 Envelope spectra at Station 30. R/R_{REF} = 1.43

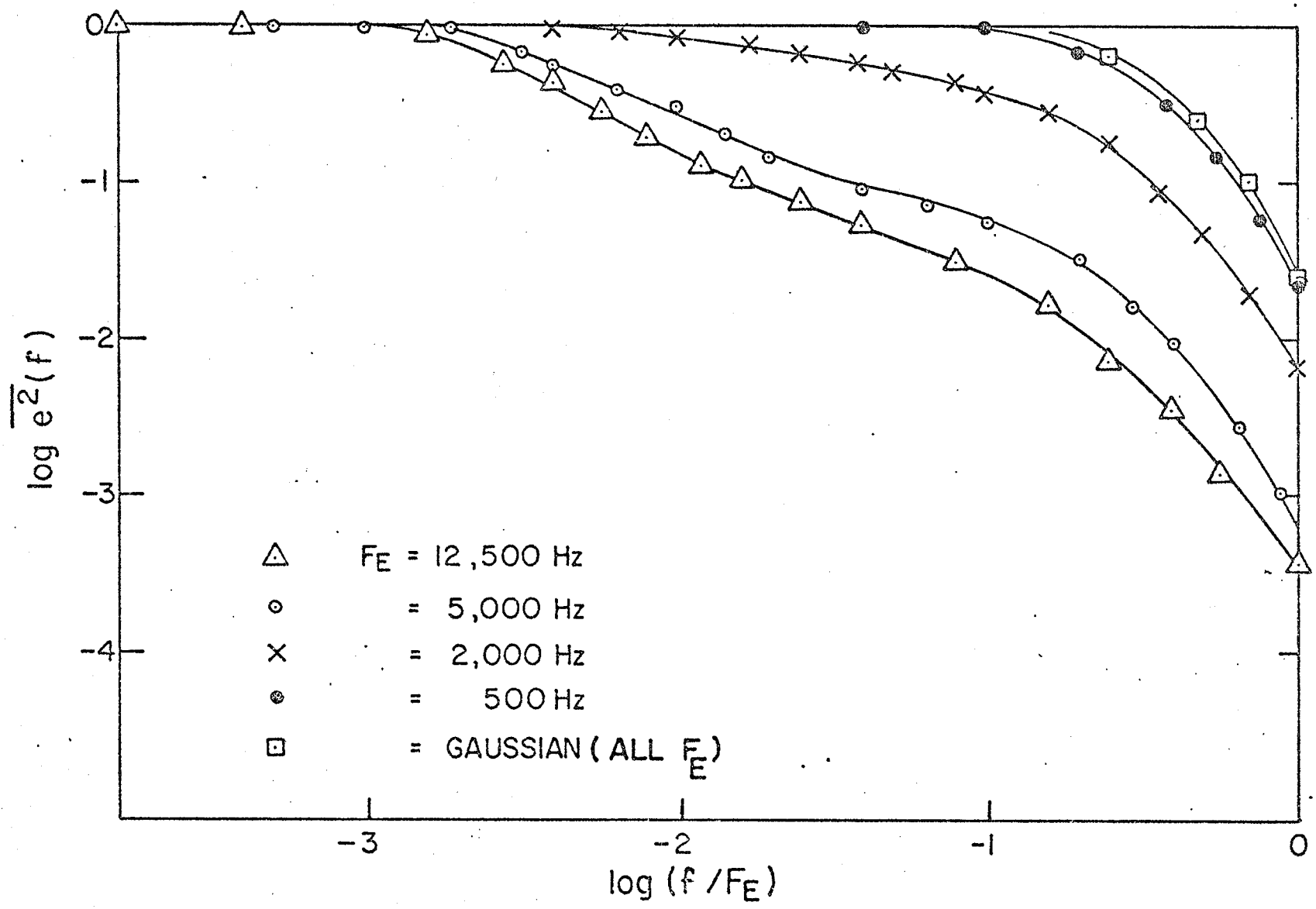

Figure 7.6 Envelope spectra at Station 30. R/R_{REF} = 1.04

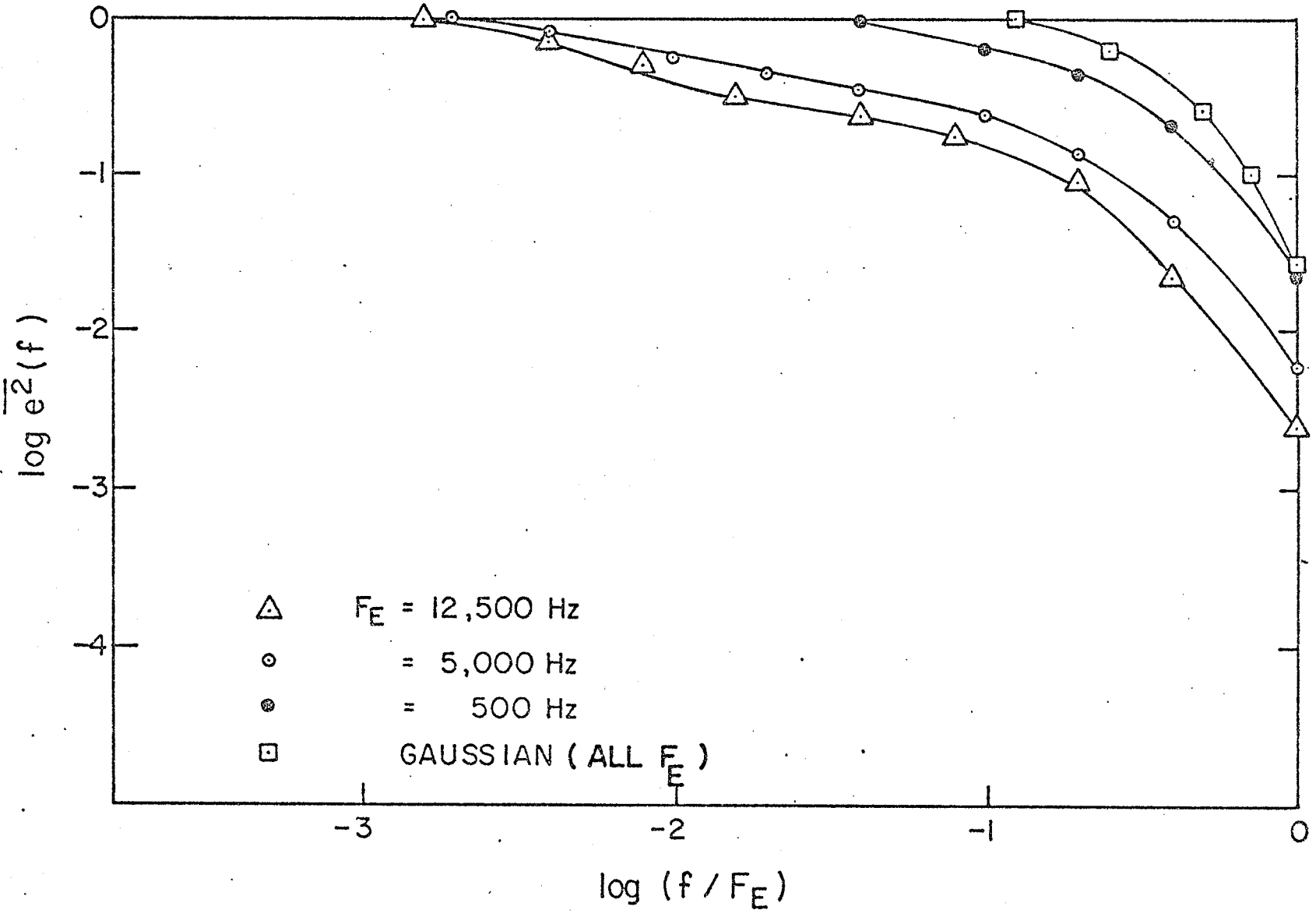

Figure 7.7 Envelope spectra at Station 30. R/R_{REF} = 0.403

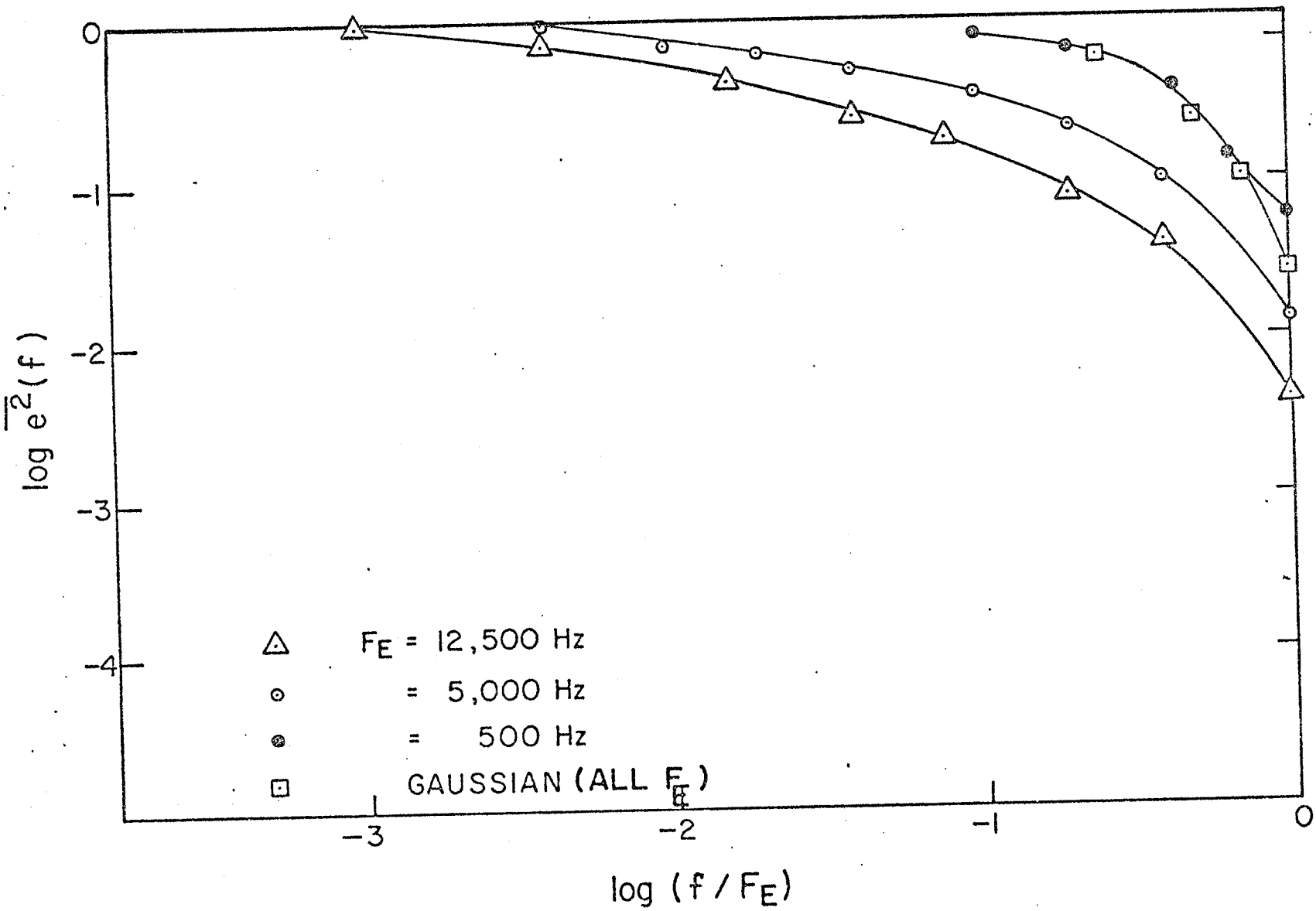

Figure 7.8 Envelope spectra at Station 30. $R/R_{REF} = 0$

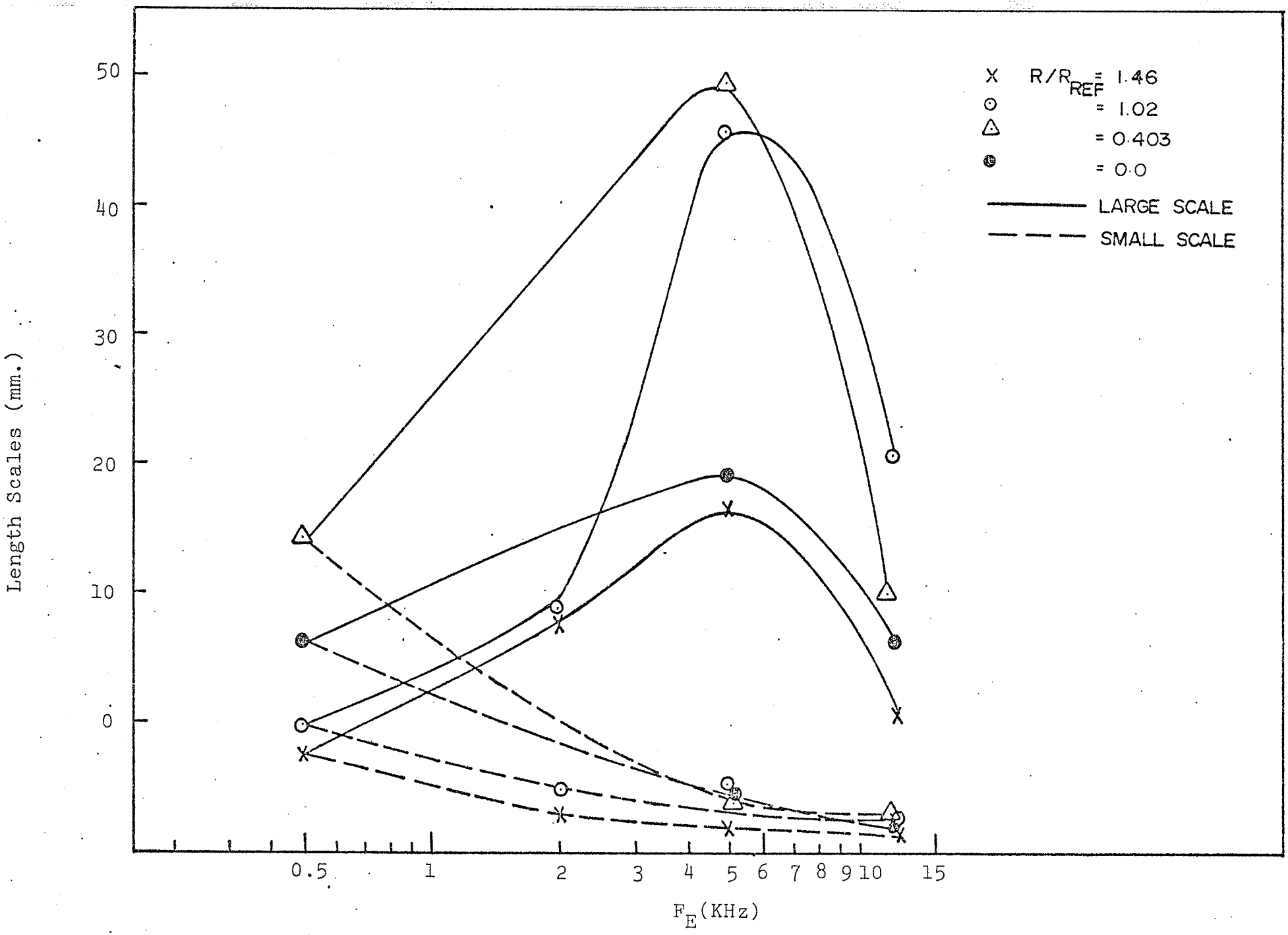

Figure 7.9 Distribution of length scales with envelope frequency at Station 30

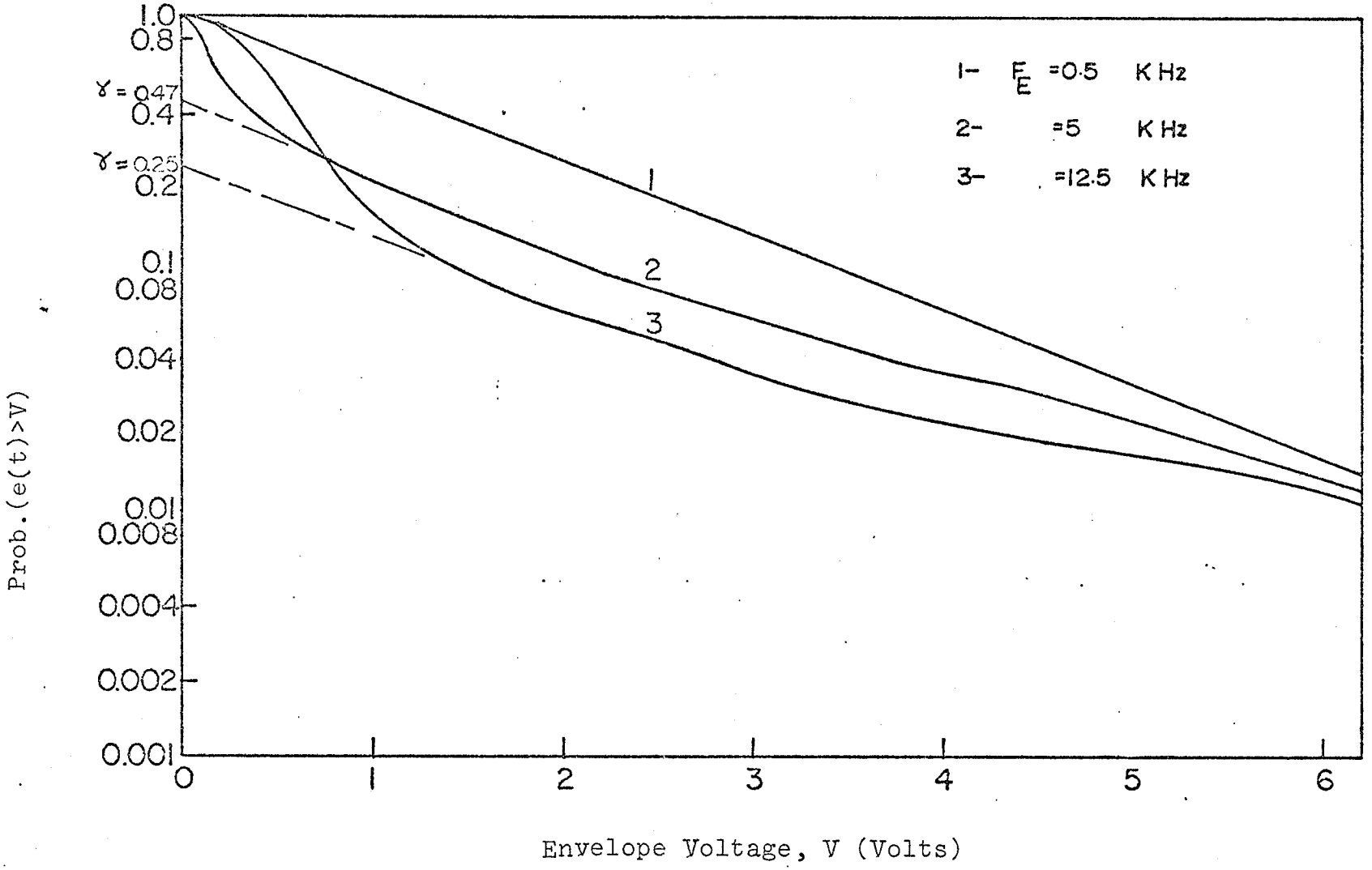

Figure 7.10 Envelope probability distributions at Station 30.
$R/R_{REF} = 1.42$

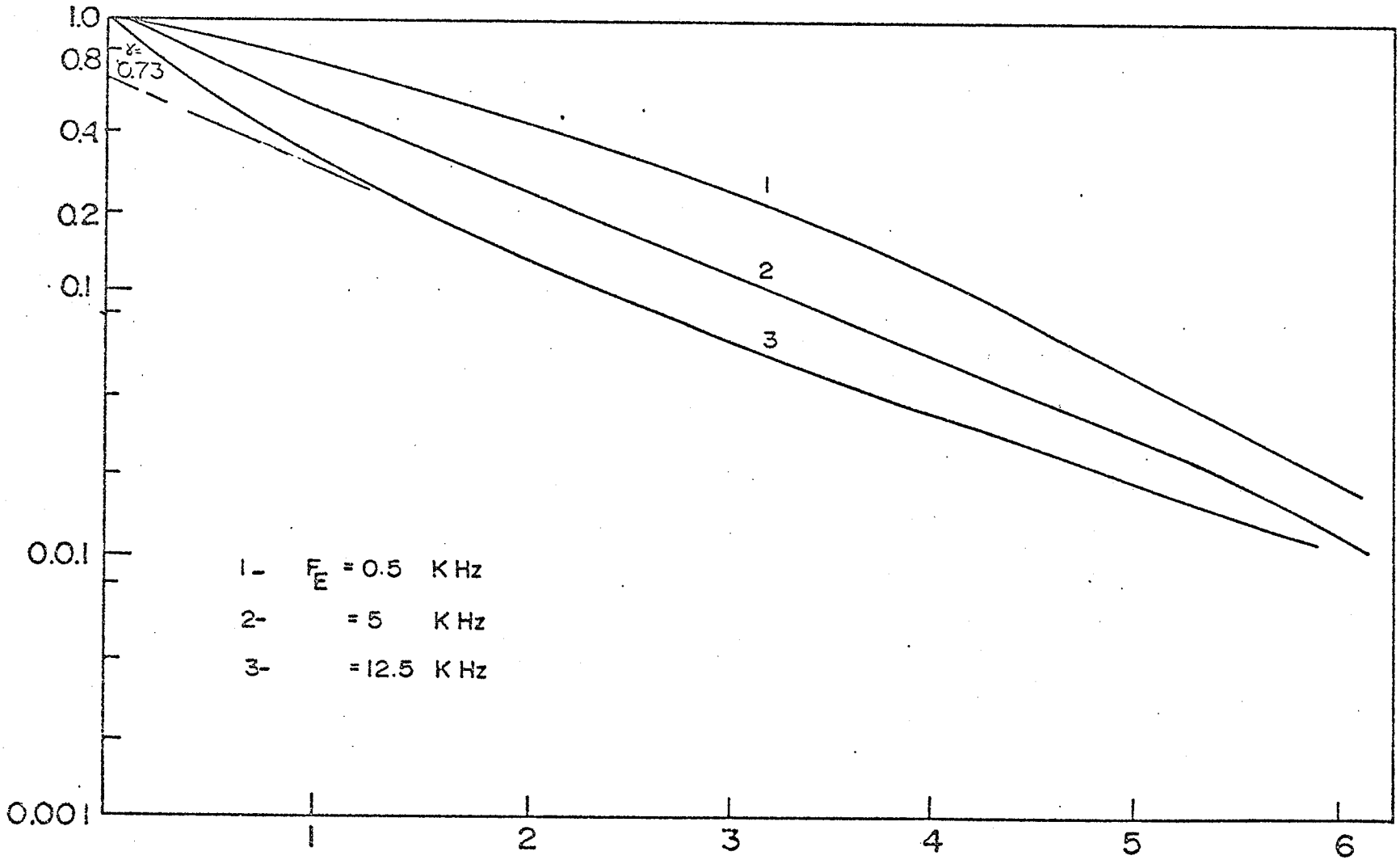

Figure 7.11 Envelope probability distributions at Station 30. $R/R_{REF} = 1.02$

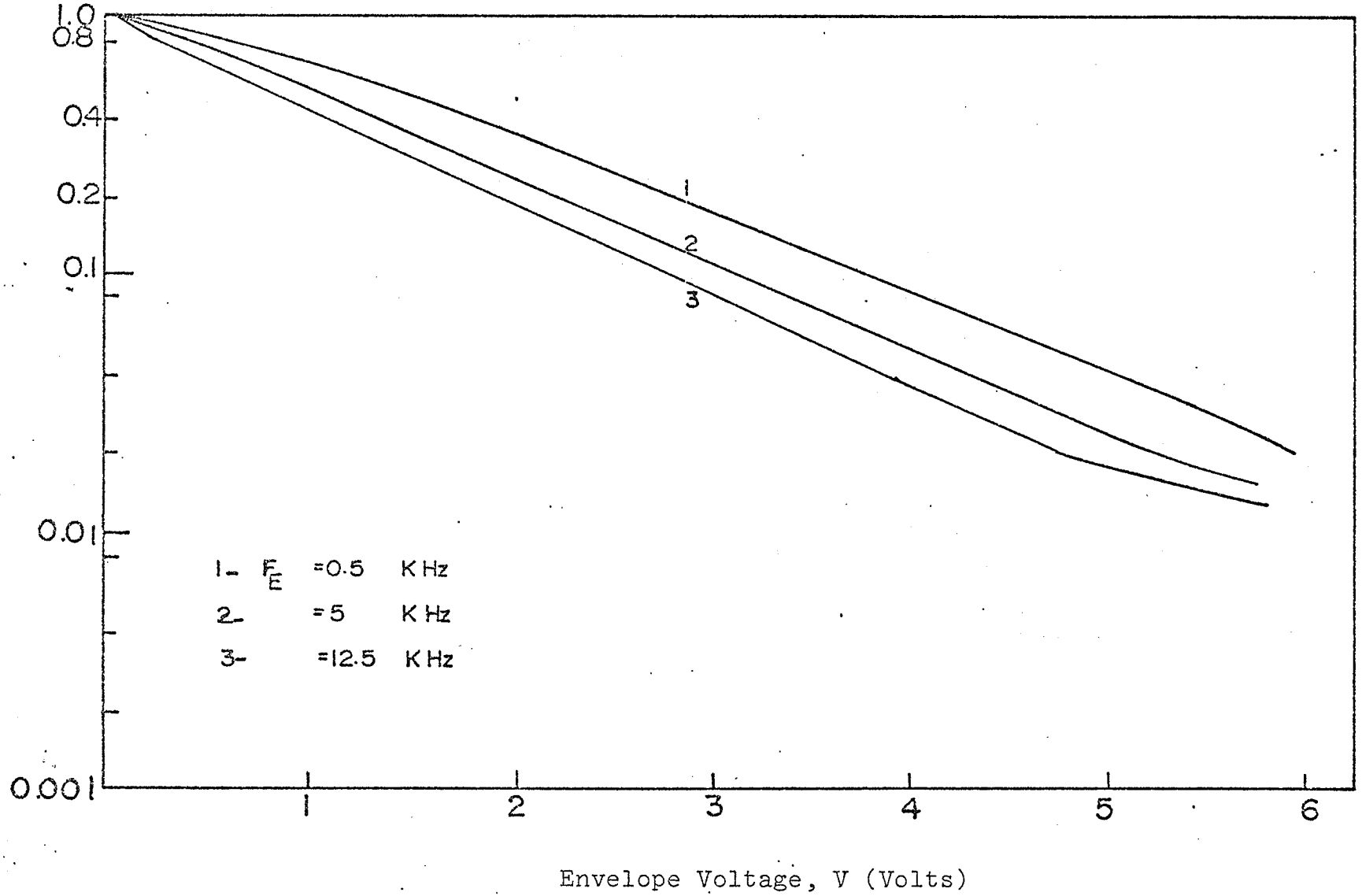

Figure 7.12 Envelope probability distributions at Station 30.
R/R_{REF} = 0.403

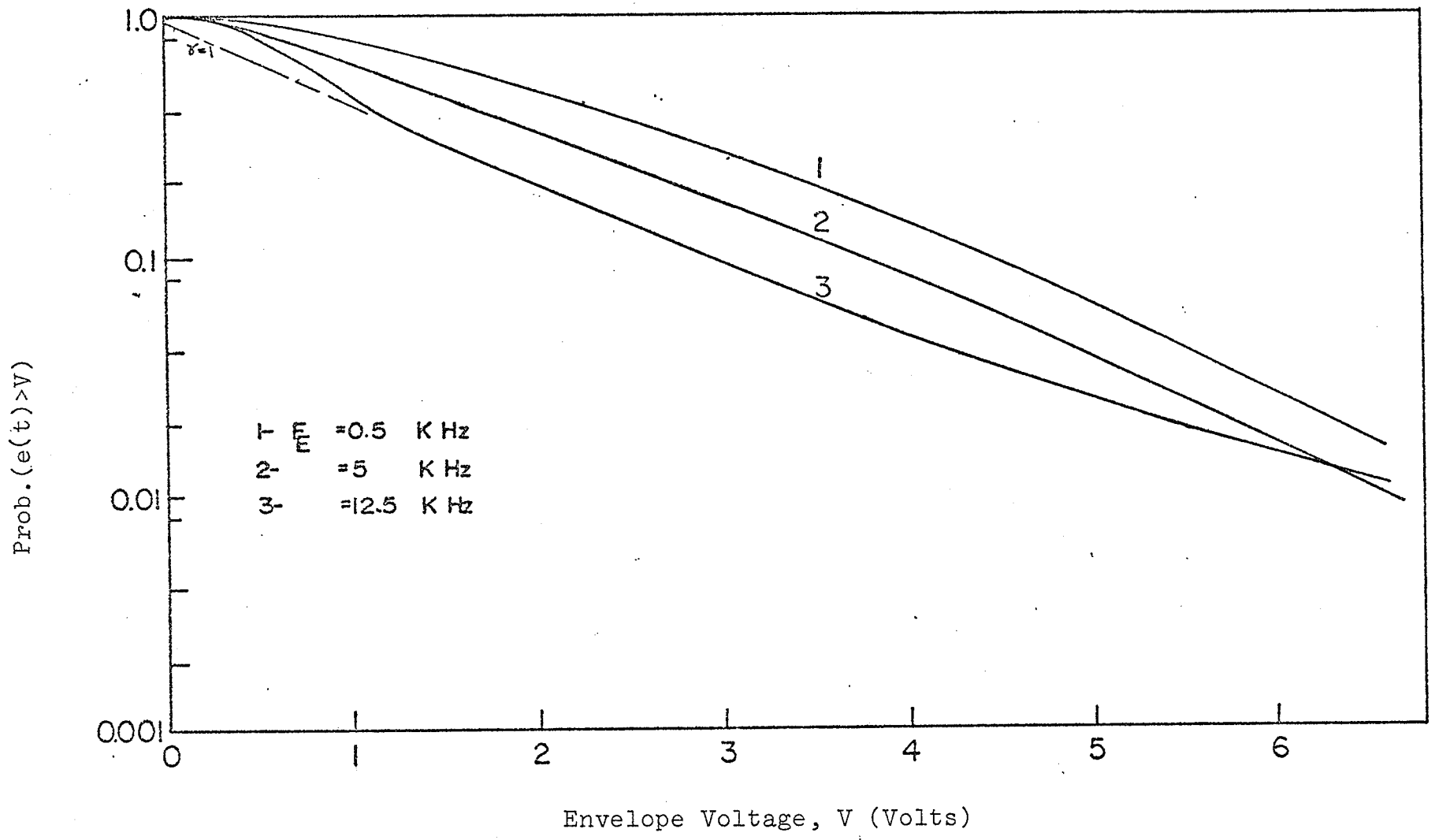

Figure 7.13 Envelope probability distributions at Station 30.
$R/R_{REF} = 0$

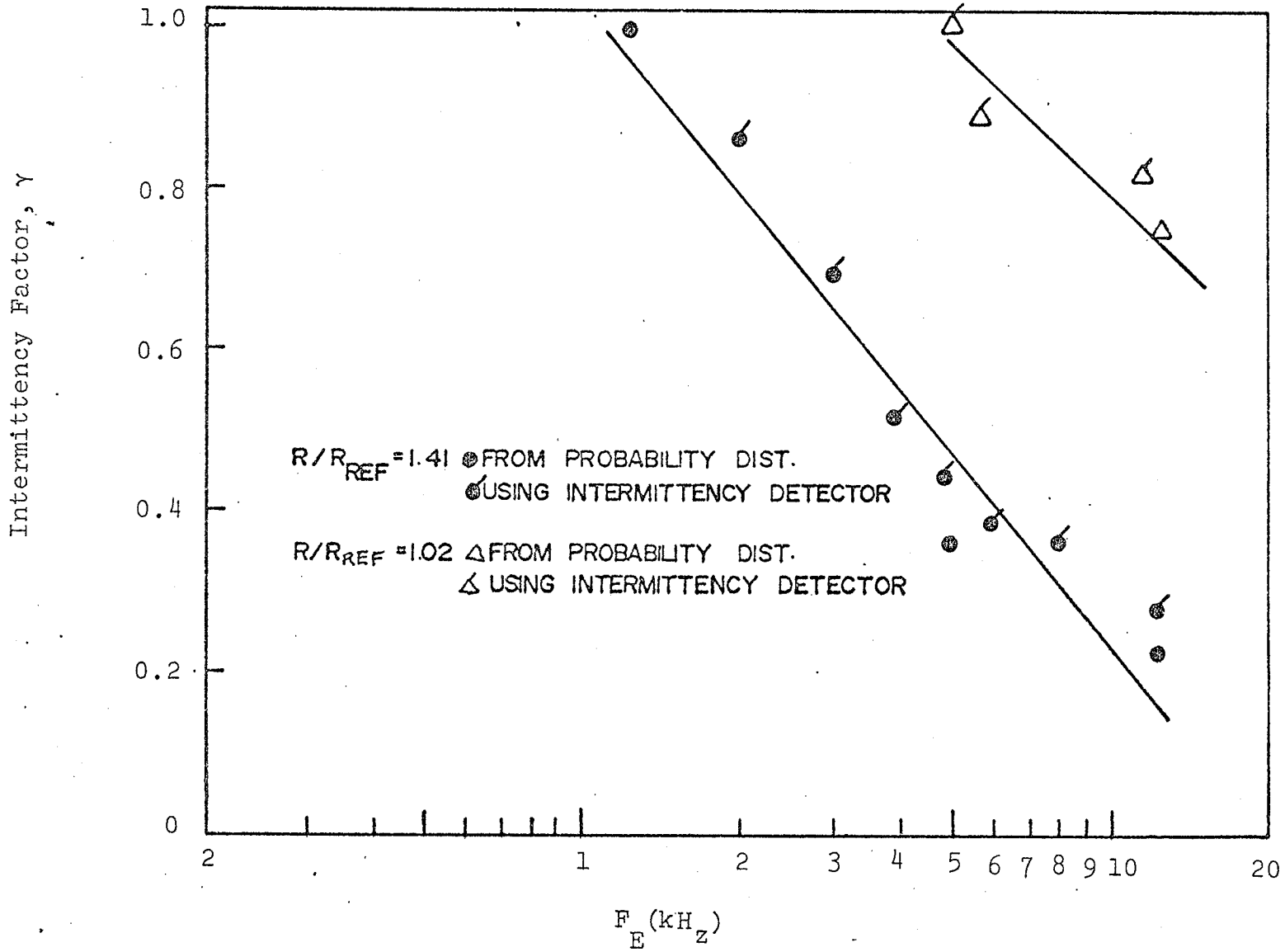

Figure 7.14 Envelope intermittency at Station 30

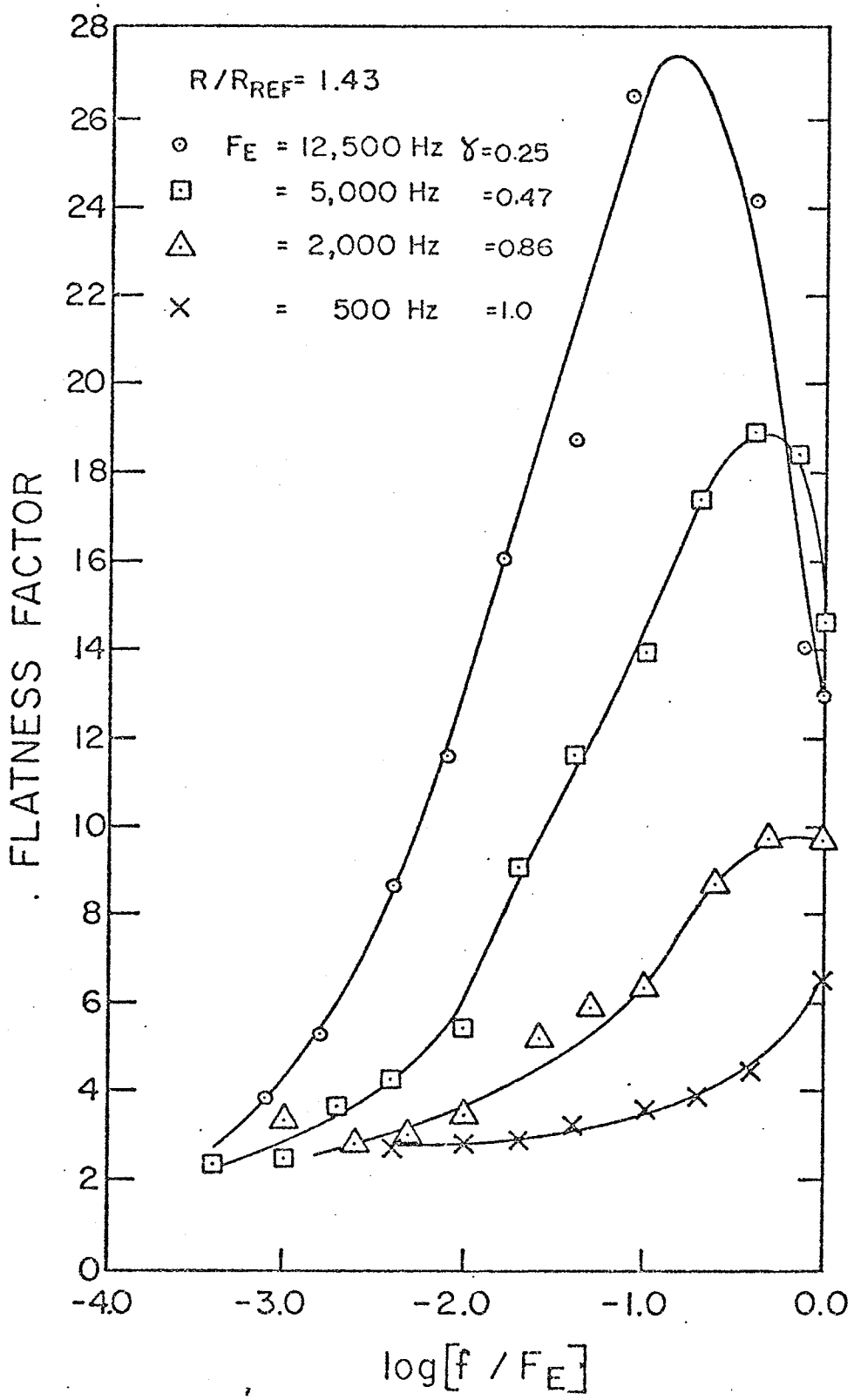

Figure 7.15 Flatness factor of narrow-band filtered envelope at Station 30

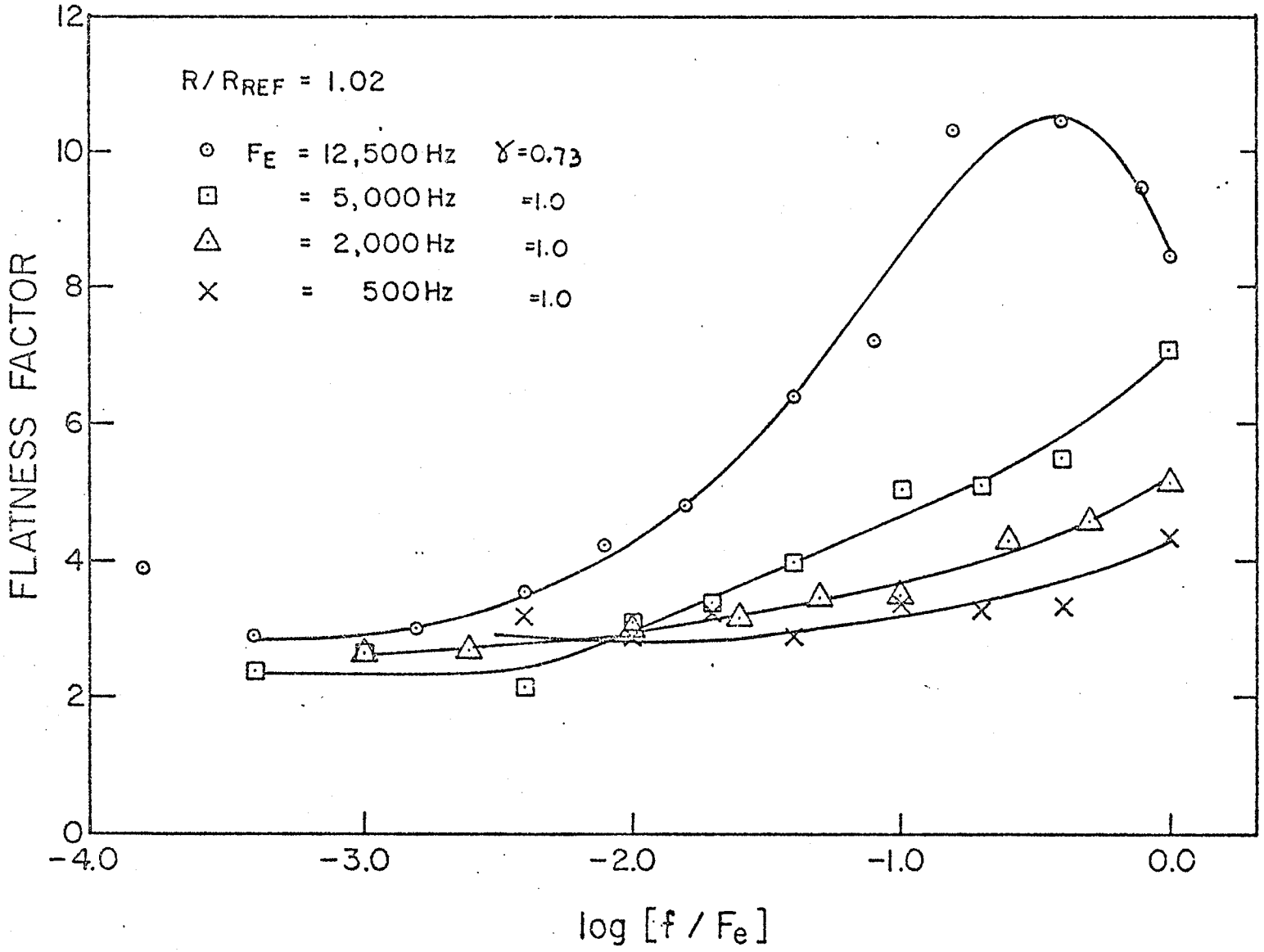

Figure 7.16 Flatness factor of narrow-band filtered envelope at Station 30

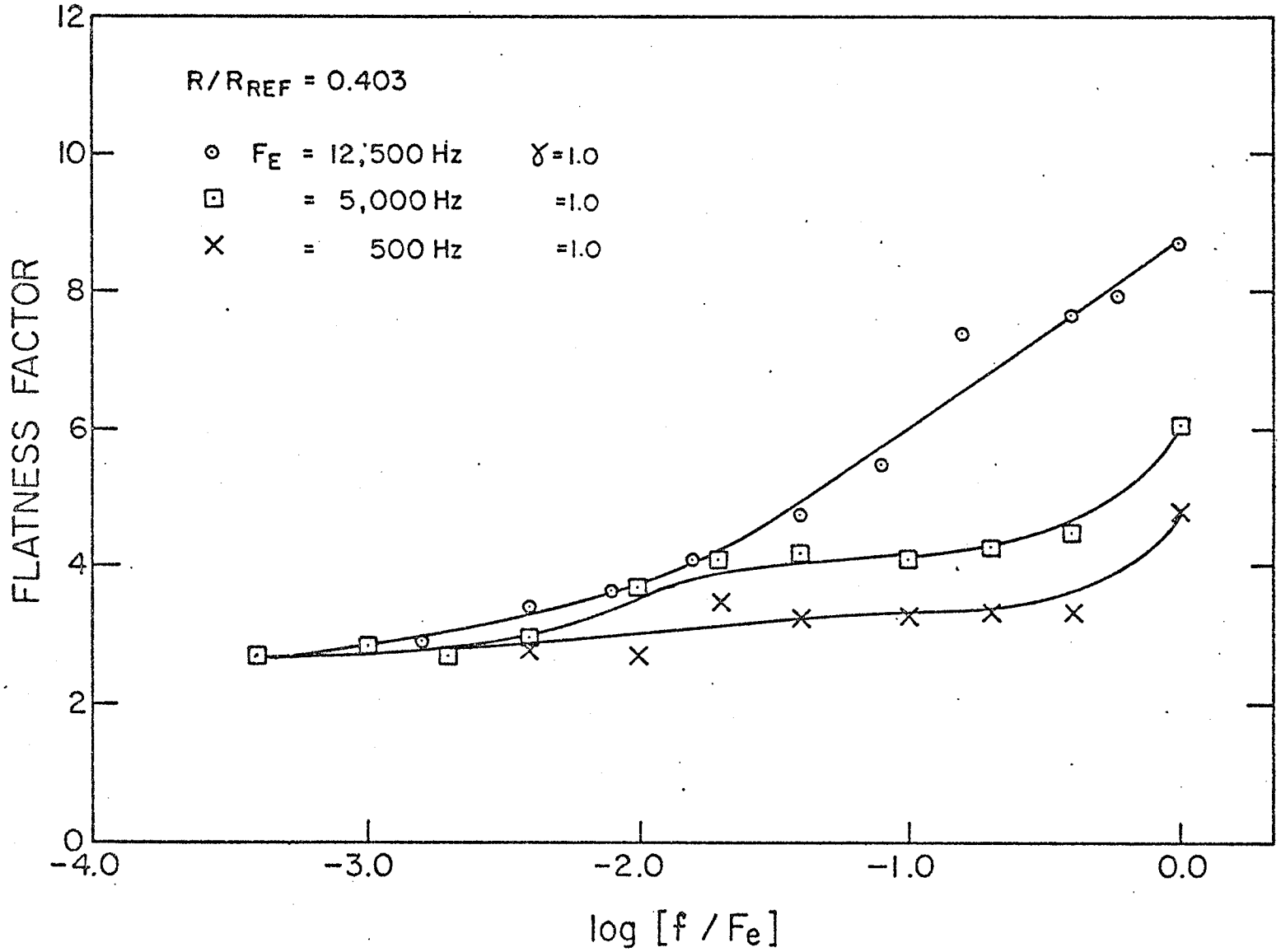

Figure 7.17 Flatness factor of narrow-band filtered envelope at Station 30

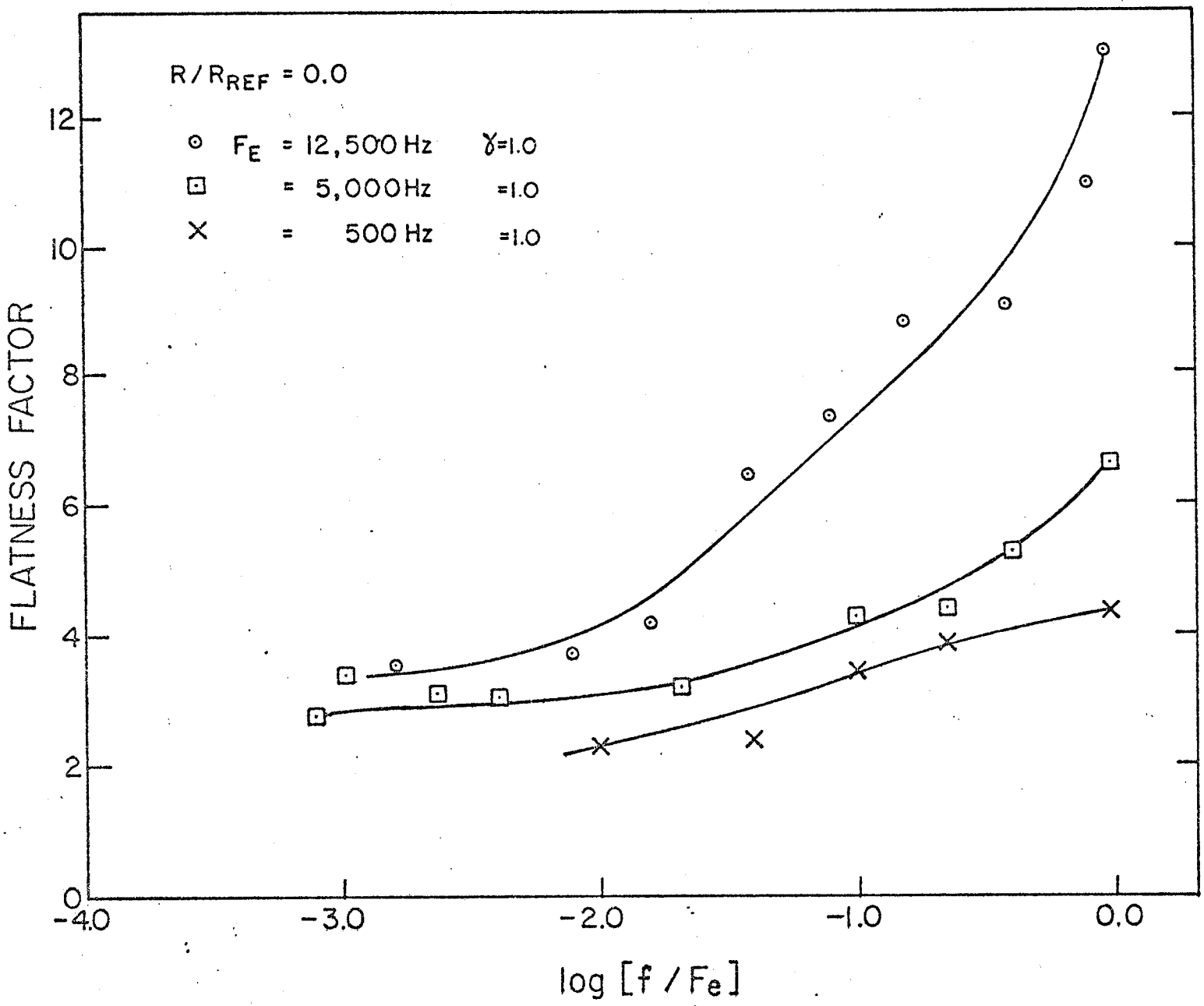

Figure 7.18 Flatness factor of filtered envelope at Station 30

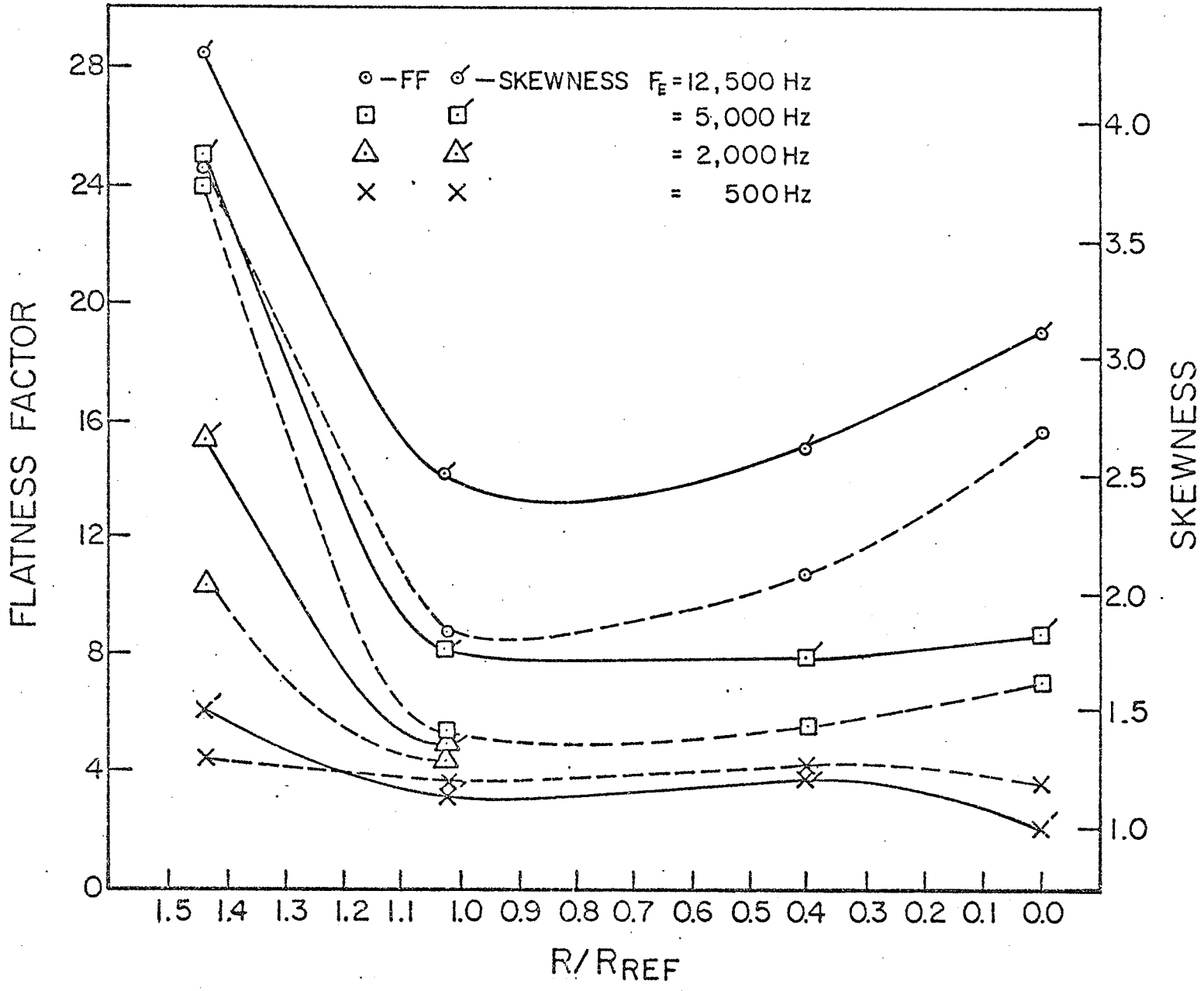

Figure 7.19 Envelope skewness and flatness factor at Station 30

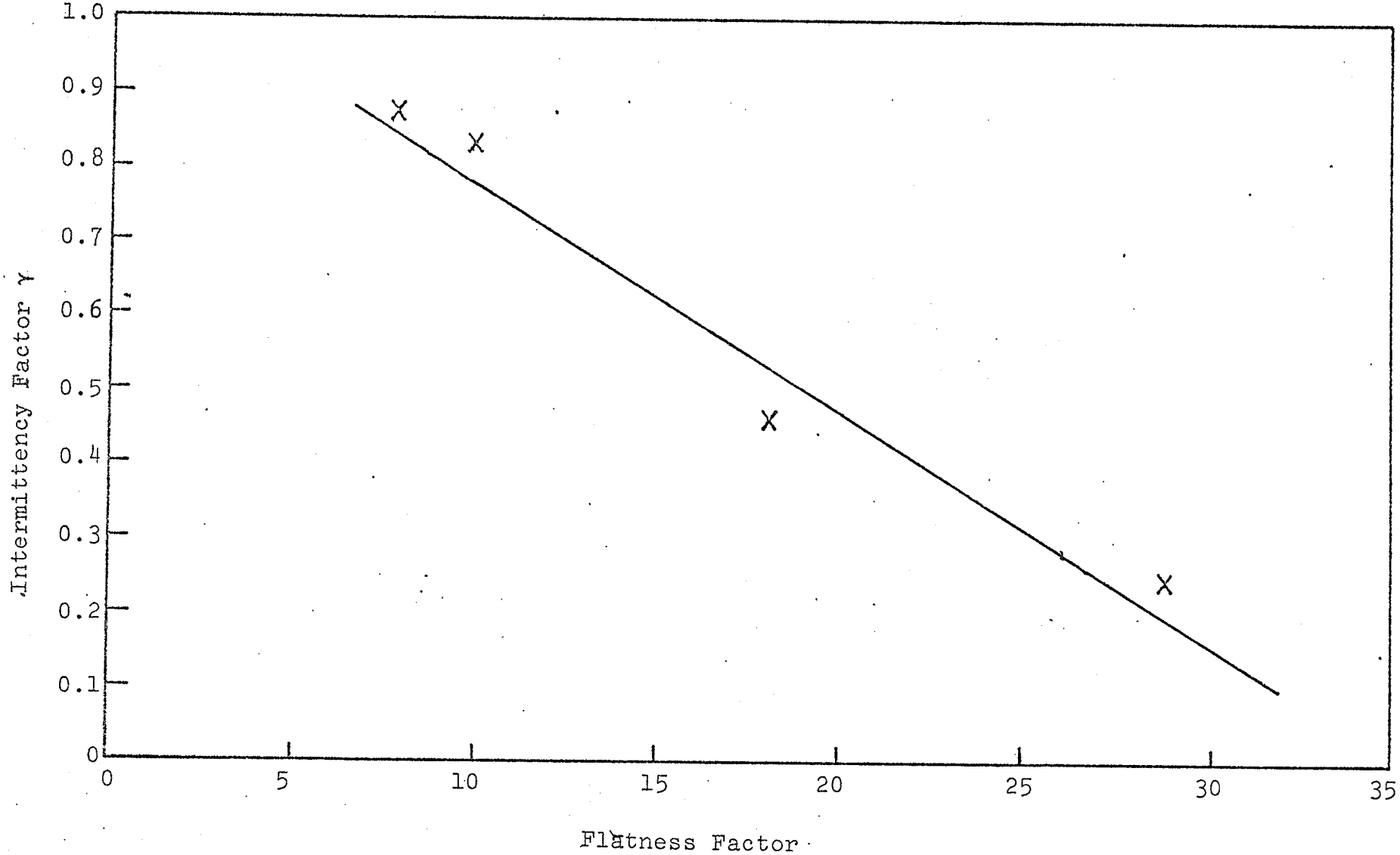

Figure 7.20 Intermittency factor of unfiltered envelope VS. peak flatness factor value of narrow-band filtered envelope

8.0 GENERAL DISCUSSION OF RESULTS

An important aspect of the present study was to investigate the developing nature of diffuser* flow. Also investigated was the wall region, assumed at the outset to have many similarities with that of pipes, channels, etc. In this chapter these aspects of diffuser turbulence are discussed further in the light of the experimental evidence obtained. For purposes of discussion, the diffuser is partitioned into three regions, A, B and C as shown in Figure 8.1. The significance of the boundaries between the various regions will be explained as the discussion develops.

Regions B and C are characterized by large turbulence production and intensities. As shown in Figure 4.14b, the maximum value of u' in these regions is nearly three times that of the centre line value at entry. Based on the present results, and those of Azad and Hummel (1971) with non-turbulent potential flow at entry, it is generally concluded that the turbulence in these regions is largely

*Actually a very specific diffuser as described in Chapter 3.

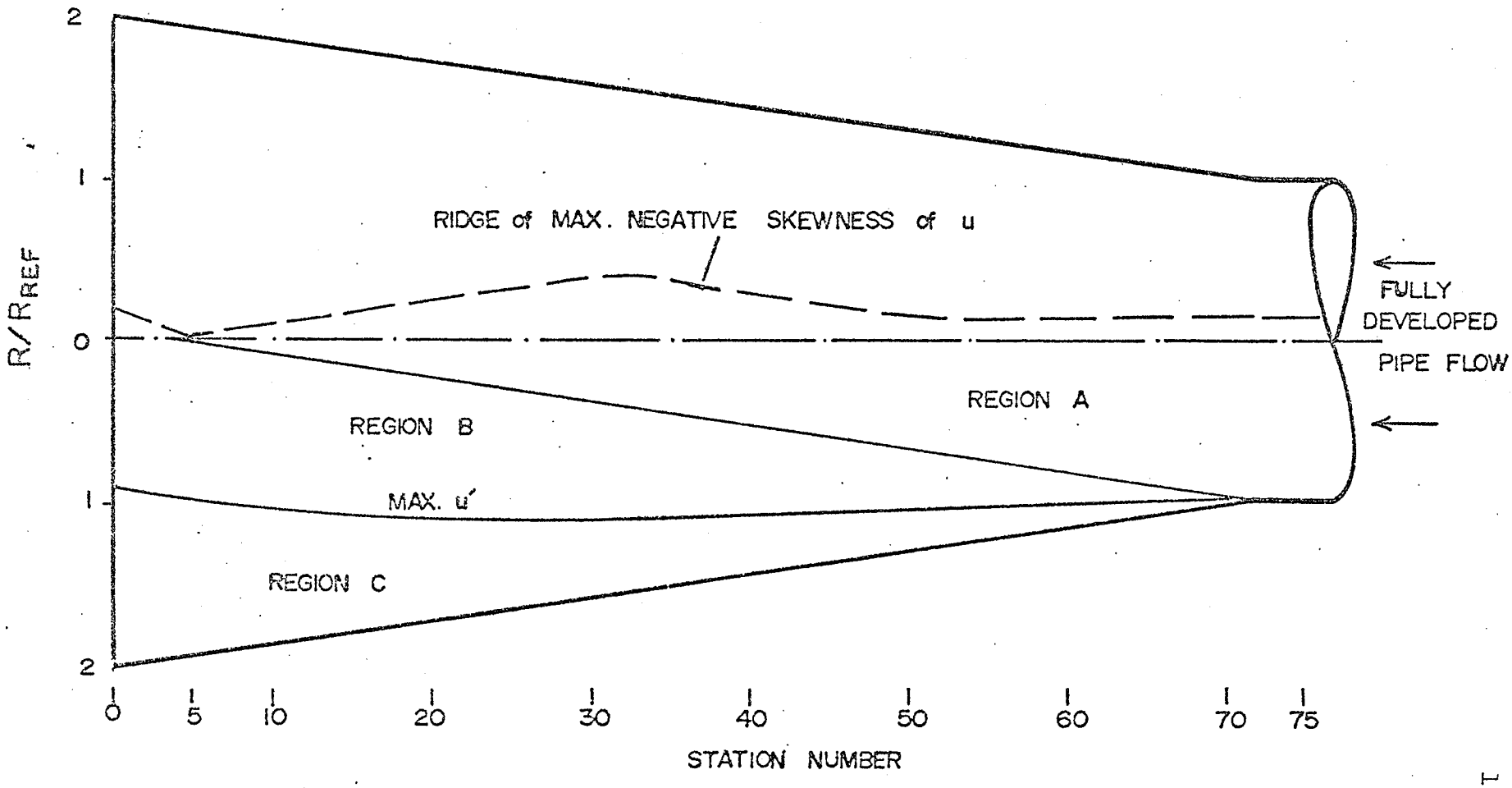

Figure 8.1 Diffuser geometry showing various flow regions

dominated by the very intense turbulence produced there and hence largely independent of the flow structure at entry.

In region A the flow is largely dependent on the type of flow at entry. For example with non-turbulent potential flow at entry, this region remains largely non-turbulent forming an intermittent interface with region B (Azad and Hummel, 1971). In the present case, as will be shown, the flow in region A also retains many of the characteristics of fully developed pipe flow.

Having shown briefly, the general characteristics of the various regions, a more detailed discussion can proceed starting with the core region which includes region A and that part of region B for which $R/R_{REF} < 0.8$. Of special interest are the skewness of u and the non-normalized truncated uv correlation measurements, also referred to as the uv components.

Figure 5.9 shows the uv components at station 75 (3 cm inside the pipe). The curves for the ejection and sweep events are approximately straight lines with slopes characteristic of such events in the core region of a fully developed pipe flow. Further down stream at station 30, (Figure 5.11) and for ($R/R_{REF} < 0.3$), the slopes of the sweeps and ejections are approximately the same as at

station 75 (in the pipe). These are therefore referred to as "pipe-like" sweeps and ejections. Wallward for ($R/R_{REF} > 0.4$), the sweeps and ejections increase more rapidly, reaching peak values at ($R/R_{REF} \approx 1$) which are about twice as large as those found in the pipe. These sweeps and ejections are associated with turbulence produced in the diffuser and would (presumably) also occur with non-turbulent flow at entry. Hence, they are referred to as "diffuser-like" sweeps and ejections.

Returning to station 75, the skewness of u shows a maximum negative value at $R/R_{REF} \approx 0.20$ (Figure 4.8). This result is consistent with the fully developed pipe flow studies of Lawn (1971). Moving further down stream, at station 55, the "pipe-like" sweeps and ejections merge gradually with the "diffuser-like" sweeps and ejections at $R/R_{REF} \approx 0.8$, (Figure 5.10) with maximum negative u skewness still occurring at $R/R_{REF} \approx 0.20$, (Figure 4.13). Thus, at this station, the structure associated with the core region of a fully developed pipe flow has been maintained toward the centre line ($R/R_{REF} < 0.7$) but has been gradually replaced towards the wall by a new type of the structure; i.e., "diffuser-like" sweeps and ejections.

Moving down stream, from station 55, the ridge of maximum negative skewness maintains its radial position,

at $R/R_{REF} \approx 0.20$, (Figure 4.13) up to about station 45 where it starts to diverge from the centre line. From station 35 onward it returns toward the centre line, increasing in value up to station 5, where it touches the centre line.

At station 30, as previously discussed and shown in Figure 5.18, the structure of the sweeps and ejections changes rather abruptly at $R/R_{REF} \approx 0.40$ from one of "pipe-like" flow near the centre line to one of "diffuser-like" flow toward the wall. This radial location also marks the approximate location of maximum negative u skewness and is further characterized by,

a) Maximum FF of u, (Figure 4.10).

b) Maximum FF of the longitudinal vorticity, (Figure 5.13).

c) A peak in the FF of $\partial u/\partial t$, (Figure 5.14).

d) Maximum negative skewness and flatness factor of the transverse velocity difference, (Figures 5.16 and 5.17).

e) The approximate outer edge ($\gamma \approx 0.1$) of the intermittent zone if the flow at the inlet is non-turbulent (Azad and Hummel, 1971).

It would thus appear that a rather abrupt change of structure does occur at $R/R_{REF} \approx 0.4$ with the boundary marking the outer edge (measured from the wall) for which "diffuser-like" ejections are effective. It is further characterized by more intermittent local shear, a conclusion based on the results of Figures 5.17 and 5.14 which show increased FF values of $\partial u/\partial y$ (estimated by the velocity difference of two probes separated in the y direction) and $\partial u/\partial x$ (estimated by $\partial u/\partial t$). Between stations 5 and 35 the boundary is coincident with the ridge of maximum negative u skewness.

At (approximately) station 5, the ridge of maximum negative skewness (Figure 4.13a) actually reaches the centre line marking the end of region A in the down stream direction. The explaination is that at approximately station 5 and down stream some of the "diffuser-like" ejections (low momentum fluid moving away from the wall) actually cross over the centre line thus becoming wallward interactions (low momentum fluid towards the opposite wall). As shown in Figure 5.12 the "pipe-like" sweeps and ejections have completely disappeared at this station. Furthermore, the wallward interactions increase toward the centre line, a feature not nearly so much in evidence for the other stations. Thus, down stream from station 5 low momentum

fluid is ejected across the centre line with equal probability from all radial directions. The resulting decrease in mean time between ejections on the centre line results in decreased values for the skewness (magnitude) and flatness factor. Thus moving down stream from station 5 the ridges of maximum negative skewness and FF diverge from the centre line as the results show (Figure 4.13a, b).

In the absence of any flow visualization experiment for the diffuser, it is interesting to speculate on the nature of the "bursting process" associated with the production of energy in regions B and C. Because of the large mean lateral vorticity in this region (which can be estimated by $\partial\bar{U}/\partial y$, the slope of the mean velocity profiles in Figure 4.16, it seems reasonable to assume that much of the large scale turbulence will be produced in the form of large lateral vortices. Using a flow visualization technique, Nychas et al (1973) have demonstrated the existence of such vortices for turbulence produced near the wall of a boundary layer. The conjecture is that such vortices would convect high (axial) momentum fluid from region B into region C (sweeps) where the fluid would "stall" or "become trapped" because of the adverse pressure gradient. The highly intermittent fine structure observed in region C would then be attributed to the high

local shear rates generated when this "blob" of stalled fluid comes in contact with or is torn apart by a higher momentum fluid parcel from further up stream, trying to displace it. The "stalled" fluid envisaged here is similar to the "decelerated" fluid discussed by Nychas et al (1973). Such a model of "stalled fluid" being torn apart by high momentum fluid seems consistent with the results given in Figures 5.21 to 5.24 which show the fine structure to be coincident with the high momentum fluid.

A major objective of the present work, was to draw comparisons between the turbulence of a conventional boundary layer and that for the diffuser (towards the wall). For the former, maximum u' and energy production both occur at $y^+ \approx 15$ with a layer of constant Reynolds stress further out from the wall. For the diffuser, Okwuobi and Azad (1973) have shown that the radial position for maximum u', energy production, and Reynolds stress all coincide at approximately the entry radius throughout. This radial position is shown in Figure 8.1 as "the line of maximum u'" and defines the boundary between regions B and C. In the analogy therefore regions C correspond to $y^+ < 15$.

In addition to those just described, the following additional similarities have been observed.

1) For both boundary layers and diffuser flow maximum u' also correspond to the position of minimum FF and zero skewness of u. This can readily be seen by comparing the results in Figure 4.13 with the results of Echelmann (1973). Furthermore for $y^+ < 15$ the skewness of u in the boundary layer is positive as it is in region C and negative for $y^+ > 15$ as it is in region B.

2) A comparison of the boundary layer data in Figure 5.4 with the diffuser data shown in Figures 5.5 to 5.12 shows that region B is dominated by ejection events as is the region, $y^+ > 15$ for the boundary layer. For the diffuser, region C is dominated by sweep events with the outward interactions larger in magnitude than the wallward interactions. This situation also exists in the region ($y^+ < 15$) for the boundary layer.

3) As discussed in section 5.7 and Chapter 7, the fine structure in region C is very intermittent. Ueda and Hinze (1975, Figure 6)

have shown that the maximum FF of the narrow-band filtered u signal is much larger at $y^+ = 5.02$ than for example at $y^+ = 21$, thus indicating increased spatial localization of the structure in the inner zone of a boundary layer.

While the number of similarities is substantial, important dissimilarities exist. For example the peak in the skewness of $\partial u/\partial t$, observed by Ueda and Hinze (1975) for a boundary layer at $y^+ \simeq 15$ does not occur for diffuser flow at $R/R_{REF} \simeq 1$ (Figure 5.14). This result strongly suggests that region C for the diffuser is quite different from the boundary layer region ($y^+ < 15$) and a more detailed comparison between the two regions is required.

For the boundary layer, the region ($y^+ < 15$) contains the viscous sublayer ($y^+ < 5$). Ueda and Hinze (1975, Figure 4) have shown that in the viscous sublayer, R_λ is less than 35 and decreasing very rapidly toward the wall. Thus one-third of the region ($y^+ < 15$) is dominated by viscosity. For the diffuser, on the other hand, (at station 30), R_λ is less than 35 for ($1.56 < R/R_{REF} < 1.575$), a result obtained by extrapolating the R_λ results of Figure 5.1 to the wall. Thus at station 30, the viscous region (corresponding to the viscous sublayer) is only about 3%

of the thickness of region C which is therefore dominated largely by inertial forces with a very narrow viscous region near the wall.

From this discussion the following flow structure is proposed for the wall region of the diffuser "far" from the inlet; i.e., between stations 0 and 65, say. Toward the inlet the flow structure must approach that of a boundary layer.

Because of the rather large inertial region between the maximum shear stress layer ($R/R_{REF} \approx 1$) and the wall, the maximum shear stress layer is viewed more as a boundary-free shear layer than a wall bounded shear layer. This effect increases in the down stream direction as region C widens. The non-zero mean velocity gradient near the wall (Figure 4.16) demands the existence of a viscous layer adjacent to the wall. It is suggested that this viscous layer is actually part of some sort of conventional boundary layer very close to the wall. Such a boundary layer would be characterized by low wall shear stress, decreasing in the down stream direction and would exist only intermittently at any given wall location because of the very intermittent nature of the large scale motion in its outer region (region C). The existence of such a layer would be demonstrated by increased turbulence

production and dissipation very close to the wall, the former already having been shown by Okwuobi and Azad (1973).

From the above discussion the tentative conclusion is that, for a diffuser, as used in the present work, the "boundary layer" may be thought of as a composite or two-stage layer with a boundary-free shear layer at approximately the entry radius and a more conventional, "intermittently existing", boundary layer very close to the wall.

9.0 CONCLUDING REMARKS

An experimental investigation of the turbulence structure in a conical diffuser with fully developed pipe flow at entry has been described. From the results the following main conclusions can be drawn.

1) For the core region near entry, the structure is similar to that of fully developed pipe flow. Moving down stream this structure is gradually replaced by a more energetic structure expanding toward the centre line from the wall. This more energetic structure, associated with turbulence produced in the diffuser, completely fills the diffuser 5 cm upstream of the exit plane. The boundary between the two types of structures becomes better defined in the down stream direction coinciding with the ridge of maximum negative u skewness between stations 5 and 35.

2) In the vicinity of $R/R_{REF} \approx 1$ the flow shows several similarities and dissimilarities with boundary layer flow in the vicinity of $y^+ = 15$. The similarities are:

a) At $R/R_{REF} \approx 1$ and $y^+ \approx 15$, u' is maximum but the flatness factor of u is minimum.

b) For $R/R_{REF} < 1$ (approx.) and $y^+ > 15$, the skewness of u is negative with ejection events making a larger contribution to $\overline{uv}$ than sweep events.

c) For $R/R_{REF} > 1$ (approx.) and $y^+ < 15$, the skewness of u is positive with sweep events making a larger contribution to $\overline{uv}$ than ejection events. Furthermore, the fine structure, in both cases becomes very intermittent.

The dissimilarities are:

a) For the boundary layer, the peak in the skewness of $\partial u/\partial t$ at $y^+ \approx 15$, does not occur in the diffuser for $R/R_{REF} \simeq 1$.

b) For the diffuser, the viscous part of the region $R/R_{REF} > 1$, is percentage-wise less than the viscous part of the boundary layer region $y^+ < 15$; i.e., the viscous sublayer.

3) $\partial u/\partial t$ is intermittent only in the vicinity of the wall where the fine structure coincides

more with high (axial) momentum fluid than low (axial) momentum fluid.

4) The envelope of narrow-band filtered u shows two length scales; one increasing with wave-number, in the inertial subrange and then decreasing again in the dissipation region, the other decreasing with wave-number throughout. A linear relationship exists between the "peak" value of the flatness factor of the filtered envelope, and the intermittency factor of the envelope itself.

5) Except near the wall, structure function measurements show the existence of an inertial subrange for a separation range of about one decade. Thus the assumptions of Kolmogoroff still have some validity for a flow as complicated as that found in a diffuser.

10.0 RECOMMENDATIONS

A number of preliminary results have been given for the envelope of narrow-band filtered u. The ultimate aim is to obtain unambiguous fine structure information and in particular, to measure the mean time or distance between bursts. To test the ultimate worth of such experimentation, it is recommended that further experiments be performed in a boundary layer where the results can be compared with those obtained by other experimenters.

BIBLIOGRAPHY

AZAD, R.S. and HUMMEL, R.H. (1971)
Measurement of the intermittency factor in diffuser flow. Can. J. Phys. 49, 2917-2930.

BAKEWELL, Jr., H.P. and LUMLEY, J.L. (1967)
Viscous sublayer and adjacent wall region in turbulent pipe flow. Phys. Fluids, 10,1880-1889.

BATCHELOR, G.K. and TOWNSEND, A.A. (1947)
Decay of vorticity in isotropic turbulence. Proc. Roy, Soc. A 190, 534-550.

BATCHELOR, G.K. and TOWNSEND, A.A. (1949)
The nature of turbulent motion at large wave-number. Proc. Roy. Soc. A 199,238-255.

BATCHELOR, G.K. (1960)
The theory of homogeneous turbulence. Cambridge University Press.

BLACKWELDER, R.F. and KOVASZNAY, L.S.G. (1972)
Time scales and correlations in a turbulent boundary layer. Phys. Fluids 15,1544-1554.

BOX, M.J., DAVIES, D., and SWANN, W.H. (1969)
Non-linear optimization techniques. Oliver and Boyd, Edinburgh.

BREMHORST, K. and WALKER, T.B. (1973)
Spectral measurements of turbulent momentum transfer in fully developed pipe flow. J. Fluid Mech. 61, 173-186.

BRODKEY, R.S., WALLACE, J.M. and ECKELMANN, H. (1974)
Some properties of truncated turbulence signals in bounded shear flows. J. Fluid Mech. 63, 209-224.

CHAMPAGNE, F.H., HARRIS, V.G. and CORRSIN, S. (1970)
Experiments on nearly homogeneous turbulent shear flow. J. Fluid Mech. 41, 81-139.

CHEN, W.Y. (1971)
Lognormality of small-scale structure of turbulence. Phys. Fluids. 14, 1639-1642.

COMTE-BELLOT, G. and CORRSIN, S. (1971)
Simple eulerian time correlation of full and narrow-band velocity signals in grid-generated, 'isotropic' turbulence. J. Fluid Mech. 48, part 2, 273-337.

CORINO, E.R. and BRODKEY, R.S. (1969)
A visual investigation of the wall region in turbulent flow. J. Fluid Mech. 37, part 1, 1-30.

CORRSIN, S. and KISTLER, A.L. (1955)
Free-stream boundaries of turbulent flows. NACA report 1244.

CORRSIN, S. (1962)
Turbulent dissipation fluctuations. Phys. Fluids 5, 1301.

ECKELMANN, H. (1973)
An experimental investigation of a turbulent channel flow with a thick viscous sublayer. Bericht Nr. 101/1973 Mak Planck Institut Fuer Stromungsforschung.

FIEDLER, H. and HEAD, M.R. (1966)
Intermittency measurements in the turbulent boundary layer. J. Fluid Mech. 25, part 4, 719-735.

FRENKIEL, F.N. and KLEBENOFF, P.S. (1975)
On the log normality of the small-scale structure of turbulence. Boundary-layer Meteorology 8, 173-200.

GAD-EL-HAL, M. and CORRSIN, S. (1974)
Measurements of the nearly isotropic turbulence behind a uniform jet grid. J. Fluid Mech. 62, part 1, 115-143.

GRASS, A.J. (1971)
Structural features of turbulent flow over smooth and rough boundaries. J. Fluid Mech. 50, part 2, 233-255.

GURVICH, A.S. and YAGLOM, A.M. (1967)
Breakdown of eddies and probability distributions for small-scale turbulence. Phys. Fluids 10, (suppl.), 59-65.

HINZE, J.O. (1959)
Turbulence, McGraw-Hill Book Co., New York, N.Y.

KIM, H.T., KLINE, S.J. and REYNOLDS, W.C. (1971)
The production of turbulence near a smooth wall in a turbulent boundary layer. J. Fluid Mech. 50, part 1, 133-160.

KISTLER, A.L. (1952)
The vorticity meter. M.Sc. Thesis, The Johns Hopkins University, Baltimore, U.S.A.

KOLMOGOROV, A.N. (1941)
C.R. Acad. Sci. (Doklady), U.S.S.R., 30, 301.

KOLMOGOROFF, A.N. (1962)
A refinement of previous hypothesis concerning the local structure of turbulence in a viscous incompressible fluid at high Reynolds number. J. Fluid Mech. 13, 81-85.

KOVASZNAY, L.S.G. (1967)
Structure of the turbulence boundary layer. Phys. Fluids 10, (suppl.), 25-30.

KUO, A.Y. and CORRSIN, S. (1971)
Experiments on internal intermittency and fine-structure distribution functions in fully turbulent fluid. J. Fluid Mech. 50, part 2, 285-319.

LAWN, C.J. (1971)
The determination of the rate of dissipation in turbulent pipe flow. J. Fluid Mech. 48, part 3, 477-505.

LU, S.S. and WILLMARTH, W.W. (1973)
Measurement of the mean period between bursts. Phys. Fluids. 16, 2012-2013.

MIDDLETON, D. (1960)
An introduction to statistical communications theory, McGraw-Hill Book Co., New York, N.Y.

MONIN, A.S. and YAGLOM, A.M. (1975)
Statistical Fluid Mechanics II. The MIT Press Cambridge, Mass. U.S.A.

MORRISON, W.R.B. (1969)
Two-dimensional frequency-wave number spectra and narrow band shear stress correlations in turbulent pipe flow. Ph.D. Thesis, University of Queensland.

NOVIKOV, E.A. (1965)
High-order correlations in turbulent flow. Isv., Atmospheric and oceanic Physics Series 1, 788-796.

NYCHAS, S.G., HERSEY, H.C. and BRODKEY, R.S. (1973)
A visual study of turbulent shear flow. J. Fluid Mech. 61, part 3, 513-540.

OKOVKHOV, A.M. (1962)
Some specific features of atmospheric turbulence. J. Fluid Mech. 13, 77-81.

OKWUOBI, P.A.C. and AZAD, R.S. (1973)
Turbulence in a conical diffuser with fully developed flow at entry. J. Fluid Mech. 57, part 3, 603-622.

PANCHEV, S. (1971)
Random functions and turbulence, Pergamon Press, Oxford.

RAO, K.N., NARASIMA, R. and NARAYANAN, M.A.B. (1971)
The "bursting" phenomenon in a turbulent boundary layer. J. Fluid Mech. 48, part 2, 339-352.

REICHERT, J.K. (1977)
A study of developing turbulent pipe flow, Ph.D. Thesis, University of Manitoba, Canada.

RUETENIK, J.R. and CORRSIN, S. (1955)
Equilibrium turbulent flow in a slightly divergent channel. 50 Jahre Grenzschichung, pp. 446-459, Brauschweig: Vieweg and Sohn.

SABOT, J. and COMTE-BELLOT, G. (1976)
Intermittency of coherent structures in the core region of fully developed turbulent pipe flow. J. Fluid Mech. 74, part 4, 767-796.

SANDBORN, V.A. (1959)
Measurements of intermittency of turbulent motion in a boundary layer. J. Fluid Mech. 6, 211-240.

SOVRAN, G. and CLOMP, E.D. (1967)
Experimentally determined optimum geometries for rectilinear diffusers with rectangular, conical or annular cross-section. Gen. Motors Symposium on Internal Flow, Amsterdam, Elsevier.

STEWART, R.W., WILSON, J.R. and BURLING, R.W. (1970)
Some statistical properties of small scale turbulence in an atmospheric boundary layer. J. Fluid Mech. 41, part 1, 141-152.

REICHERT, J.K. and AZAD, R.S. (1976)
Non asymtotic behavior of developing turbulent pipe flow. Can. J. Phys. 54, 268-278.

TAYLOR, G.I. (1938)
Production and dissipation of vorticity in a turbulent fluid. Proc. Roy. Soc. A 164, 15-23.

TENNEKES, H. and LUMLEY, J.L. (1972)
A first coarse in turbulence, MIT Press, Mass.

TENNEKES, H. (1968)
Simple model for the small-scale structure of turbulence. Phys. Fluids. 11, 669-671.

TOWNSEND, A.A. (1951)
On the fine structure of turbulence. Proc. Roy. Soc. A208, 534-542.

TRUPP, A.C. (1973)
The structure of turbulent flow in triangular array rod bundles. Ph.D. Thesis, University of Manitoba, Canada.

UEDA, H. and HINZE, J.D. (1975)
Fine-structure turbulence in the wall region of a turbulent boundary layer. J. Fluid Mech. 67, part 1, 125-143.

VAN ATTA, C.W. and CHEN, W.Y. (1970)
Structure functions of turbulence in the atmospheric boundary layer over the ocean. J. Fluid Mech. 44, part 1, 145-159.

VAN ATTA, C.W. and YEH, T.T. (1973)
The structure of internal intermittency in turbulent flows at large Reynolds number: experiments in scale similarity. J. Fluid Mech. 59, part 3, 537-559.

WALLACE, J.M., ECKELMANN, H. and BRODKEY, R.S. (1972)
The wall region in turbulent shear flow. J. Fluid Mech. 55, part 1, 39-48.

WILLMARTH, W.W. and LU, S.S. (1972)
Structure of the Reynolds stress near the wall, J. Fluid Mech. 55, part 1, 65-92.

WILLMARTH, W.W. (1975)
Structure of turbulence in boundary layers, Advances in Applied Mechanics, Vol. 15, Academic Press, New York, N.Y.

YAGLOM, A.M. (1966)
The influence of fluctuations in energy dissipation on the shape of turbulence characteristics in the inertial interval. Soviet Physics Doklady 11, 26-29.

ZARIC, Z. (1974)
Statistical analysis of wall turbulence phenomena. Advances in Geo physics, Vol. 18A, Academic Press.

ZARIC, Z. (1974)
Etude statistique de la turbulence parietale. Ph.D. Thesis, University of Belgrade.

APPENDIX A

Vorticity Probe Calibration

The vorticity probe, consisting of four hot-wires connected in the configuration of a Wheatstone bridge is shown schematically in Figure A.1. A single anemometer is connected across terminals A - D heating the wires and measuring the down stream velocity U. The down stream vorticity ξ, is obtained as the voltage difference between terminals B and C. Corrsin and Kistler (1955) have given a detailed description of such a probe. The probe was custom made by DISA with geometry as shown in Figure A.2. Each active wire was 3.6Ω at 23°C.

Calibration was by rotating the probe using a Type 4-MTA/T mercury slipringless transmitter manufactured by The Vibro-Meter Corporation, Fribourg, Switzerland. Rotation was provided by a small d.c motor whose speed could be easily controlled and measured to within 1% using a stroboscopic light. A rotation rate of n revolutions/second corresponds to a vorticity of $2\pi n$ radians/sec. A variable velocity, irrotational flow was provided by placing the probe on the centre line of the contraction cone of the wind tunnel described by Trupp (1973).

Originally, as described by Corrsin and Kistler (1955) this type of probe was used only in the constant current mode. For the present work a DISA 55M01 constant

temperature anemometer was used. Figure A.3 shows the vorticity output from the probe for various mean velocities and rotation rates. These voltages are of the order of a few millivolts and were measured using a Fluke 335 differential voltmeter. Clearly the vorticity readings depend on the mean velocity and a way had to be found to remove this dependency. Analysis of the data showed that if the vorticity output from the probe were multiplied by $U^{0.65}$, the dependency would be largely removed. Using only summing and a square root circuit, $U^{0.65}$ can be approximated by,

$$U^{0.65} = K_1 U^{0.5} + K_2 U$$

where

$$K_1 \simeq 0.94$$
$$K_2 \simeq 0.138$$

Figure A.4 shows a schematic diagram of the vorticity measuring system. Operational amplifiers A1 and A2 were specially selected for low input drift since, as shown in Figure A.3 the difference of the inputs was very small (of the order of a few millivolts). The BALANCE control was set for minimum change in output ξ for various mean velocities, but with the probe not rotating. The ZERO control was set for best zero value of ξ with various mean

velocities, and also with the probe not rotating. The "constants", K_1 and K_2, were adjusted experimentally by potentiometers to minimize any effect of the mean velocity on the vorticity output, ξ.

Figure A.5 shows the compensated vorticity output voltages for various mean velocities and vorticities (simulated by rotation). Maximum error was estimated to be approximately 5%.

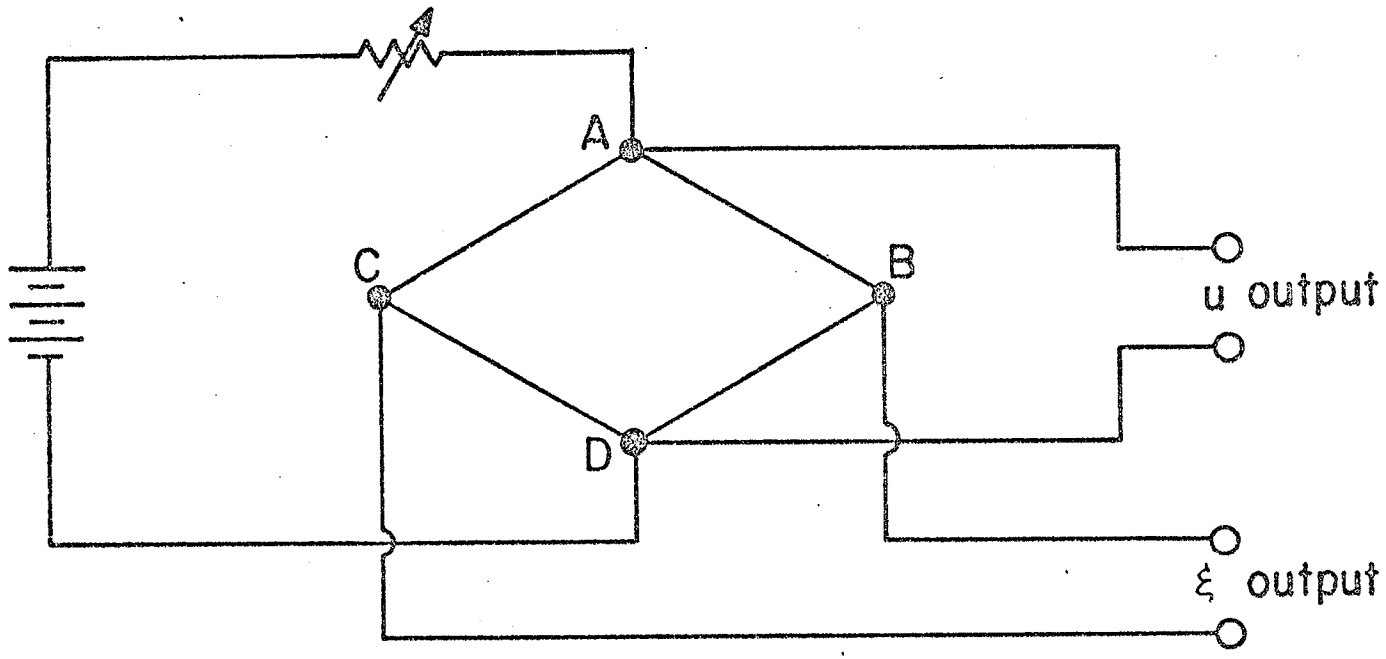

Figure A-1 Schematic diagram of vorticity probe

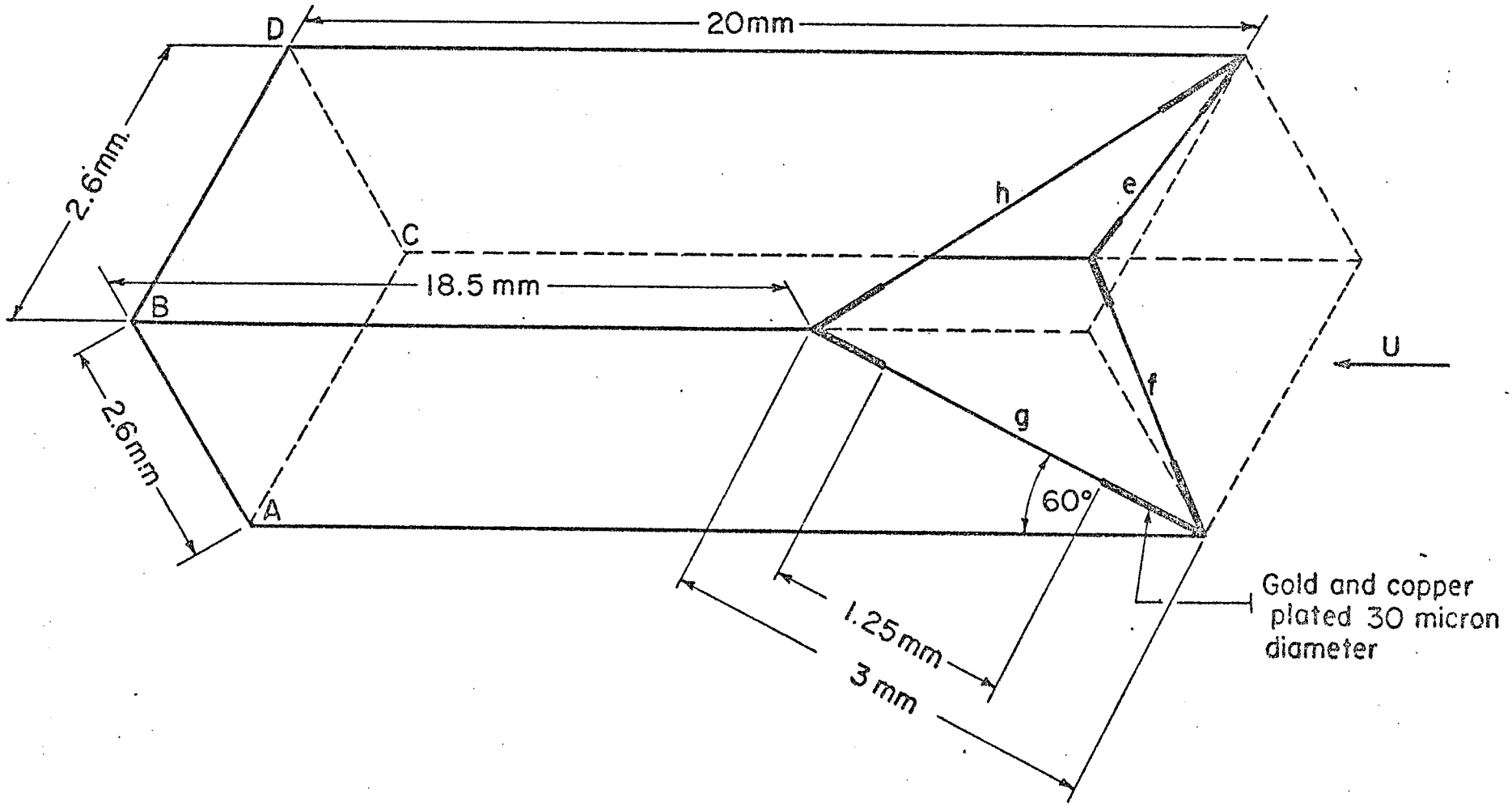

Figure A-2 Vorticity probe geometry

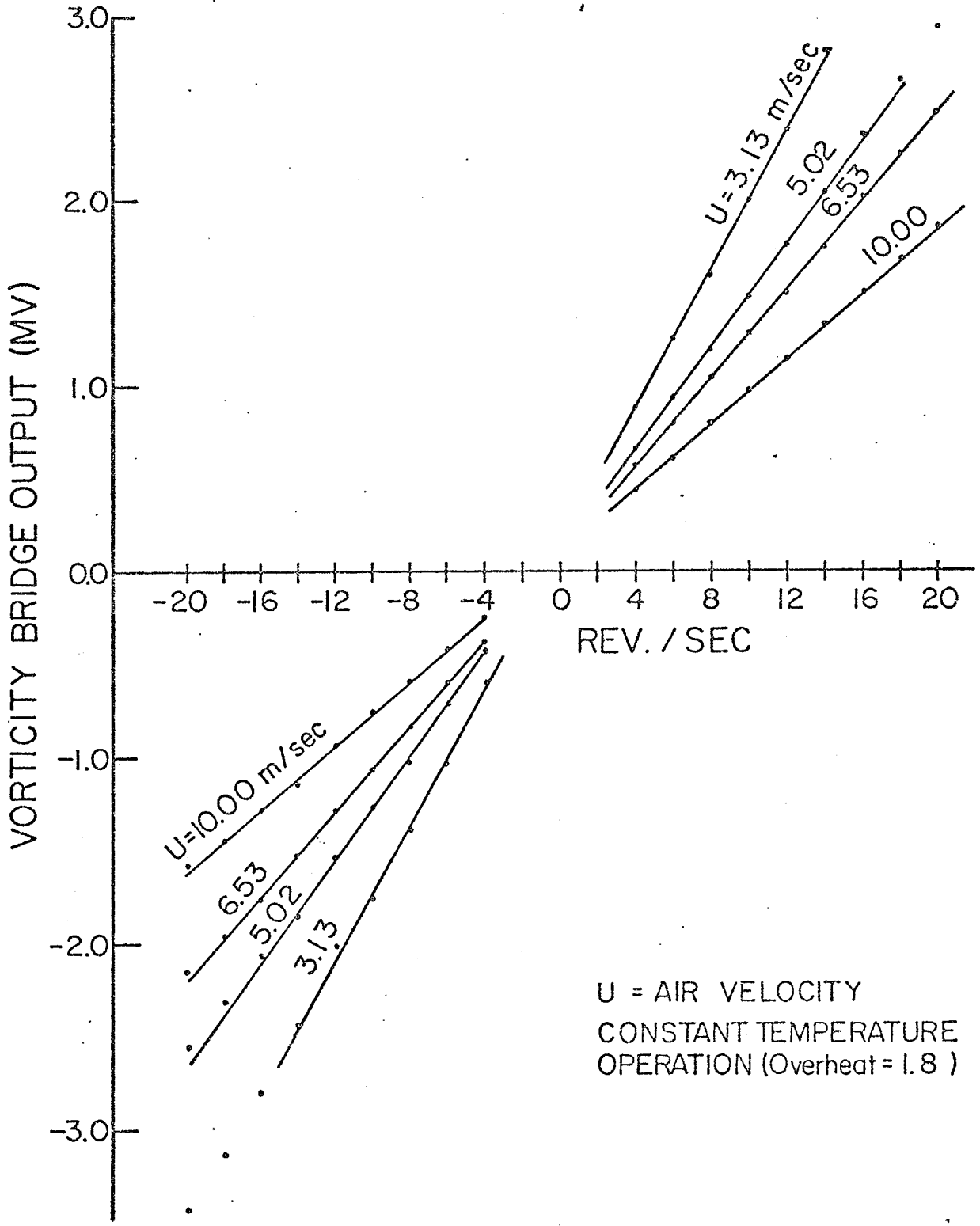

Figure A-3 Vorticity probe output voltage as a function of rotation rate and mean velocity

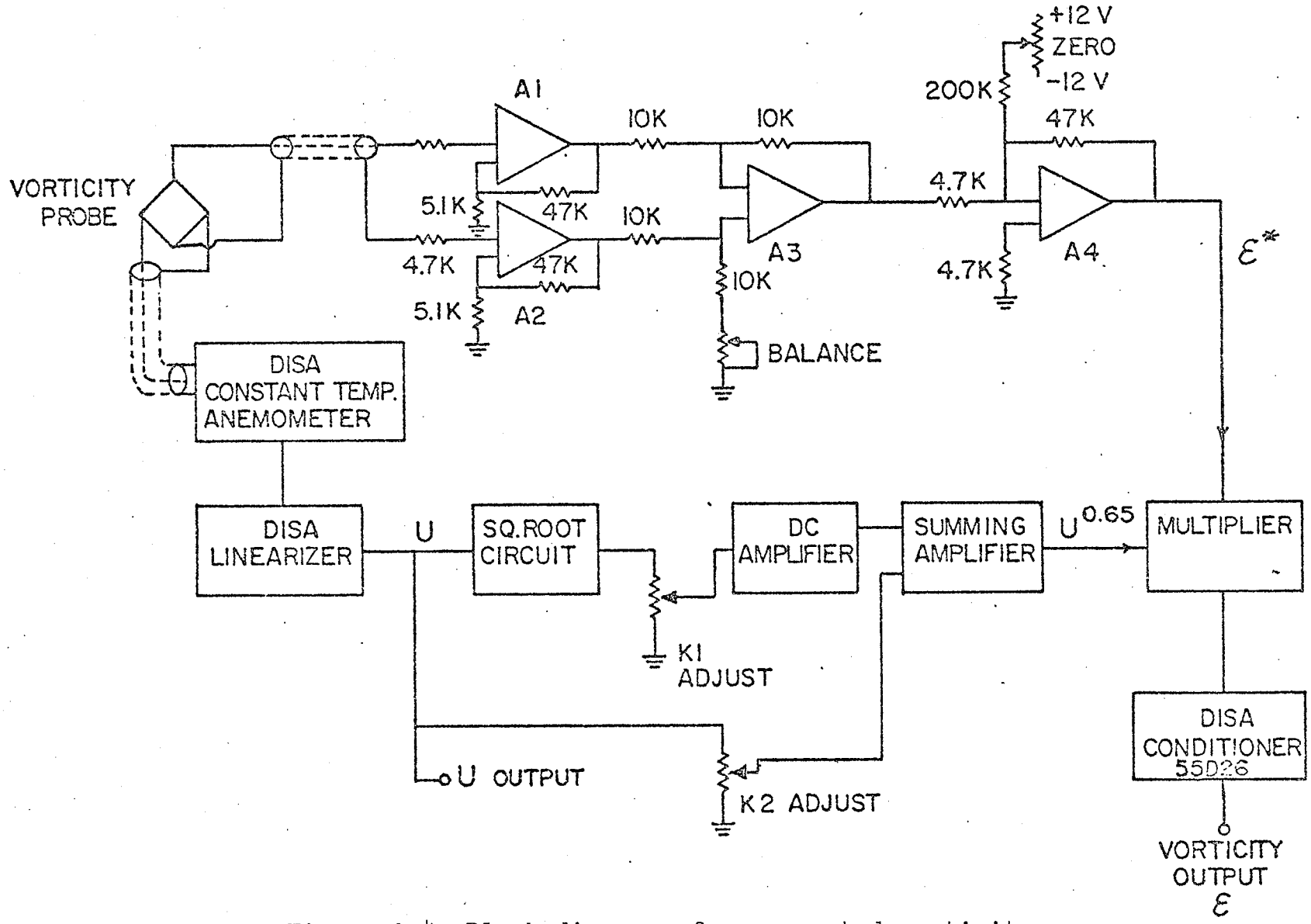

Figure A-4 Block diagram of compensated vorticity measuring system

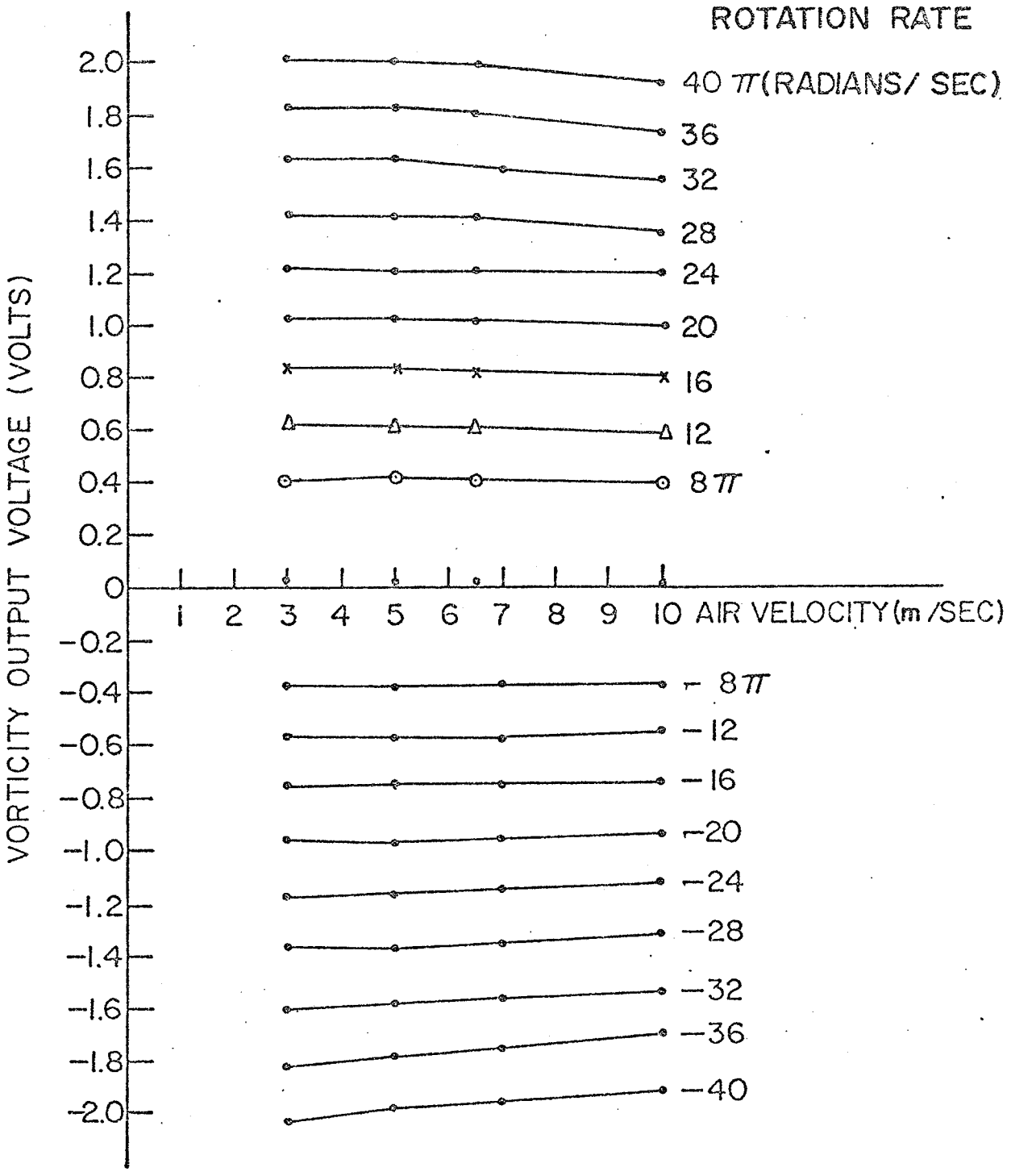

Figure A-5 Characteristics of compensated vorticity measuring system

APPENDIX B

Normalizing Procedure For Probability Density Functions

This Appendix describes the technique adopted for normalizing the experimentally obtained probability density functions (PDF's). These were obtained in the form of graphs drawn by an xy recorder with the horizontal and vertical scales arbitrary. The graphs were then "faired" on a light table and a sufficiently large number of point pairs $(f_1(x_1), x_1)$ read manually from the resulting graph. The mean value, $\bar{U}$, was measured directly using a d.c. voltmeter.

A properly normalized PDF is defined such that;

a) $$\int_{-\infty}^{\infty} f(x)dx = 1 \qquad (1)$$

b) $$\int_{-\infty}^{\infty} x\, f(x)dx = \bar{U}. \qquad (2)$$

$f(x)$ and x are found from the measured points $f_1(x_1)$ and x_1, using the linear relationships,

$$f(x) = C\, f_1(x_1) \qquad (3)$$

$$x = D\, x_1 \qquad (4)$$

where C and D are constants to be found.

By substituting (3) and (4) into (1) and (2) respectively, it is easily shown that;

$$C = \frac{\int_{\infty}^{\infty} x_1 \, f_1(x_1) \, dx_1}{\bar{U} \left[\int_{-\infty}^{\infty} f_1(x_1) \, dx_1 \right]^2}$$

and

$$D = \frac{\bar{U} \int_{-\infty}^{\infty} f_1(x_1) \, dx_1}{\int_{-\infty}^{\infty} x_1 \, f_1(x_1) \, dx_1} .$$

These constants were readily found using numerical integration and the properly normalized PDF then found from (3) and (4).

V I T A

RUDOLF HENRY HUMMEL

1932	Born, January 26, in Winnipeg, Canada
1951	Graduated from St. Paul's High School, Winnipeg
1955	Graduated B.Sc. (Electrical Engineering), The University of Manitoba
1955-56	Microwave Engineer - Manitoba Telephone System
1956-57	Radar Engineer - Canadian Aviation Electronics Montreal, Canada
1957-59	Telecommunications and Radar Engineer - Federal Electric Corporation - Paramus, New Jersey
1959-60	Post Graduate Work in Electrical Engineering, The University of Manitoba
1961-68	Electronic Research and Development Engineer Nuclear Enterprises Ltd., Winnipeg
1968-69	M.Sc. student - The University of Manitoba
1970	Graduated M.Sc. (Fluid Mechanics and Turbulence) The University of Manitoba
1969-72	Ph.D student - The University of Manitoba
1972-77	Part-time Ph.D student; Electronic Engineer and partner, TRIMET Instruments Ltd., 1792 St. Mathews Avenue, Winnipeg, Canada

REPORTS AND PUBLICATIONS

1. W.B. Reid, R.H. Hummel	Pulse Shape Discrimination in Organic Scintillators Canadian Nuclear Technology Jan. - Feb., 1966
2. K.I. Roulston, W.B. Reid, R.H. Hummel	Some Recent Advances in Nuclear Electronics Physics in Canada 21, 31 (1965)
3. W.B. Reid, R.H. Hummel	A Radiation Analyzer Which Detects and Sorts Neutrons, Gamma Rays, and Ionizing Particles Nuclear Enterprises Internal Report March, 1963
4. R.H. Hummel	On the Design and Performance of a Time to Amplitude Converter Nuclear Enterprises Internal Report 1967
5. R.S. Azad, R.H. Hummel	Measurements of the Intermittency Factor in Diffuser Flow Canadian Journal of Physics 49, 2917 (1971)
6. D.P. Kostiuk, R.H. Hummel, R.S. Azad	An Instrument for Measuring Pressure in Turbulent Boundary Layers Rev. of Scientific Instruments 42, 1127 (1971)